

**The role of Ephrin and HGF/c-MET pathway in regulating Vasculogenic
mimicry in breast cancer and possible effects of phytochemicals**

**Thesis submitted to
JADAVPUR UNIVERSITY**



in partial fulfillment of the requirements

for the award of the degree of

DOCTOR OF PHILOSOPHY (Science)

BY

DEBARPAN MITRA

(INDEX NO.: 97/18/Life. Sc./25)

Department of Signal Transduction and Biogenic Amines

Chittaranjan National Cancer Institute

37, S.P Mukherjee Road, Kolkata- 700026

India

DR. NABENDU MURMU, PhD

Senior Scientific Officer, Assistant Director Grade

Head-Dept. of Signal Transduction and Biogenic Amines



Chittaranjan National Cancer Institute

An autonomous body under the Ministry of Health
and Family Welfare, Govt. of India

37, S. P. Mukherjee Road, Kolkata - 700026

Phone: 2475 9313, 2476 5101 (Extn. 322)

Fax: 2475 7606

Email: nabendu.murmu@cnci.ac.in
nabendu64@gmail.com

CERTIFICATE FROM THE SUPERVISOR

This is to certify that the thesis entitles “**The role of Ephrin and HGF/c-MET pathway in regulating Vasculogenic mimicry in breast cancer and possible effects of phytochemicals**” submitted by **Sri Debarpan Mitra**, who got his name registered on 27th February, 2018 (**INDEX NO.: 97/18/Life. Sc./25**) for the award of Ph.D. (Science) degree of Jadavpur University, is absolutely based upon his own work under my supervision and that neither this thesis nor any part of it has been submitted for either any degree/diploma or any other academic award anywhere before.

डॉ० नबेंदु मुरुमु / Dr. Nabendu Murmu Ph.D
वरिष्ठ वैज्ञानिक अधिकारी, सहायक संचालक ग्रेड
Sr. Scientific Officer, Assistant Director Grade
विभाग प्रमुख सिग्नल ट्रांसडक्शन और बायोजेनिक एमाइंस/
Head Department of Signal Transduction and Biogenic Amines
चितरंजन राष्ट्रीय कैंसर संस्थान
Chittaranjan National Cancer Institute
स्वास्थ्य और परिवार कल्याण मंत्रालय
Ministry of Health & Family Welfare
कालकता-700 026 / Kolkata-700 026


30.06.2023

(Dr. NABENDU MURMU)

DECLARATION

I hereby declare that the thesis entitled, **“The role of Ephrin and HGF/c-MET pathway in regulating Vasculogenic mimicry in breast cancer and possible effects of phytochemicals”** submitted to Jadavpur University, for the award of PH.D (Science) degree, is a record of original research work carried out by me under the supervision of Dr. Nabendu Murmu, Head of the Department, Senior Scientific Officer, Assistant Director Grade, Dept. of Signal Transduction and Biogenic Amines (STBA), Chittaranjan National Cancer Institute, 37, S.P. Mukherjee Road, Kolkata- 700026, India. This work has not been submitted elsewhere for any other degree/diploma or any academic award.

Place: KOLKATA

Date: 30.06.2023



(DEBARPAN MITRA)

DEDICATION

This thesis in its entirety is dedicated to my creators

Mrs. Suparna Mitra

&

Mr. Debashis Mitra

They are the sole reason for my mental and physical well-being, for being the titans who does the herculean task of holding my world together. They are my only true well-wishers in this world and I am eternally grateful to them for the patience and support they provide constantly.

Acknowledgement

I am eternally grateful to the Director, CNCI for providing me the opportunity of conducting my research work at Chittaranjan National Cancer Institute, Kolkata and also for providing the necessary funding.

I am indebted to Dr. Nabendu Murmu, H.O.D, Dept. of Signal Transduction and Biogenic Amines, Chittaranjan National Cancer Institute, Kolkata for taking me under his wing and generously providing necessary guidance and support all throughout this work. Without his supervision and inputs this work would only be a fantasy. I am thankful to him for seeing the potential and having faith in me all throughout the course of this work.

Most importantly, I would like to acknowledge the patience and the vast knowledge and care that Dr. Biswanath Majumder, Oncology Division, Bugworks Research, C-CAMP, Bangalore and Dr. Pradip K. Majumder, Department of Cancer Biology, Praesidia Biotherapeutics, 1167Massachusetts Avenue, Arlington, MA has so patiently shared with me over the years. Their vital inputs have in many ways made me a better thinker and also a better researcher.

I would also like to thank my seniors, Dr. Gaurav Das, Dr. Sayantan Bhattacharyya, Dr. Sudipta Ray, Dr. Paramita Ghosh and Dr. Sreyashi Mitra for being the beacons of light whenever I lost my way and also in times of dire need.

I am thankful to Ms. Depanwita Saha, Ms. Rimi Mukherjee, Mr. Debojit talukdar, Ms. Aritri Bhattacharya and Mr. Subhabrata Guha for being the best of colleagues that one can hope for and for providing the much needed moral boost whenever things went awry.

I would also like to convey my gratitude to Dr. Neyaz Alam, Department of Surgical Oncology, Chittaranjan National Cancer Institute, Kolkata and Dr. Saunak Mitra Mustafi, Department of Pathology, Chittaranjan National Cancer Institute, Kolkata for their valuable clinical insights.

Finally, I would like to acknowledge the Research Advisory committee of Jadavpur University for evaluating this work.

Chapter Index

Chapter No.	Chapter name	Page No.
1.	Review of Literature	1-39
2.	Objectives of the research	40-125
	Chapter A: To determine the influence of the c-MET and Ephrin pathways in regulating Vasculogenic Mimicry in breast cancer tissues.	43-70
	Chapter B: To determine the expressional regulation of the c-MET and Ephrin pathways influencing Vasculogenic mimicry in breast cancer.	71-93
	Chapter C: To demonstrate the potential synergistic effect of the phytochemical Lupeol along with chemotherapeutic drugs in regulation of vasculogenic mimicry.	94-125
3.	CONCLUSIONS	126-128
4.	BIBLIOGRAPHY	129-143
5.	PUBLICATIONS	144

Figure Index

Figure No.	Figure Name	Page No.
1	Hallmarks of Cancer	5
2	Activation of a Proto-oncogene to an Oncogene	6
3	Types of Cancer	8
4	Cancer Development Stages	10
5	Chemical structure of Lupeol	35
6	Flow chart describing the inclusion/exclusion criteria of patients in our study	48
7	CD-31/PAS dual staining of invasive ductal carcinoma of breast tissue section	53
8	IHC profile of proteins in the VM-positive breast cancer cohort	57
9	Kaplan–Meier plots for DFS and OS	63
10	Flow chart describing the inclusion/exclusion criteria of patients in our study (II)	75
11	Treatment failure and evaluation of the underlying mechanism of non- response in TNBC recurrence, post treatment with 5FU	84
12	Graphs representing the IHC scores vs various treatment arms and also microvascular density	85
13	Representative image depicting evaluation of siRNA mediated silencing by Western blot post-transfection	88
14	Evaluation of the effect of individual and dual knock down of c-MET and EphA2 genes on MDA MB 231 in the presence of HGF	89
15	Graphs pertaining to Fig. 16	90
16	in vivo evaluation of the effect of individual/dual silencing of c-MET and EphA2 in the presence	91

	of HGF	
17	Combination of Lupeol and 5FU induces cytotoxicity on MCF-7 cells and also reduces their wound healing potential	107
18	Combination of Lupeol and 5FU induces cytotoxicity on MDA-MB-231 cells and reduces their wound healing potential.	108
19	Graphs representing the relative cell viability of WRL-68 cells	108
20	Induction of apoptosis by the combination regimen of Lupeol and 5FU on MCF-7 cells	110
21	Induction of apoptosis by the combination regimen of Lupeol and 5FU on MDA-MB-231 cells	111
22	Evaluation of the combinatorial effect of 5FU and Lupeol on MDA-MB 231 cells	114
23	Graphs pertaining to Fig. 24	115
24	Evaluation of the effect of the combination of Lupeol and 5FU on the stemness of TNBC cells	117
25	Histopathological evaluation of the effect of the various in vivo treatment	118
26	In vivo evaluation of the combinatorial effect of 5FU and Lupeol in a TNBC syngeneic mice model	121
27	Evaluation of the combinatorial effect of 5FU and Lupeol in ex vivo explant culture model	123
28	Schematic representation of the synergistic effect of Lupeol and 5FU	128

Table Index

Table No.	Table Name	Page No.
1	Example of Tumor-suppressor Genes	7
2	Various stages of breast cancer	21
3	Demographic and pathological profiles of patients with breast cancer	52
4	Relationship of VM, phospho-EphA2, phospho-MET and clinicopathological parameters in invasive ductal carcinoma of breast.	55-56
5	Correlation between VM, phospho- EphA2, phospho-MET and relevant proteins in invasive ductal carcinoma of breast.	57
6	Relationship of phospho-EphA2, phospho-MET and VM double positive status and clinicopathological parameters in invasive ductal carcinoma of breast.	60
7	Univariate analysis for DFS	64
8	Univariate analysis for OS	65
9	Multivariate Cox proportionality hazard model on DFS	66
10	Multivariate Cox proportionality hazard model on OS.	67
11	Demographic and pathological profiles of TNBC patients (N=135)	76
12	Demographic and pathological profiles of TNBC patients (N=15) used for ex vivo explant culture	77
13	Association between the differential expressional status of phospho-EphA2 in the 5FU/Other SOC treated cohort	86

14	Association between the differential expressional status of phospho-c-MET in the 5FU/Other SOC treated cohort	86
15	Association between the differential expressional status of phospho-EphA2 levels in the responder and non-responder groups.	86
16	Association between the differential expressional status of phospho-c-MET levels in the responder and non-responder groups	86
17	Determination of effective dose and combination effect	106
18	Various serum parameters of mice after treatment with HGF, 5FU or Lupeol, alone or in combination	119



CHAPTER 1

Review of Literature

INTRODUCTION

Cancer is a class of disease characterized by dysregulated cellular growth, evasion of apoptosis and invasion into adjacent tissue/organs. Cancer results from failures of the mechanisms that usually control the growth and proliferation of cells. During normal development and throughout adult life, intricate genetic control systems regulate the balance between cell birth and senescence, in response to growth signals, growth-inhibiting signals, and death signals. Cellular proliferation and death rates determine the rate of growth and adult body size. In some adult tissues, cell proliferation occurs continuously as a constant tissue-renewal strategy. Intestinal epithelial cells, for instance, live for just a few days before they die and are replaced; certain white blood cells are replaced just as rapidly, and skin cells commonly survive for only 2–4 weeks before being shed. The cells in many adult tissues, however, normally do not proliferate except during healing processes. Such stable cells (e.g., hepatocytes, heart muscle cells, neurons) can remain functional for long periods or even for the entire lifetime of an organism. Cancer occurs when the mechanisms that maintain normal proliferation rates malfunction to cause excess cell division [1].

Genetic damage, which is frequently brought on by substances, hormones, and even viruses that promote tumor growth, is what causes the loss of cellular regulation that lead to the majority or all cases of cancer. Cancer development has been linked to mutations in three main types of genes. Normal proto-oncogenes that undergo mutations become oncogenes, whose by-products are overly active in promoting cell development. Gene expression is often enhanced or a hyperactive gene product is produced as a result of oncogenic alterations. Normal tumor-suppressor genes prevent growth, thus mutations that render them inactive promote unfavorable cell proliferation. Genome maintenance genes, a third class of genes frequently connected to

cancer, are involved in preserving the integrity of the genome. When these genes are inactivated, cells acquire additional genetic changes at an increased rate including mutations that cause the deregulation of cell growth and proliferation and lead to cancer. Many of the genes in these three classes encode proteins that help regulate cell proliferation (i.e., entry into and progression through the cell cycle) or cell death by apoptosis; others encode proteins that participate in repairing damaged DNA [2].

The cancer-forming process, called oncogenesis or tumorigenesis, is interplay between genetics and the environment. Most cancers arise after genes are altered by cancer-causing chemicals, known as carcinogens, or by errors in their copying and repair. Even if the genetic damage occurs in only one somatic cell, division of this cell will transmit the damage to its daughter cells, giving rise to a clone of altered cells. Rarely, however, does mutation in a single gene lead to the onset of cancer. More typically, a series of mutations in multiple genes creates a progressively more rapidly proliferating cell type that escapes normal growth restraints, creating an opportunity for additional mutations. The cells also acquire other properties that give them an advantage, such as the ability to escape from normal epithelia and to stimulate the growth of vasculature to obtain oxygen. Eventually the clone of cells grows into a tumor. In some cases, cells from the primary tumor migrate to new sites, where they form secondary tumors, a process termed metastasis. Most cancer deaths are due to invasive, fast-growing metastasized tumors [3].

Time plays an important role in cancer. It may take many years for a cell to accumulate the multiple mutations that are required to form a tumor, so most cancers develop later in life. The requirement for multiple mutations also lowers the frequency of cancer compared with what it would be if tumorigenesis were triggered by a single mutation. However, huge numbers of cells are, in essence, mutagenized and tested for altered growth during our lifetimes, a powerful

selection in favor of these mutagenized cells, which, in this case, we do not want. Cells that proliferate quickly become more abundant, undergo further genetic changes, and can become progressively more dangerous. Furthermore, cancer occurs most frequently after the age of reproduction and therefore plays little role in reproductive success [4].

Clinically, the origin of a malignancy is frequently determined by the embryonic tissue. Malignant tumors are categorized as carcinomas if they originate from epithelia like endoderm (the lining of the intestine) or ectoderm (the lining of the skin and the neural tissue), and sarcomas if they originate from mesoderm (the precursors of muscle, blood, and connective tissue). The most typical sort of malignant tumor is a carcinoma. (more than 90 percent). The majority of tumors are solid masses, although a subset of sarcomas called leukemia develops as separate cells in the blood. (The term leukemia, which means "white blood" in Latin, refers to the massive multiplication of leukemic cells that can make a patient's blood seem milky) [5].

Hallmarks of Cancer:

The hallmarks of cancer comprise six biological capabilities acquired during the multistep development of human tumors. The hallmarks constitute an organizing principle for rationalizing the complexities of neoplastic disease (Fig. 1). They include sustaining proliferative signaling, evading growth suppressors, resisting cell death, enabling replicative immortality, inducing angiogenesis, and activating invasion and metastasis. Underlying these hallmarks are genome instability, which generates the genetic diversity that expedites their acquisition, and inflammation, which fosters multiple hallmark functions. Conceptual progress in the last decade has added two emerging hallmarks of potential generality to this list—reprogramming of energy metabolism and evading immune destruction. In addition to cancer cells, tumors exhibit another

dimension of complexity: they contain a repertoire of recruited, ostensibly normal cells that contribute to the acquisition of hallmark traits by creating the “tumor microenvironment.” Recognition of the widespread applicability of these concepts will increasingly affect the development of new means to treat human cancer [6].

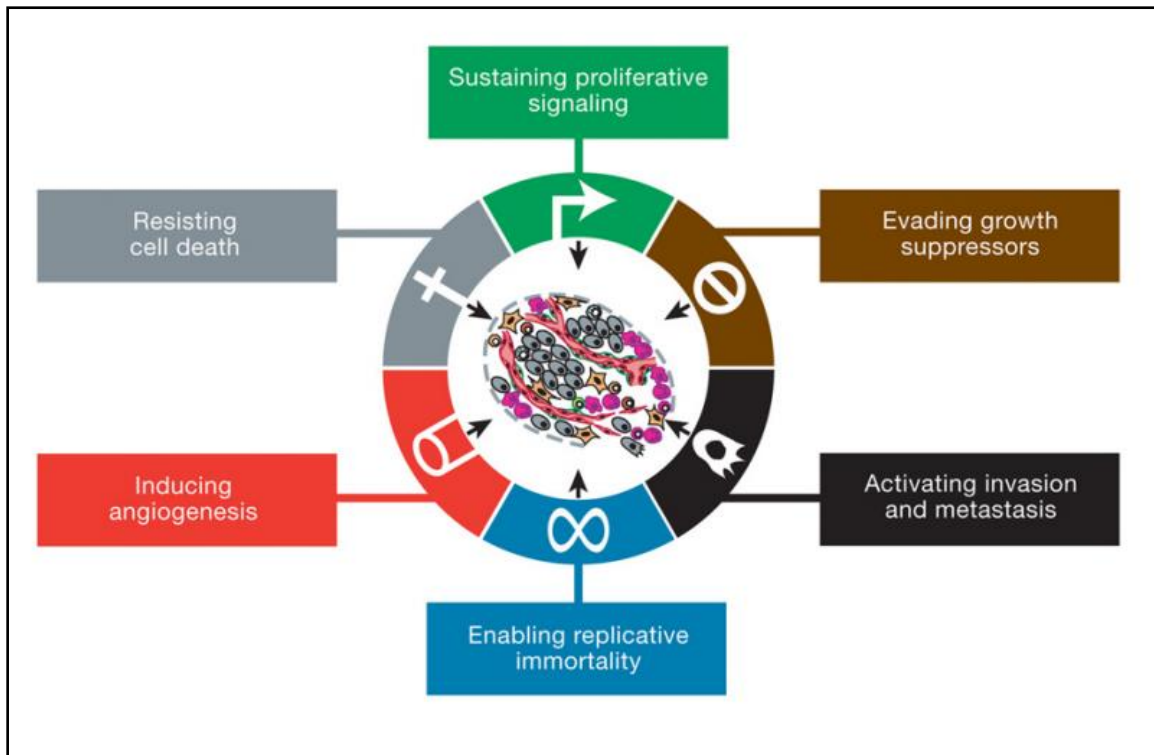


Fig. 1: Hallmarks of Cancer [6].

Oncogene and Proto-oncogene:

A proto-oncogene is a normal cellular gene involved in some aspect of cell growth and proliferation (Fig. 2). When proto-oncogenes are mutated or subject to dysregulation, the change in expression can lead to uncontrolled cell proliferation, or cancer. The mutated form of a protooncogene that can induce cancer is called an oncogene, from the Greek word *ónkos* (which means “mass” or “tumor”) [7].

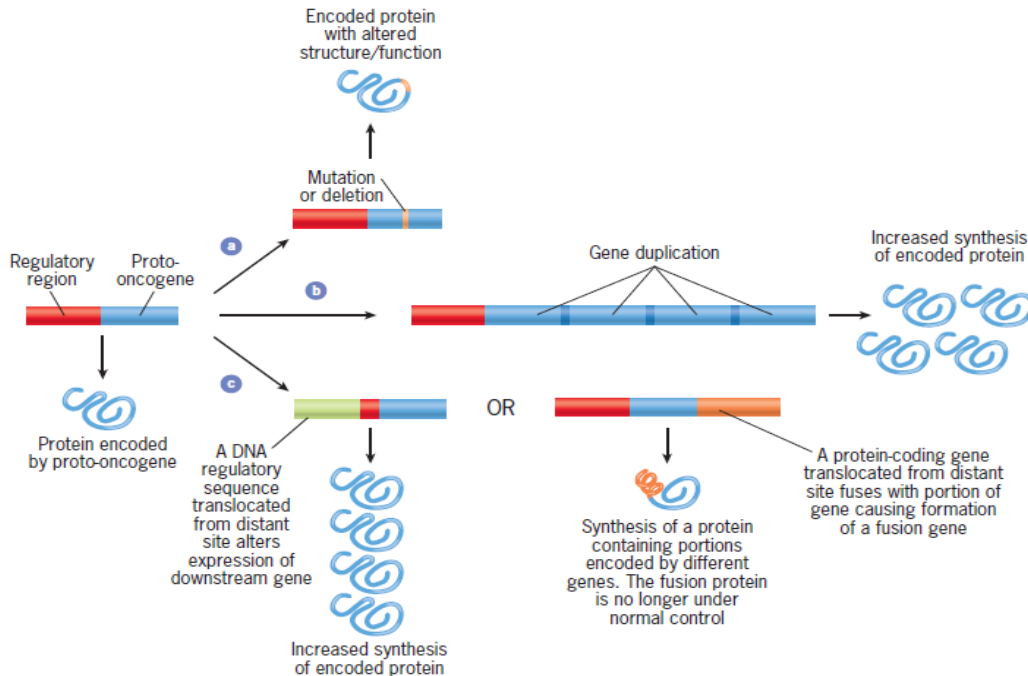


Fig. 2: Activation of a Proto-oncogene to an Oncogene [7].

Activation can be accomplished in several ways as indicated in this figure. In pathway a, a mutation in the gene alters the structure and function of the encoded protein. In pathway b, gene amplification results in overexpression of the gene. In pathway c, a rearrangement of the DNA brings a new DNA segment into the vicinity or up against the gene, altering either its expression or the structure of the encoded protein [7].

Tumor-Suppressor Genes:

Tumor-suppressor genes, or anti-oncogenes, encode proteins that inhibit cell proliferation. In their normal state, tumor-suppressor genes prevent cells from progressing through the cell cycle inappropriately, functioning like brakes on a car. A release of this inhibition is what can lead to cancer induction (Table 1). The prototype of this category of oncogenes is Rb, the retinoblastoma gene. Hereditary retinoblastoma is a rare childhood cancer in which tumors develop from neural

precursor cells in the immature retina. The affected child inherits a mutated Rb allele; later, somatic inactivation of the remaining Rb allele is what leads to tumor growth. Unlike oncogenes where a single allele alteration can lead to unregulated growth, tumor-suppressor genes require a “two-hit” disabling sequence, as one functional allele is typically sufficient to suppress the development of cancer [8].

Gene	Cancer Type	Protein Function	Hereditary Syndrome	Chromosome Location
<i>APC</i>	Colon carcinoma	Cell adhesion	Familial adenomatous polyposis (FAP)	5q21–q22
<i>BRCA1</i>	Breast cancer	Has possible transcription activation domain; interacts with DNA damage repair machinery	Breast cancer and ovarian cancer	17q21
<i>BRCA2</i>	Breast cancer	Has possible transcription activation domain; interacts with DNA damage repair machinery	Breast cancer	13q12–q13
<i>DCC</i>	Colon carcinoma	Cell adhesion	Involved in colorectal cancer	18q21.3
<i>NF1</i>	Neurofibromas	GTPase activating protection	Neurofibromatosis type I	17q11.2
<i>NF2</i>	Schwannomas and meningiomas	Links cell surface glycoprotein to the actine cytoskeleton?	Neurofibromatosis type II	22q12.2
<i>p16</i>	Melanoma and others	Cdk inhibitor	Familial melanoma	9p21
<i>RB</i>	Retinoblastoma	Cell cycle and transcription regulation	Retinoblastoma	13q14.1–q14.2
<i>TP53</i>	Wide variety	p53 is a transcription factor	Li–Fraumeni syndrome	17p13.1
<i>VHL</i>	Kidney carcinoma, pancreatic tumors, and others	Transcription elongation	von Hippel–Lindau syndrome	3p26–p25
<i>WT1</i>	Nephroblastoma	Transcription activator or repressor depending on cell	Wilms tumor 1	11p13

Table 1: Example of Tumor-suppressor Genes [8].

Types of Cancer:

There are five main types of cancer (Fig. 3). These include:

- ✚ *Carcinoma*. This type of cancer affects organs and glands, such as the lungs, breasts, pancreas and skin. Carcinoma is the most common type of cancer.
- ✚ *Sarcoma*. This cancer affects soft or connective tissues, such as muscle, fat, bone, cartilage or blood vessels.
- ✚ *Melanoma*. Sometimes cancer can develop in the cells that pigment your skin. These cancers are called melanoma.
- ✚ *Lymphoma*. This cancer affects your lymphocytes or white blood cells.
- ✚ *Leukemia*. This type of cancer affects blood [9].

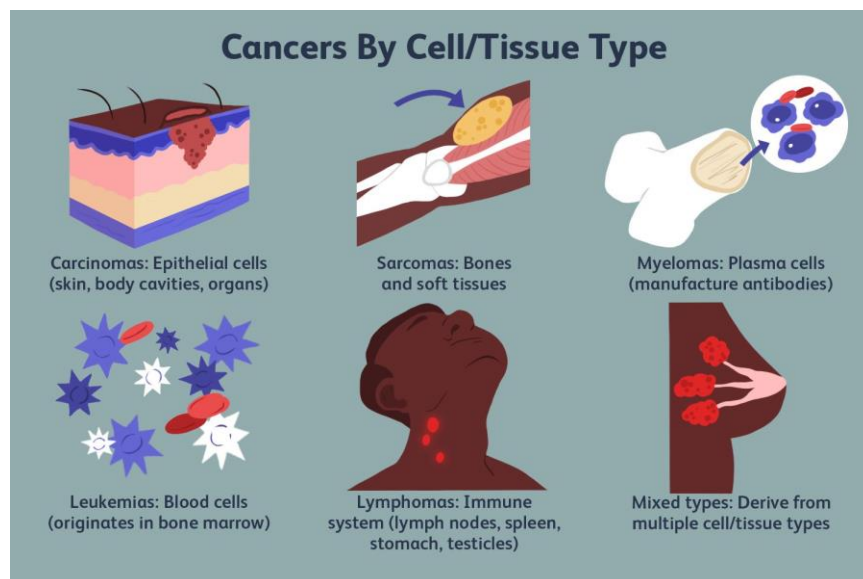


Fig. 3: Types of Cancers [9].

Cancer Development:

A single mutated cell begins to proliferate abnormally, giving rise to a proliferative cell population. Additional mutations followed by selection for more rapidly growing cells then result in progression first to benign adenomas of increasing size and then to a malignant carcinoma (Fig. 4). The cancer cells then invade the underlying connective tissue and penetrate blood and lymphatic vessels, thereby spreading throughout the body [10].

Carcinogenesis:

The terms carcinogenesis, cancer inducing factors or carcinogenic factors more adequate for what happens during tumor cell transformation, with the mention that the term carcinogenesis defines the initiation of a tumor, and oncogenesis its maintenance and subsequent evolution.

Tumors develop in those tissues in which cellular homeostasis have been disturbed by hyperplastic, dysplastic or regenerative changes. Clinical and experimental data have proved that during the division process the cell is more susceptible to carcinogenic factors than at rest. Human and veterinary oncology can provide such examples: hyperplastic endometrial and mammary processes that are submitted to hormonal fluctuations represent the usual background for the appearance of cancer; bronchial carcinoma in smokers invariably appears against a dysplastic or metaplastic background of the airways; bone cancer usually occurs at a young age, when physiological osteogenesis is active. These examples demonstrate that the oncogenic process is more frequent in tissues with increased cellular activity [2].

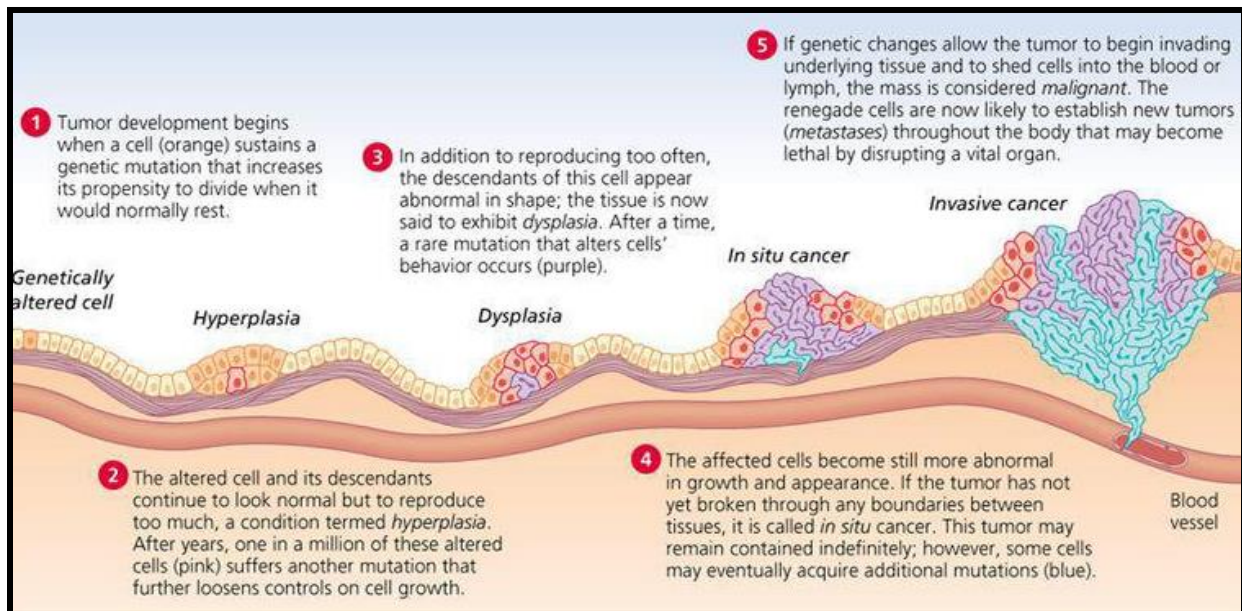


Fig. 4: Cancer Development Stages [11].

Metastasis of Cancer:

The spread of cancer cells from the place where they first formed to another part of the body. In metastasis, cancer cells break away from the original (primary) tumor, travel through the blood or lymph system, and form a new tumor in other organs or tissues of the body. The new, metastatic tumor is the same type of cancer as the primary tumor. For example, if breast cancer spreads to the lung, the cancer cells in the lung are breast cancer cells, not lung cancer cells.

After the cancerous cells have grown to form a primary tumor, matrix metalloproteinases (MMPs) are activated. These enzymes allow the cancer cells to invade local tissues by degrading basement membranes. These MMPs are either directly produced by the cancer cells or the extracellular matrix is stimulated by the cancer cells to produce them.

The invading cancer cells then undergo a process called epithelial to mesenchymal transition (EMT), in which the cells repress E-cadherins and upregulate N-cadherins. This process is due to

the production of EMT-inducing transcription factors and allows cells to adopt a mesenchymal phenotype, aiding the ability of cells to intravasate into the blood stream. N-cadherins also have decreased intracellular adhesion in comparison to E-cadherins, permitting further local tissue invasion.

The cancerous cells can then enter the blood stream or lymphatic system in a process called intravasation, by squeezing through the surface of a blood vessel. Once within the circulatory system, they disseminate to distinct sites of the body and become lodged into the capillaries of other organs [12].

These cells then undergo extravasation by moving through the vessel membranes and forming micro-metastases. At this point, the cancerous cells can form colonies, forming secondary tumors. These new tumors will then stimulate additional angiogenesis, triggered by hypoxia, forming a new blood supply to support further growth and metastasis.

Most cancerous cells will not survive this process, particularly due to the hydrodynamic stresses of migrating in the blood stream and the immune system. One protective mechanism utilized by migrating cancerous cells includes the formation of heterotypic clumps, in which they bind to platelets and evade the immune system.

It is the overall function of the various protective mechanisms to allow a small minority of around 1 in 10,000 cells to survive and form secondary tumors.

Breast Cancer:

Breast cancer is the commonest cause of cancer death in women worldwide. Rates vary about five-fold around the world, but they are increasing in regions that until recently had low rates of the disease. Many of the established risk factors are linked to estrogens. Risk is increased by early menarche, late menopause, and obesity in postmenopausal women, and prospective studies have shown that high concentrations of endogenous estradiol are associated with an increase in risk. Childbearing reduces risk, with greater protection for early first birth and a larger number of births; breastfeeding probably has a protective effect. Both oral contraceptives and hormonal therapy for menopause cause a small increase in breast-cancer risk, which appears to diminish once use stops. Alcohol increases risk, whereas physical activity is probably protective. Mutations in certain genes greatly increase breast cancer risk, but these account for a minority of cases [13].

The breast is composed of two main types of tissues i.e., glandular tissues and stromal (supporting) tissues. Glandular tissues house the milk producing glands (lobules) and the ducts (the milk passages) while stromal tissues include fatty and fibrous connective tissues of the breast. The breast is also made up of lymphatic tissue-immune system tissue that removes cellular fluids and waste [14].

There are several types of tumors that may develop within different areas of the breast. Most tumors are the result of benign (non-cancerous) changes within the breast. For example, fibrocystic change is a non-cancerous condition in which women develop cysts (accumulated packets of fluid), fibrosis (formation of scar-like connective tissue), lumpiness, and areas of thickening, tenderness, or breast pain [15].

Most breast cancers begin in the cells that line the ducts (ductal cancers). Some begin in the cells that line the lobules (lobular cancers), while a small number start in the other tissues.

Risk Factors:

Menarche and the menstrual cycle

The older a woman is when she begins menstruating, the lower her risk of breast cancer (Kelsey *et al.*, 1993). For each 1-year delay in menarche, the risk decreases by around 5%. There is also evidence that, although age at menarche is related to breast cancer risk at all ages, the effect may be stronger in younger (premenopausal) women. Other menstrual factors, such as cycle length and regularity, have not been consistently related to risk of breast cancer [16].

Childbearing

Childbearing seems to have a dual effect on risk of breast cancer; it is increased in the period immediately after a birth, but this excess risk gradually diminishes and, in the longer term, the effect of a birth is to protect against the disease. Compared with nulliparous women, women who have had at least one full-term pregnancy have, on average, around a 25% reduction in breast-cancer risk. Furthermore, increasing protection is seen with increasing numbers of full-term pregnancies, such that women with five or more children have about half the risk of nulliparous women [17].

Endogenous hormones

During the past decade, several prospective cohort studies have examined the relation between serum concentrations of hormones and breast-cancer risk. For postmenopausal women, the studies have shown a positive association between serum estradiol concentrations and risk;

postmenopausal women with high serum estradiol concentrations have a risk around twice that of women with lower concentrations of this hormone. A positive association has also been observed in at least some studies with other sex hormones, with prolactin, and with insulin-like growth factor 1 [18].

Oral contraceptives

The risk of breast cancer is increased by around 25% in current users of combined oral contraceptives, but the excess risk falls after cessation of use, such that 10 or more years after use stops, no significant increase in risk is evident. Use of combined oral contraceptives is associated with a larger excess of localized cancers than those that have spread beyond the breast. This finding has raised the possibility that the increased risk of breast cancer in recent users of oral contraceptives may be partly due to increased surveillance [19].

Other exogenous hormones: Diethylstilbestrol and fertility drugs

Treatment for infertility may entail exposure to a variety of hormonally active drugs, including clomiphene citrate, human menopausal gonadotropin, and gonadotropin-releasing hormone. Most studies investigating the risk of breast cancer in relation to such exposure have not detected any increase in risk, but they have been hampered by small numbers and the inability to account for important potential confounding factors. One recent study reported a significant, transient excess of breast cancer in the 12 months after ovarian stimulation for in vitro fertilization [20].

Genetic causes

Family history has long been known to be a risk factor for breast cancer. Both maternal and paternal relatives are important. The risk is highest if the affected relative developed breast

cancer at a young age, had cancer in both breasts, or if she is a close relative. First-degree relatives, (mother, sister, daughter) are most important in estimating risk. Several second-degree relatives (grandmother, aunt) with breast cancer may also increase risk. Breast cancer in a male increases the risk for all his close female relatives. BRCA1 and BRCA2 are abnormal genes that, when inherited, markedly increase the risk of breast cancer to a lifetime risk estimated between 40 and 85%. Women who have the BRCA1 gene tend to develop breast cancer at an early age [21]. So far at least five germline mutations that predispose to breast cancer have been identified or localised. These include mutations in the genes BRCA1, BRCA2, P53, PTEN, and ATM. Mutations in BRCA1 and BRCA2 can cause high risks of breast cancer, especially, and ovarian cancers. Germline mutations in P53 predispose to the Li-Fraumeni cancer syndrome (including childhood sarcomas and brain tumors, as well as early-onset breast cancer) and those in PTEN are responsible for Cowden disease (of which breast cancer is a major feature). High-risk alleles probably account for most of the families with four or more breastcancer cases, for around 20–25% of the familial breast cancer risk overall, and for around 5% of all breast cancers [22].

Alcohol and smoking

Observational studies have repeatedly shown that alcohol consumption is associated with a moderate increase in the risk of breast cancer; risk increases by roughly 10% per 10 g alcohol (1 unit) consumed per day.²⁶ Within the range of light to moderate alcohol intake, breast-cancer risk seems to increase linearly, so an intake of around 30 g alcohol (3 units) per day is associated with an increase of about 30% in breast-cancer risk. Studies have not shown higher risks at higher consumption or among women with alcoholism. Many studies have examined the relation between smoking and breast-cancer risk, and overall, they show no association [23].

Types of Breast Cancer:

According to site

Non-Invasive Breast Cancer

Cells that are confined to the ducts and do not invade surrounding fatty and connective tissues of the breast. Ductal carcinoma in situ (DCIS) is the most common form of non-invasive breast cancer (90%). Lobular carcinoma in situ (LCIS) is less common and considered a marker for increased breast cancer risk [24].

Invasive Breast Cancer

Cells that break through the duct and lobular wall and invade the surrounding fatty and connective tissues of the breast. Cancer can be invasive without being metastatic (spreading) to the lymph nodes or other organs [25].

Frequently occurring Breast cancer

Lobular carcinoma in situ (LCIS, lobular neoplasia):

The term, "in situ," refers to cancer that has not spread past the area where it initially developed. LCIS is a sharp increase in the number of cells within the milk glands (lobules) of the breast [26].

Ductal carcinoma in situ (DCIS):

DCIS, the most common type of non-invasive breast cancer, is confined to the ducts of the breast. For example, ductal comedo carcinoma [27].

Infiltrating lobular carcinoma (ILC)

ILC is also known as invasive lobular carcinoma. ILC begins in the milk glands (lobules) of the breast, but often spreads (metastasizes) to other regions of the body. ILC accounts for 10% to 15% of breast cancers [28].

Infiltrating ductal carcinoma (IDC):

IDC is also known as invasive ductal carcinoma. IDC begins in the milk ducts of the breast and penetrates the wall of the duct, invading the fatty tissue of the breast and possibly other regions of the body. IDC is the most common type of breast cancer, accounting for 80% of breast cancer diagnoses [29].

Less commonly occurring Breast cancer

Medullary carcinoma:

Medullary carcinoma is an invasive breast cancer that forms a distinct boundary between tumor tissue and normal tissue. Only 5% of breast cancers are medullary carcinoma [30].

Tubular carcinoma:

Tubular carcinomas are a special type of infiltrating - (invasive) breast carcinoma. Women with tubular carcinoma generally have a better prognosis than women with more common types of invasive carcinoma. Tubular carcinomas account for around 2% of breast cancer diagnoses [31].

Inflammatory breast cancer

Inflammatory breast cancer is the appearance of inflamed breasts (red and warm) with dimples and/or thick ridges caused by cancer cells blocking lymph vessels or channels in the skin over

the breast. Though inflammatory breast cancer is rare (accounting for only 1% of breast cancers), it is extremely fast-growing [32].

Paget's disease of the nipple

A rare form of breast cancer that begins in the milk ducts and spreads to the skin of the nipple and areola, Paget's disease of the nipple only accounts for about 1% of breast cancers [33].

Phyllodes tumor

Phyllodes tumors (also spelled "phyllodes") are can be either benign (non-cancerous) or malignant (cancerous). Phyllodes tumors develop in the connective tissues of the breast and may be treated by surgical removal. Phyllodes tumors are very rare; less than 10 women die of this type of breast cancer each year in the United States [25].

Signs and Symptoms:

- ✓ Detection of a breast mass is the most common breast complaint for which women seek medical advice. Approximately 90 percent of all breast masses are caused by benign lesions. Smooth and rubbery masses are usually associated with fibroadenoma in women in their 20s and 30s or cysts in women in their 30s and 40s.
- ✓ Breast pain is also a common presenting problem. Mastalgia is rarely associated with breast cancer and is usually related to fibro-cystic changes in premenopausal women. Postmenopausal women receiving estrogen replacement therapy may also present with breast pain caused by fibrocystic changes. The pain of fibrocystic conditions is associated with diffuse lumpy breasts.

- ✓ Erythema, edema and retraction of the skin or nipple are associated with malignancies. Another common presenting problem is nipple discharge. Discharge from a breast carcinoma is usually spontaneous, bloody, associated with a mass and localized to a single duct in one breast.
- ✓ Examination of the breast should be performed in the upright (sitting) and supine positions with the woman's hands behind her head. The breasts should be inspected for differences in size, retraction of the skin or nipple, prominent venous patterns and signs of inflammation. The flat surface of the fingertips should be used to palpate the breast tissue against the chest wall. The axillary and supraclavicular areas should be checked for adenopathy. The nipple should be gently squeezed to check for discharge.
- ✓ A mass that is suspicious for breast cancer is usually solitary, discrete and hard. In some instances, it is fixed to the skin or the muscle. A suspicious mass is usually unilateral and nontender. Sometimes, an area of thickening that is not a discrete mass may represent cancer. Breast cancer is rarely bilateral when first diagnosed. [34]

Breast Cancer Screening:

Breast cancer screening means checking a woman's breasts for cancer before there are signs or symptoms of the disease. All women need to be informed by their health care provider about the best screening options for them [35].

Mammogram

A mammogram is an X-ray of the breast. For many women, mammograms are the best way to find breast cancer early, when it is easier to treat and before it is big enough to feel or cause

symptoms. Having regular mammograms can lower the risk of dying from breast cancer. At this time, a mammogram is the best way to find breast cancer for most women of screening age [35].

Breast Magnetic Resonance Imaging (MRI)

A breast MRI uses magnets and radio waves to take pictures of the breast. Breast MRI is used along with mammograms to screen women who are at high risk for getting breast cancer. Because breast MRIs may appear abnormal even when there is no cancer, they are not used for women at average risk [36].

Stages of Breast Cancer

When cancer is diagnosed, a stage is assigned to it, based on how advanced it is. The stage helps doctors determine the most appropriate treatment and the prognosis (Table 2). Stages of breast cancer may be described generally as in situ (not invasive) or invasive. Stages may be described in detail and designated by a number (0 through IV) [37].

Stage	Description
In situ carcinoma	
0	The tumor is confined, usually to a milk duct or milk-producing gland, and has not invaded surrounding breast tissue.
Localized and regional invasive cancer	
I	The tumor is less than ¾ inch (2 centimeters) in diameter and has not spread beyond the breast.
IIA	The tumor is ¾ inch or less in diameter and it has spread to one to three lymph nodes in the armpit, microscopic amounts have spread to lymph nodes near the breastbone on the same side as the tumor, or both or The tumor is larger than ¾ inch but smaller than 2 inches (5 centimeters) in diameter but has not spread beyond the breast.
IIB	The tumor is larger than ¾ inch but smaller than 2 inches in diameter, and it has spread to one to three lymph nodes in the armpit, microscopic amounts have spread to lymph nodes near the breastbone on the same side as the tumor, or both or The tumor is larger than 2 inches in diameter but has not spread beyond the breast.
IIIA	The tumor is 2 inches or less in diameter and has spread to four to nine lymph nodes in the armpit or has enlarged at least one lymph node near the breastbone on the same side as the tumor or The tumor is larger than 2 inches in diameter and has spread to up to nine lymph nodes in the armpit or to lymph nodes near the breastbone.
IIIB	The tumor has spread to the chest wall or skin or has caused breast inflammation (inflammatory breast cancer).
IIIC	The tumor can be any size plus at least one of the following: It has spread to 10 or more lymph nodes in the armpit. It has spread to lymph nodes under or above the collar bone.
	It has spread to lymph nodes in the armpit and has enlarged at least one lymph node near the breastbone on the same side as the tumor.
	It has spread to four or more lymph nodes in the armpit, and microscopic amounts have spread to lymph nodes near the breastbone on the same side as the tumor.
Metastatic cancer	
IV	The tumor, regardless of size, has spread to distant organs or tissues, such as the lungs or bones, or to lymph nodes distant from the breast.

Table 2: Various stages of breast cancer [37].

Management of Breast Cancer:

Following approaches are to be made for the management of breast cancer. They are as follows;

Surgery

Depending on the stage and type of the tumor, lumpectomy (removal of the lump only), or surgical removal of the entire breast (mastectomy) is performed. Standard practice requires the surgeon to establish that the tissue removed in the operation has margins clear of cancer, indicating that the cancer has been completely excised. If the removed tissue does not have clear margins, further operations to remove more tissue may be necessary. This may sometimes require removal of part of the pectoralis major muscle, which is the main muscle of the anterior chest wall. More recently, the technique of sentinel lymph node (SLN) dissection has become popular, as it requires the removal of far fewer lymph nodes, resulting in fewer side effects. Advances in sentinel lymph node mapping over the past decade have increased the accuracy of detecting sentinel lymph node from 80% using blue dye alone to between 92% and 98% using combined modalities [38].

Surgery for breast cancer consists of two main options.

In breast-conserving surgery, only the tumor and an area of normal tissue surrounding it are removed. Breast conserving surgery includes the following:

Lumpectomy: A small amount of surrounding normal tissue is removed. **Wide excision:** Also called as partial mastectomy in which somewhat larger amount of the surrounding normal tissue is removed.

Quadrantectomy: About one fourth of the breast is removed.

Mastectomy: All breast tissue is removed.

Radiation Therapy

Radiation therapy involves using high energy X-rays or gamma rays that target a tumor or post-surgery tumor site. These radiations are very effective in killing cancer cells that may remain after surgery or recur where the tumor was removed. In addition to this treatment implanted radioactive catheters (brachytherapy), similar to those used in prostate cancer treatment, can be used. However this treatment option has been superseded by electron beam radiotherapy to the breast scar. Radiation therapy for breast cancer is usually performed after surgery and is an integral component of breast-conserving therapy. The dose of radiation must be strong enough to ensure the elimination of cancer cells. Treatments are typically given over a period of five to seven weeks, performed five days a week[39].

Triple Negative Breast Cancer:

Triple-negative breast cancer (TNBC) accounts for 15% to 20% of breast cancer cases and is characterized by the absence of estrogen, progesterone, and human epidermal growth factor 2 receptors. Though TNBC is a highly heterogenic and aggressive disease, TNBC patients have better response to neoadjuvant therapy compared to other breast cancer subtypes. Nevertheless, patients with residual disease have a very poor prognosis, with higher probability of relapse and lower overall survival in the first years after diagnosis [40].

TNBC makes up 10-30% of all breast cancers. It is associated with younger age and higher stage at diagnosis, higher nuclear grade and mitotic activity, and poorer prognosis [41]. Within the TNBC designation are heterogeneous characteristics. TNBC can be categorized by its morphological appearance: infiltrating ductal carcinoma, not otherwise specified (NOS),

medullary carcinoma, adenoid cystic carcinoma, myoepithelial carcinoma, squamous carcinoma, metaplastic carcinoma, apocrine carcinoma, secretory carcinoma, or carcinoma arising in the background of micro-glandular adenosis. Despite TNBC having a more aggressive nature as a whole, there are subtypes that are much more indolent. For example, adenoid cystic carcinomas are considered slow growing, with a very good prognosis status post-surgical excision [42]. Based on genetic expression profiling, TNBC has been categorized into six TNBC subtypes: basal-like 1 (BL1), basal-like 2 (BL2), immunomodulatory (IM), mesenchymal (M), mesenchymal stem-like (MSL) and luminal androgen receptor (LAR) [43]. The intrinsic molecular BLBC subtype has controversially been considered synonymous with TNBC. It is called basal-like for its expression of markers for basal type cells (CK5/6, CK14, CK17, EGFR), and is defined as ER/PR/HER2 negative, CK5/6 positive, and/or positive for EGFR. Although it has been argued that TNBC and BLBC are the same subtype, not all TNBC express basal cell markers characteristic of BLBC; positivity for basal markers is associated with poorer prognosis than TNBC overall, and may be seen across the different genetic subtypes of TNBC [44]. BLBC typically has a worse prognosis, but when treated with adjuvant chemotherapy, patients with BLBC showed longer disease free survival when compared to patients with TNBC as a whole. Despite better response rates of TNBC versus non-TNBC to chemotherapy, overall prognosis is still poor [45]. Furthermore, better response rates may be due to BLBC being grouped with TNBC, thus patients with non-BLBC TNBC fare the worst. Claudin-low breast cancer, similar to BLBC is found mostly in TNBC, and represents 25-39% of all TNBC. In molecular cluster analysis, it is found in close proximity to BLBC; however claudin-low tumors do not consistently express basal keratins. Furthermore, it has characteristics of mesenchymal and MSL molecular subtypes, which are also seen by IHC, with positive vimentin and N-cadherin. It is

called claudin-low because of its lack of expression of tight-junction components, claudin-3, claudin-4, and claudin-7. This type is associated with poor prognosis, as well as poorer sensitivity to chemotherapy than BLBC [46].

More recently, Burstein, et al. revisited the grouping of TNBC, and redefined subtypes into four, rather than six, subtypes using RNA and DNA gene expression profiling. Subtype 1 tumors have AR, ER, prolactin and ErbB4 signaling despite being ER negative via IHC. This subtype highlights ER negative tumors that may still respond to ER antagonists. They correlate with the tumors previously categorized as LAR subtype, and subsequently have been termed the LAR subtype. Subtype 2 highly express growth factors and genes otherwise only seen with osteocytes and adipocytes and show pathways regulated in breast cancer. This subtype correlates with the mesenchymal stem-like subtype and claudin-low tumors, and have been termed the mesenchymal (MES) subtype. Subtype 3 exhibits down regulation of immune regulating pathways and cytokine pathways with basal-like expression. It has been termed the basal-like immunosuppressed (BLIS) subtype. Subtype 4 has basal-like expression, but has upregulation of immune-regulating pathways, and has been termed the basal-like immune activated (BLIA) subtype. The BLIA subtype has the best prognosis, while the BLIS subtype has the poorest prognosis. The prognostic implications of BLIA vs BLIS subtypes are of interest because of the observation that tumor-infiltrating lymphocytes (TILs) in TNBC are associated with better prognosis. The International TILs Working Group 2014, recently proposed a possible standardized method to be used to assess TILs in breast cancers by H&E evaluation. However, there are still no recommendations for clinically relevant TIL thresholds [47]. Currently, the only treatment for patients with TNBC is chemotherapy. In patients who receive neoadjuvant chemotherapy and show a pathological complete response on resection, prognosis is very good.

However, in patients who do not show a pathological complete response, they have a worse prognosis with a higher incidence of recurrences. Thus there is an urgent need to find targeted therapies and stratify patients by treatment options [48].

Vasculogenic Mimicry:

The term *angiogenesis* describes the formation of new vessels from pre-existing vessels. The term *vasculogenesis* describes the formation of new vessels *de novo*. In 1999, Maniotis et al. [49] described the formation of fluid-conducting channels by highly aggressive and genetically dysregulated melanoma cells. There was no term available to describe this phenomenon. The channels developed by aggressive tumor cells are not vessels architecturally but they function to transport plasma and perhaps red blood cells. The formation of these channels is not an angiogenic event: they do not arise from pre-existing vessels, and despite the fact that they develop *de novo*— a feature shared with vasculogenesis — the channels are clearly not blood vessels. Thus, the term *vasculogenic mimicry* was coined [49], [50] to describe the formation of these channels by aggressive tumor cells —*vasculogenic* because the channels do not form from pre-existing vessels despite the fact that they distribute plasma and may contain red blood cells — and *mimicry* because the channels are not blood vessels and merely mimic the function of vessels.

The initial description of vasculogenic mimicry was vigorously challenged[51]. Nevertheless, work of the past 5 years by independent laboratories throughout the world has provided convincing evidence that vasculogenic mimicry is both novel and significant. Moreover, vasculogenic mimicry provides a pathway for perfusion that is independent of angiogenesis.

Vasculogenic Mimicry: Implications for cancer therapeutics

The microcirculation of uveal melanomas is heterogeneous[52], containing pre-existing normal vessels that are incorporated into the lesion [53], mosaic vessels lined by both tumor cells and endothelium [52], angiogenic vessels, and extravascular patterned matrix in highly aggressive tumors. If one wished to design a therapeutic approach to cancer that deprived tumors of a blood supply, the treatment of only angiogenic vessels would still leave other perfusion mechanisms intact and might result in incomplete therapy. Thus, treatment strategies that target the tumor microcirculation must not only target angiogenesis, but also take into account non-angiogenic pathways of tumor perfusion and metastasis [54], [55]. Therapeutic strategies that target angiogenesis may not be effective in blocking or disrupting vasculogenic mimicry of the patterned matrix type: as mentioned earlier, neither TNP-450nor endostatin [56] inhibits vasculogenic mimicry *in vitro*. Furthermore, because vasculogenic mimicry has now been documented histologically in a wide variety of cancers, it would be prudent to target this process therapeutically.

Vasculogenic mimicry of the patterned matrix type may favor metastasis through two mechanisms. First, as a non-vascular and thus non-endothelial cell-lined channel, tumor cells in the patterned matrix may be exposed to the flow of plasma. As Folkman [57] noted with reference to mosaic vessels, the exposure of tumor cells to blood flow may facilitate metastasis. Tumor cells also migrate along extracellular matrix scaffolds, and the physical connection between these patterns and vessels may facilitate hematogenous dissemination of cancer. Second, because extravascular matrix patterns of vasculogenic mimicry are generated by highly invasive tumor cells – poorly invasive cells do not generate such patterns [58] – matrix patterns are markers of the presence of a highly invasive tumor cell phenotype which can be targeted.

Several interesting strategies for targeting vasculogenic mimicry have emerged. Sanz et al. [59] reported targeting vasculogenic mimicry with antibody fragments to laminin and were able to disrupt the formation of networks of cellular cords – the tubular form of vasculogenic mimicry – *in vitro*, but the disruption of the patterned matrix was not illustrated. As discussed in detail above, Liu et al. [60] also successfully targeted the tumor cell-lined tubes which may have been generated by vasculogenic mimicry. There are considerable opportunities to develop new therapeutic strategies targeting vasculogenic mimicry of the patterned matrix type. Because the generation of the extravascular patterned matrix requires both an invasive tumor cell phenotype and a permissive tumor matrix microenvironment, vasculogenic mimicry affords an opportunity to investigate and therapeutically target a crucial phenotypic malignant switch.

VM in breast cancer:

VM has been identified in numerous types of highly aggressive tumors including breast cancer. Only two years later from the first report of VM in melanoma, a group in Japan identified the presence of blood pooling without a lining of ECs on hyper vascularized xenografts of inflammatory breast cancer. Remarkably, these cells were able to form tube-like structures and loops *in vitro*, and were associated with lung metastasis *in vivo*, representing the first evidence of VM in breast cancer [61]. These results helped to establish the relationship between angiogenesis and VM. Shirakawa et al. observed that the hyper vascularized zone in the tumor periphery contained vessels lined by ECs positive to murine CD31, consistent with angiogenesis, while the central highly hypoxic area of the tumor exhibited channels that were PAS positive, presented weak expression of human integrin $\alpha_v\beta_3$ and lacked ECs, consistent with VM. Altogether, this suggested that in some instances, tumors can develop hybrid vascular networks combining angiogenesis and VM to efficiently obtain oxygen and nutrients [62], [63]. In addition, structural

heterogeneity (mosaic vessels) has also been described in solid tumors, including breast cancer, where a vessel may be lined by ECs in some parts and by tumor cells in others, forming hybrid vascular structures associated with intravasation and systemic dissemination of cancer cells [64]. Since it has been demonstrated that VM can enhance metastasis after an anti-angiogenic treatment [65], research in the VM field will surely improve cancer therapeutics.

TNBC chemotherapy drugs and efficacy evaluation:

Compared to other types of breast cancer, TNBC has limited treatment options, is prone to recurrence and metastasis, and has a poor prognosis. The main reason is that the expression of ER, PR, and HER2 are all negative, making specific endocrine therapies and targeted therapies ineffective. Therefore, chemotherapy has become the main approach for the treatment of TNBC. In recent years, a large body of literature has shown that the use of neoadjuvant chemotherapy regimens in the treatment of TNBC has a significantly higher pathological remission rate than for hormone receptor-positive breast cancer and can significantly improve the prognosis of TNBC patients [66]. The national comprehensive cancer network guidelines recommend using combination regimens based on taxane, anthracycline, cyclophosphamide, cisplatin, and fluorouracil. At present, taxel/docetaxel + adriamycin + cyclophosphamide (TAC), docetaxel + cyclophosphamide (TC), adriamycin + cyclophosphamide (AC), cyclophosphamide + methotrexate + fluorouracil (CMF), cyclophosphamide + adriamycin + fluorouracil (CAF), and cyclophosphamide + epirubicin + fluorouracil + paclitaxel/docetaxel (CEF-T) are the preferred adjuvant regimens for TNBC. Therefore, the selection of appropriate chemotherapy drugs and the optimization of chemotherapy regimens are important for ensuring good treatment outcome and prognosis of TNBC patients.

5-Fluorouracil:

5-Fluorouracil (5-FU) is a fluoropyrimidine anticancer drug that disrupts cellular metabolism by inhibiting the synthesis of purines and pyrimidines, which disrupts DNA synthesis and RNA translation in target cells. In this way, 5-FU promotes cell death during cell division. In order to exert its cytotoxic activity, 5-FU must be enzymatically converted to a nucleotide by ribosylation and phosphorylation [67]. Approximately 90% of the administered dose of 5-FU is catabolized by dihydropyrimidine dehydrogenase in the liver, peripheral blood mononuclear cells, intestinal mucosa, pancreas, lungs and kidneys; the remaining 10% is excreted unchanged in the urine [68]. 5-FU is an important chemotherapeutic drug and has been used for about 40 years. 5-FU is used in most of the standard chemotherapeutic protocols for solid cancers of the colon, breast, stomach, liver, and pancreas, among others. Moreover, 5-FU is able to induce differentiation in human tumor cells; however, it is highly toxic to both tumor cells and normal cells [69].

Clinical Pharmacology of 5-Fluorouracil:

5-Fluorouracil is one of only a few clinically useful antineoplastic drugs that have been rationally designed on the basis of knowledge of tumor biochemistry. Experimental studies had demonstrated that certain tumors (rat hepatomas) utilized exogenous uracil more avidly than healthy tissues [70]. The uracil was necessary for sustaining nucleic acid synthesis required for tumor growth. This led to the hypothesis that if a pyrimidine analogue could be synthesized with physicochemical properties similar to uracil, it might interfere with nucleic acid synthesis and slow tumor growth [71]. In attempting to design a uracil analogue that would interfere with tumor cell growth, consideration was given to fluorine. Earlier studies had shown that by substituting fluorine for a hydrogen, a relatively non-toxic molecule (e.g. acetate) could be

converted into one with increased toxicity (e.g. fluoroacetate) [72]. In addition, the van der Waal's radius of the fluorine atom (1.35Å) was similar to that of hydrogen (1.2Å), thus minimizing alteration of the molecular conformation and increasing the likelihood that such a molecule could be uracil. The hydrogen at the '5' position appeared particularly attractive for substitution since most mammalian cells obtain the thymidine-5'-triphosphate (dTTP) needed for DNA synthesis from 2'-deoxyuridine-5'-monophosphate (dUMP) by replacing the hydrogen on the '5' carbon with a methyl group to form thymidine-5'-monophosphate (dTMP). Lastly, it was hypothesized that the carbon-fluorine bond would be more stable with less chemical reactivity, thereby preventing substitution of the methyl group at the '5' position of the uracil analogue [i.e. 5-fluoro-2'-deoxyuridine-5'-monophosphate (FdUMP)]. 5-Fluorouracil was originally synthesised by Duschinsky from acyclic precursors [73]. This method is still utilised in the commercial synthesis of the drug. An alternative method of synthesis using direct fluorination of uracil by trifluoromethyl hypofluorite has also been described [74]. 5-Fluorouracil is more acidic than its natural pyrimidine analogue and is also more soluble in aqueous solutions. It is stable in solution at physiological pH for weeks. On exposure to ultraviolet irradiation, it forms an alkali-labile, acid-stable compound that has been identified as 5-fluoro-5-hydroxy-5,6-dihydrouracil [75, pp. 5-].

Metabolism:

There are two main pathways for the incorporation of 5-FU into nucleic acids. It is metabolised initially to nucleotides including fluoridine 5'-triphosphate (FUTP) and 5-fluoro-2'-deoxyuridine-5'-monophosphate (FdUMP), although it is unclear which is the most important pathway clinically [76]. 5-Fluorouracil is inactivated initially by conversion to 5-fluorodihydrouracil by the enzyme dihydropyrimidine dehydrogenase (DHPD) [77]. This occurs in all tissues, but its

activity is most intense in the liver, which therefore plays a major role in the degradation of 5-FU.

There have been case reports of severe 5-FU toxicity, associated in some cases with an inherited DHPD deficiency; such a deficiency has been shown to result in reduced 5-FU. In the clinical series discussed below, there is a noticeable variation in the toxicity, and this could in part be due to inter-patient variation in the metabolism of 5-FU. The inhibition of thymidylate synthase (TS) is undoubtedly one of its main mechanisms of action, since this leads to depletion of TMP and thus inhibition of DNA synthesis. In the presence of 5,10-CH₂-tetrahydrofolate (THF), FdUMP forms a tightly bound covalent bond with TS. Folinic acid (5-formyl-tetrahydrofolate) is converted to 5,10-CH₂-THF, and thus causes stabilisation of the quaternary complex of FdUMP bound to TS, hence the current interest in increasing the efficacy of 5-FU by the concomitant administration of folinic acid (leucovorin). The other main mechanism of the action of 5-FU is via its incorporation into RNA, after conversion to FUTP. The nuclear RNA is then processed into cytoplasmic rRNA, and this probably also contributes to its cytotoxicity [78].

Toxicity:

Several enzymes are involved in the capecitabine metabolism. The dihydropyrimidinedehydrogenase enzyme (DPD) metabolizes about 80% of the administered 5-FU into the inactive metabolite 5,6-dihydro-5-fluorouracil. The remaining 20% is converted into active metabolites that cause the inhibition of thymidylate synthase (TYMS) and RNA/DNA damage. Several genotypes of the DPD have been associated with reduced enzyme activity that could lead to severe toxic adverse events of fluoropyrimidine. The most used pharmacogenetic test to predict DPD activity is based on the detection of IVS14 p 1G > A polymorphism in the

DPYD gene, which leads to the production of an inactive protein and severe toxicity in about one-half of carrier patients. Moreover, a decreased value of 5FUDR is linked to DPYD haplotype, and it could be related to adverse events development; however, this polymorphism has a low frequency. Other enzymes are involved in 5-FU metabolism, and their polymorphisms could result in increased and unexpected toxicities such as MTHFR (methylenetetrahydrofolate reductase), one of the most relevant enzyme that regulates intracellular folate levels that affect DNA synthesis and methylation and TYMS [79].

Symptoms 5-FU Toxicity:

- ✓ Diarrhea
- ✓ Encephalopathy
- ✓ Mucositis
- ✓ Myelotoxicity
- ✓ Nausea and vomiting
- ✓ Skin reactions

The prognosis of TNBC patients can be greatly improved by the use of neoadjuvant chemotherapy regimens, which have been demonstrated to have a significantly greater pathological remission rate than those used to treat hormone receptor-positive breast cancer in recent years. For the reason of severe toxicity of 5 FU we have to use another combinational with 5-FU as a combination therapy in breast cancer treatment [80].

Lupeol, a novel anti-inflammatory and anti-cancer dietary triterpene

Lupeol a triterpene (also known as Fagarsterol) found in white cabbage, green pepper, strawberry, olive, mangoes and grapes was reported to possess beneficial effects as a therapeutic and preventive agent for a range of disorders. Last 15 years have seen tremendous efforts by researchers worldwide to develop this wonderful molecule for its clinical use for the treatment of variety of disorders. These studies also provide insight into the mechanism of action of Lupeol and suggest that it is a multi-target agent with immense anti-inflammatory potential targeting key molecular pathways which involve nuclear factor kappa β (NF κ B), cFLIP, Fas, Kras, phosphatidylinositol-3-kinase (PI3K)/Akt and Wnt/ β -catenin in a variety of cells. It is noteworthy that Lupeol at its effective therapeutic doses exhibit no toxicity to normal cells and tissues. This mini review provides detailed account of preclinical studies conducted to determine the utility of Lupeol as a therapeutic and chemopreventive agent for the treatment of inflammation and cancer [81].

Sources of Lupeol

Lupeol, is found in vegetables such as white cabbage,pepper, cucumber, tomato, in fruits such as olive, fig, mango,strawberry, red grapes and in medicinal plants such as American ginseng, Shea butter plant, Tamarindusindica, Allanblackiamonticola, Himatanthussucuuba, Celastruspaniculatus, Zanthoxylumriedelianum, Leptadeniahastata, Crataevanurvala, Bombax ceiba and Sebastianiaadenophora used by native people in North America, Latin America, Japan, China, Africa and Caribbean islands [82].

Chemical structure and analysis:

The chemical structure of Lupeol is presented in Fig. 5. The chemical formula of Lupeol is C₃₀H₅₀O and its melting point is 215–216°C. Properties computed from the structure of Lupeol

show that it has a molecular weight of 426.7174 (g/mol), H-Bond donor 1, H-Bond acceptor 1, rotatable bond count 1, exact mass 426.386166, mono isotopic mass 426.386166, topological polar surface area 20.2, heavy atom count 31, formal charge 0, complexity 766, isotope atom count 0, defined atom stereo center count 10, and bonded unit count 1 (PubChem, NIH library, Compound ID 259846). The infra-red spectrum of Lupeol shows the presence of a hydroxyl function and an olefinic moiety which show their presence in the spectrum at 3235 and 1640 cm⁻¹, respectively. The molecular formula depicts the presence of 6° of unsaturation, out of them one can be satisfied by an olefinic function. The presence of seven methyl singlets and an olefinic function in the ¹H NMR spectrum revealed that Lupeol is pentacyclic triterpenoid type in nature. Study conducted by Martelanc et al. using high-performance liquid chromatographic (HPLC) method with UV and mass spectrometric (MS) showed that Lupeol exhibits a parent ion peak at m/z 409 [M+H⁺]⁺ [83].

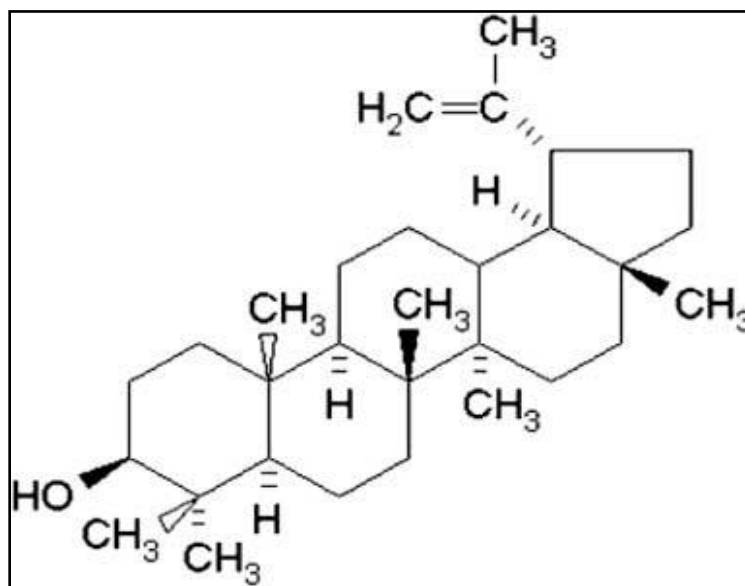


Fig. 5: Chemical structure of Lupeol (PubChem, NIH library, Compound ID 259846)

Lupeol and cancer:

Recent studies have shown that diets rich in phytochemicals can significantly reduce cancer risk by as much as 20% [84]. Epidemiological data suggest that the phytosterols content of the diet is associated with a reduction in common cancers including cancers of the colon, breast, and prostate. Data emanating from molecular studies with various tumorigenic models suggest that phytosterols modulate host systems potentially enabling more robust antitumor responses such as enhancing immune recognition of tumor cells, altering hormone-dependent growth of endocrine tumors and modulating sterol biosynthesis and references therein [85]. A number of triterpenoids have shown promise as antineoplastic agents and exhibit antiproliferative activity when tested against various cancer cell lines. These triterpenoids include members belong to the cycloartane, lupane, friedelane, dammarane, ursane, oleanane, limonoid and cucurbitacin family [86]. Recent reports showed that triterpenes directly inhibit tumor growth, cell cycle progression, and induce the apoptosis of tumor cells under in vitro and in vivo situations and references therein. Mutations that occur through DNA strand breaks have been shown to form the precursors of cancer development, and cells harboring mutations are at high risk to transform into neoplastic phenotype. During the course of tumorigenesis, mutations get accumulated thus transforming neoplastic cells into malignant carcinomas. It is noteworthy that Lupeol was reported to exhibit strong anti-mutagenic activity under in vitro and in vivo systems. Earlier reports have shown that Lupeol inhibits the chemically-induced DNA damage under in vitro conditions [87]. Topical application of Lupeol (200 µg/mouse) prevents 7, 12-dimethylbenz (a) anthracene (DMBA)-induced DNA damage (DNA strand breaks) in murine skin [88]. Recently, Lupeol was shown to inhibit the Benzo(a)pyrene (B(a)P), a well-known mutagen-induced genotoxicity in a mouse model. This study showed that pretreatment with Lupeol (1 mg/animal) for 7 days prior to B(a)P

administration significantly decreased B(a)P-induced clastogenicity and caused an increase in mitotic index [89].

Lupeol inhibits tumor promotion in two stage skin carcinogenesis in a mouse model. Topical application of Lupeol (40 mg/ kg/three times a week) for 28 weeks was shown to significantly decrease tumor burden, tumor multiplicity and increase tumor latency period in the mouse model. The anti-tumor promotion effects of Lupeol were observed to be associated with its potential to modulate signaling pathways such as nuclear factor kappa β (NF κ β) and the phosphatidylinositol 3-kinase (PI3K) /Akt (protein kinase B pathway), which are reported to play an important role during tumorigenesis [90]. Tumor promoters {such as 12-o-tetradecanoylphorbol 13-acetate (TPA)} are known to activate NF κ β signaling thus resulting in the translocation of activated NF κ β to the nucleus where it acts as a transcriptional factor.

Tumor promoters {such as 12-o-tetradecanoylphorbol 13-acetate (TPA)} are known to activate NF κ β signaling thus resulting in the translocation of activated NF κ β to the nucleus where it acts as a transcriptional factor. NF κ β is known to activate several target genes which are required for the tumor growth. Lupeol was shown to significantly inhibit the NF κ β translocation and its DNA binding activity in a mouse model of skin tumorigenesis. Recent studies have shown the emergence of PI3K/Akt signaling as a potential molecular target for chemotherapeutic and chemo-preventive agents [91, pp. 13-]. There was evidence that Lupeol ameliorates TPA-induced PI3K/Akt signaling in murine skin. Further, Lupeol was observed to significantly inhibit the activity of ornithine decarboxylase (ODC) protein which is a well-known biomarker of tumor promotion. Lupeol was tested against human melanoma tumor cells in vitro and in a xenograft athymic nude mouse model [92]. Lupeol inhibits growth of highly metastatic tumors of human melanoma origin by modulating ratio of Bcl-2 and Bax protein levels in vitro and in vivo. The

most important observation in this study was that no toxic effect on normal human melanocytes was observed at a dose at which Lupeol kills malignant melanoma cells. Lupeol significantly inhibits the growth of metastatic melanoma cells harboring constitutive activation of Wnt/b-catenin signaling. The potential of Lupeol to inhibit the growth or metastatic spread of melanoma cells. Lupeol was shown to significantly inhibit the migration of human melanoma cells through disassembling the actin cytoskeleton [93]. These studies suggest that Lupeol itself being non-toxic to normal cells could be used as a chemo-preventive as well chemotherapeutic agent against skin cancer and breast cancer. Neo-angiogenesis is a hallmark of cancer invasion and metastasis [94]. It is noteworthy that Lupeol (50–30 μ g/ml) is shown to exhibit anti-angiogenic property in an in vitro tube formation model of human umbilical venous endothelial cells.

Androgens are the key factors in the initiation or progression of breast cancer and are known to induce oxidative stress which is marked by the generation of reactive oxygen species (ROS) and depletion in the levels of antioxidant enzymes [95]. Lupeol has been shown to inhibit the generation of ROS and restore the depleted antioxidant levels within breast tissue of androgen pretreated mice. Studies with various cancer cells have shown that Lupeol adopts multipronged strategy to inhibit the growth of human cancer cells and by inducing apoptosis. The mechanistic pathways targeted by Lupeol in cancer cells are Wnt/ β -catenin signaling and Fas-apoptotic machinery. Lupeol was reported to decrease the expression level of several genes which are directly or indirectly associated with Wnt/b-catenin signaling in cancer cells [96]. Lupeol was observed to target axin, GSK3b, MMP-2, ERBB-2 and c-myc. Lupeol modulates the microtubule assembly and the protein level of its regulatory molecules such as Stathmin and Survivin in prostate cancer cells thus causing G2/M cell cycle arrest. Lupeol induces G2/M cell cycle arrest in cancer cells by inhibiting the cyclin regulated signaling pathway.

Lupeol and toxicity studies:

Lupeol has been reported to exhibit no toxicity in animal studies [81]. Lupeol administered orally in a dose of 2 g/kg has been reported to produce no adverse effects in rats and mice, and after 96 h of observation no mortality was recorded. Lupeol tested at doses 40–200 mg/kg under various protocols (long or short-term treatment) did not show any systemic toxicity effect in animals. Lupeol (2 mg/animal, equivalent to 80 mg/kg) applied topically (three times/ week) for 28 weeks did not produce any toxicity in mice. Mice receiving oral administration of Lupeol (0.5–40 mg/kg) for seven consecutive days did register no mortality or other toxic signs [97]. Recent studies showed that mice receiving intraperitoneal administration of Lupeol (20 mg/kg/2 days) did not show any sign of toxicity or mortality.

Several factors must be taken into consideration when the evidence for the inhibition of carcinogenesis and alleviation of other diseases by Lupeol is examined. These include the effective dose used and the time of exposure. Although animal studies have enhanced our understanding of the possible action of Lupeol in decreasing carcinogenesis and ameliorating inflammation, one must apply caution in extrapolating the information obtained in animal studies to humans, because of biological differences [98].



CHAPTER 2
OBJECTIVES

OBJECTIVES OF THE RESEARCH

Despite of the vast amount of awareness, in-depth research and various clinical trials being conducted every year, the underlying mechanisms involved in cancer recurrence and resistance to conventional treatments still remains an enigma. The emerging fields of therapy have their own lacunae which directly impact patient survival and their quality of life. The abysmal failures of certain conventional therapies along with their severe side effects indicate a dire need for deeper exploration into the machinations that are responsible for this. With advancement in technology and more research on breast cancer, it has vastly improved patient survival. In spite of that, certain subsets of breast cancer still remain elusive and evade the current therapeutic modalities. This results in recurrence and poor disease free survival of the patients. Vasculogenic mimicry is such a phenomenon which has recently gained traction due to its potential in contributing to the recurrence and therapeutic resistance of solid tumors. Although, the exact mechanism through which this phenomenon is triggered or being operated is a matter of exploration and we intend to do exactly that in our work here. Also, the use of plant products as therapeutic agents has been practiced in India since ancient times. This involves rediscovering or traditional methodologies and digging deeper into the actual science behind the causative effects of the plants involved in these therapies in order to potentially use the active compounds as adjuvant to conventional therapy. This may result in decreasing the overall drug load without compromising on efficacy and simultaneously reducing its adverse effects. Aligning with these, the objectives of this work can be found distributed in the following chapters:

- A. To determine the influence of the c-MET and Ephrin pathways in regulating Vasculogenic Mimicry in breast cancer tissues.

- B. To determine the expressional regulation of the c-MET and Ephrin pathways influencing Vasculogenic mimicry in breast cancer.
- C. To demonstrate the potential synergistic effect of the phytochemical Lupeol along with chemotherapeutic drugs in regulation of vasculogenic mimicry.



CHAPTER A

To determine the influence of the c-MET and Ephrin pathways in regulating Vasculogenic Mimicry in breast cancer tissues.

Introduction

Breast cancer is the most commonly diagnosed malignancy accounting for 1 in 4 cases among women[99]. Although a widespread understanding of the molecular subtypes of breast cancer has led to the evolution of molecularly guided personalized therapies and improved response rate, a large number of patients do not get any durable benefit [100]. The better understanding of the molecular and phenotypic basis of disease progression, recurrence and metastasis is an unmet need for effective management of the diseases. One of the established factors implicated in tumor growth and survival is the formation of endothelial-lined vascular channels which supply the growing tumor with nutrients and oxygen, thus providing a survival advantage to the cancer cells under local selective pressure[101]–[103]. This has long been established as a hallmark of tumorigenesis[6]. Tumor angiogenesis classically was considered to be the only unique perfusion network within tumor microenvironment and influences outcome of rationally selected therapy [104]. However, efforts to inhibit angiogenesis in clinical setting very often fail due to adaptive resistance[105]–[107]. Thus, it is imperative to critically investigate the emerging mechanisms that underline the failure of the conventional therapies in treating breast cancers. In 1999, Maniotis et al. [49] first described a novel pseudovascular network which was independent of angiogenic vessels. It was elucidated that a class of dysregulated tumor cells formed channels mimicking the native endothelial vasculature in highly aggressive tumors and thereafter was termed as vasculogenic mimicry (VM) [108]. This work showed for the first time that VM channels can also act as an alternative network for providing the tumor with adequate

nourishment and a route for dissemination. The process involves extracellular matrix (ECM) remodeling akin to angiogenesis that can be detected by simple Periodic Acid–Schiff (PAS) staining. Hence, VM is often distinguished from the endothelial-lined vessels by combining PAS staining with histochemistry using established endothelial markers such as CD-31 or CD-34 [109], [110]. Since the monumental discovery of VM, the phenomenon has been implicated in the increased aggressive behavior, invasiveness, metastatic potential and poor survival in patients in several malignancies like lung cancer, liver cancer, gastric cancer, ovarian cancer, prostate cancer and breast cancer [111]–[117]. Among the Eph family of receptor tyrosine kinases (RTKs), Ephrin type-A receptor 2 (EphA2) has been found to have the strongest connection with tumor progression[118]–[121]. Through regulating a diverse signaling network, the EphA2 receptor is known to mediate convergent and divergent effects. The canonical pathway involves the putative ligand and kinase-dependent form of EphA2 which is mediated by cell-surface anchored ephrinA ligands such as ephrinA1 [118]. This kinase-dependent pathway has several outcomes such as inhibition of oncogenic Akt/mTORC1 and RAS-ERK signaling along with suppression of cell adhesion, induction of migration and invasion. By promoting tumor angiogenesis, it facilitates cancer cell dissemination[118], [120]–[123]. Contrastingly, EphA2 can also behave exclusively as an oncoprotein via the non-canonical pathway activation in ligand-independent manner. Ligand independent promotion of cell migration and invasion is driven by the EphA2 phosphorylation at the specific S897 residue present in the segment that links the kinase domain with the sterile alpha motif (SAM) domain[118]. This particular phosphorylation is mediated via serine/threonine kinases such as PKA, Akt and RSK which in turn enhances cell migration, invasion, metastatic potential and also cancer stem-cell-like features [119]–[122], [124], [125]. Further, Ligand independent signaling was supported by the

ratios of ephrina1/EphA2 expression in human breast cancer[126]. Recently,EphA2 has been implicated as a major driver of VM formation in several malignancies including melanoma, prostate cancer, head and neck cancer, gastric cancer and ovarian cancer [127]–[131]. Moreover, the ligand-independent phosphorylation of EphA2 has been established as the initiating event of tubule formation in MDCK cells[132]. However, this specific phosphorylation of the EphA2 receptor and its mechanistic link with VM along with its possible prognostic effect are yet to be elucidated in case of breast cancer. Several target molecules of EphA2 have been identified namely, focal adhesion kinase (FAK), extracellular signal regulated kinases (ERK) and laminin 5Y2 which mediate cellular proliferation, increased migratory potential and actas an indicator of ECM remodeling [133]. Here, we evaluated the expression status of these effector molecules in a breast cancer cohort and determined the association of clinical parameters with VM and phospho-EphA2 (S897) expression. Finally, we determined the association between VM, the phosphorylation of EphA2 receptor with prognosis and survival in clinical breast cancer patients.

The proto-oncogene MET, also known as the N-methyl-N'-nitroso-guanidine human osteosarcoma transforming gene, codes for the c-MET hepatocyte growth factor (HGF) receptor tyrosine kinase.The mitogen-activated protein kinase (MAPK), phosphatidylinositol 3-kinase (PI3K), v-src avian sarcoma (Schmidt-Ruppin A-2) viral oncogene homolog (SRC), and signal transducer and activator of transcription (STAT) signaling pathways are all activated as a result of the binding of HGF. Normal cell morphogenesis, motility and scattering, proliferation, and protection from apoptosis all depend on c-MET activity. The MET pathway is crucial for wound healing, post-injury recovery, and the development of degenerative illnesses as renal and lung fibrosis [125], [134]–[137]. Malignancies of all types, including non-small cell lung cancer

(NSCLC), gastrointestinal cancer, and hepatocellular carcinoma (HCC), are frequently found to express MET abnormally.

Materials and methods

Patient samples

This study encompasses 124 patients diagnosed with invasive ductal carcinoma (IDC) of the breast who had undergone surgery at the Chittaranjan National Cancer Hospital, Kolkata in the year 2012 to 2013. The relevant clinic-pathologic and demographic parameters were obtained for each of the patients from their clinical records. Two pathologists separately confirmed the presence of IDC of breast in the selected formalin-fixed paraffin-embedded (FFPE) blocks. The Institute Ethical Committee approved this study and the declarations of Helsinki ethical principles or its later amendments were stringently followed. Written informed consent was not required as this was a retrospective study and prior to analysis all patient information was anonymised. Patients who had undergone hormone therapy, chemotherapy or radiation before the surgery or with a history of recurrence/distant metastasis were excluded (Fig.6). Overall survival (OS) was defined as the time interval (in months) from the date of primary surgery till the date of breast cancer-related death. Disease-Free survival (DFS) was defined as the time interval (in months) from the date of primary surgery till first documentation of local recurrence or distant metastasis.

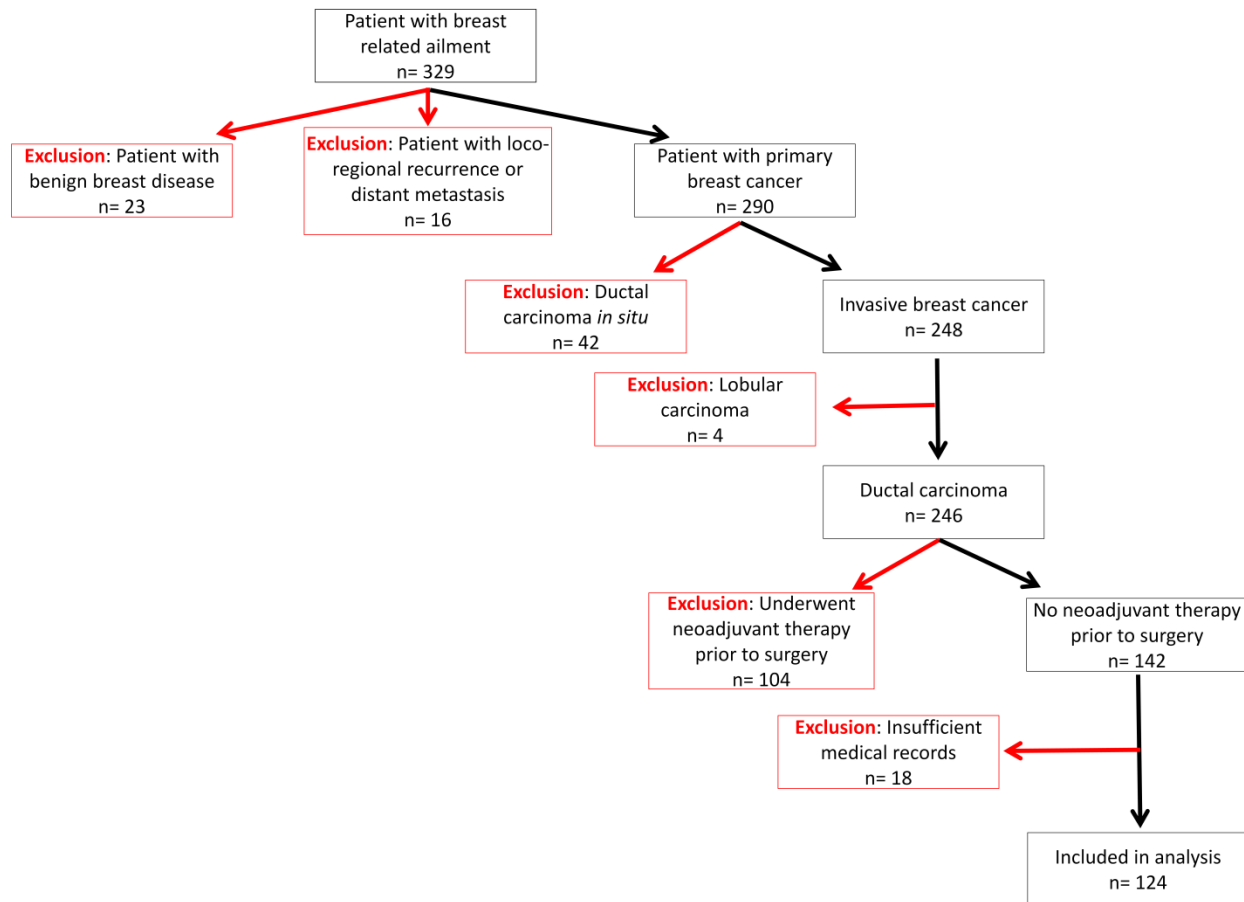


Fig. 6: Flow chart describing the inclusion/exclusion criteria of patients in our study

Immunohistochemistry/PAS dual staining

Thin sections of 4 μm each was made from the FFPE tissue blocks and were de-waxed in xylene and rehydrated in graded alcohols. Endogenous peroxidase was quenched (using 3% H_2O_2 solution in Methanol) followed by heat induced epitope retrieval in citrate buffer (0.01 mol/L; pH 6.0). Immunohistochemical staining (IHC) for CD-31 was performed by incubating the tissue sections for 1 h at room temperature, followed by DAB (3,3'-Diaminobenzidine) detection method according to the manufacturer's protocol (DAB 150 Kit, Merck). After performing CD-31 staining, the sections were incubated in 0.5% Periodic Acid solution for 10 min, followed by water wash for 5 min. The sections were next incubated in

undiluted Schiff's reagent in a dark chamber for 15 min. Samples were finally washed in lukewarm water for color development and counterstained with Mayer's haematoxylin. Prior to microscopic examination, the stained samples were dehydrated using graded alcohols, clarified with xylene and cover-slip mounted using DPX. The whole cohort was stratified into VM-positive and VM negative groups based on this dual staining method and evaluated by qualified pathologist (SM and SV). The expressional status of the proteins of interest namely phospho-EphA2 (S897), phospho-MET, phospho-p44/42 MAPK (ERK1/2)(Thr202/Tyr204), were observed by IHC along with PAS for both of the stratified VM cohorts. Laminin-5 (Y2 chain) expression was examined by performing IHC alone in immediate next section in order to avoid stain overlapping as the protein (tagged with the DAB chromogen) is expressed in the extracellular matrix of the tumor—the common target for PAS. Primary antibodies used in this study were rabbit monoclonal anti-PECAM-1/CD-31 (clone M-20, 1:100 dilution; Santa Cruz Biotechnology), rabbit monoclonal anti-Phospho-EphA2 (S897), (clone D9A1, 1:100 dilution; Cell Signaling Technology), rabbit polyclonal anti p-Met (Tyr 1349, 1:200, Santa Cruz Biotechnology), rabbit monoclonal anti-Phospho-p44/42 MAPK (phospho-ERK1/2) (Thr202/Tyr204) (clone D13.14.4E, 1:200 dilution; Cell signaling Technology) and mouse monoclonal anti-Laminin-5 (Y2 chain) (clone D4B5, 1:50 dilution; Merck). After performing CD-31/PAS dual staining, the tissue sections were observed under high power magnification of a bright-field microscope. VM or endothelial-lined vessels were identified by the various morphological patterns described earlier in literature [138] and the patient cohort was stratified accordingly. Then, IHC was performed to detect the proteins of interest in the stratified samples and IHC scoring was performed by taking the stain intensity and percentage of positive cells into account. While evaluating the stain intensity, “0” indicated negative staining, “1” indicated weak

positive staining, “2” indicated moderate staining and “3” indicated strong staining. Subsequently, the percentage of positive cells per field was manually evaluated in 10 different fields and scored by qualified pathologist (SM) using the following method—“0” for < 10% positive cells, “1” for < 25%, “2” for < 50% and “3” for > 50% [139], [140]. The sum of the stain intensity and positive cell score resulted in the staining index, which was used to determine the final result for each sample. A sample was defined as positive when the staining index was greater than 1. Immunohistochemical scoring was performed by pathologist blinded to relevant patient data including outcomes. Phospho-EphA2(S897) and phospho-MET expression were observed only in the cytoplasm although for phospho-ERK 1/2 both nuclear as well as cytoplasmic expressions were noted. Laminin 5Y2 was exclusively expressed in the extracellular matrix within tumor zones. Photomicrographs were taken using the Carl Zeiss trinocular bright-field microscope (model:PrimoStar) and the Zen 2.3 (blue edition) software was utilized for image acquisition and analysis.

Statistical analysis

Association among the VM phenotype, phospho-EphA2, phospho-MET status and the clinicopathological parameters were performed by conducting two-tailed Chi square tests. Correlation between VM, phospho-EphA2, phospho-MET, phospho-ERK 1/2 and Laminin 5Y2 were conducted by Spearman correlation test. These tests were performed using Graph-Pad Prism version 7.00 software (California, USA). Survival curves were computed by the Kaplan–Meier method and the differences in survival time (months) was compared using the Log-rank test. Independent risk factors were determined by utilizing the univariate and multivariate Cox proportional hazard regression model where disease-free survival (DFS) and overall survival

(OS) was calculated. These statistical analyses were conducted using the SPSS 17 software (SPSS Inc, Chicago, IL, USA). P value less than 0.05 was considered to be significant.

Results

Demographic and clinicopathological data of breast cancer patients

The clinicopathological and demographic data of the breast cancer patients are listed in Table 3. Parameters those are considered as vital for prognosis and diagnosis of breast cancer including age at which the disease was diagnosed, grade, tumor size, nodal status, ER, PR and HER2 status are listed in the table. The Nottingham Prognostic Index (NPI) was derived by applying the following formula, $NPI = 0.2 \times \text{pathological tumor size (cm)} + \text{histological grade (1-3)} + \text{lymph node stage}$. According to the NPI score, the patients were divided into three subgroups: good (≤ 3.4), moderate (3.41–5.4) and poor (> 5.4)[141]. At the end of the follow-up period (median follow-up period was 70 months with a range of 13–80 months), 32 (25.81%) patients had died due to clinically confirmed loco-regional recurrence (6.45%) or distant metastasis (19.35%) and 73 (58.87%) individuals were alive with the rest being lost to follow-up or died due to cardiovascular or respiratory disorders unrelated to breast cancer. They were considered as censored during further analysis.

Parameters	N (%)
Age at diagnosis (years)	
≤ 50	74 (59.68)
>50	50 (40.32)
Grades	
1	40 (32.26)
2	64 (51.61)

3	20 (16.13)
T stage	
T1	32 (25.81)
T2	81 (65.32)
T3	11 (8.87)
N stage	
N ₀	50 (40.32)
N ₁	38 (30.65)
N ₂	26 (20.97)
N ₃	10 (8.06)
Nottingham Prognostic Index	
Good prognosis	62 (50)
Moderate prognosis	57 (45.97)
Poor prognosis	5 (4.03)
ER	
Negative	32 (25.81)
Positive	92 (74.19)
PR	
Negative	49 (39.52)
Positive	75 (60.48)
HER2	
Negative	102 (82.26)
Positive	22 (17.74)
Triple negative status	
No	110 (88.71)
Yes	14 (11.29)

Table 3: Demographic and pathological profiles of patients with breast cancer

Association of VM and phospho-EphA2 (S897) expression with clinicopathological features

Vasculogenic mimicry in invasive ductal carcinoma (IDC) of the breast tissues was detected by CD-31/PAS dual staining. This method clearly distinguishes CD-31-positive endothelial from extracellular matrix remodeled PAS-positive vasculogenic mimicry (VM) entity and thus has proven to be a gold standard for detection of VM [110], [142](Fig. 7).

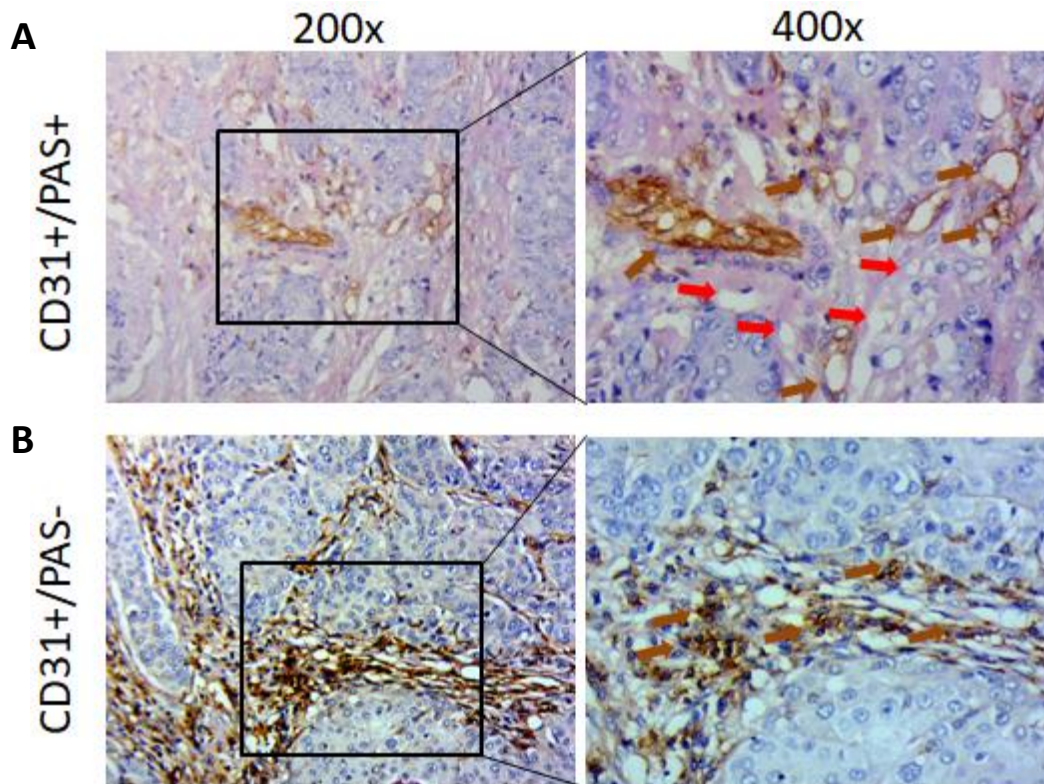


Fig. 7: CD-31/PAS dual staining of invasive ductal carcinoma of breast tissue section: A) Red arrows denote PAS-positive VM; B) Black arrows indicate endothelial cells showing CD-31 expression.

It was also observed that the PAS-positive regions tend to anastomose with the CD-31-positive endothelial-lined vessels which led us to believe that the PAS-positive VM regions enhance the vasculature already present in the tumor by connecting the endothelial hubs in tumor

microenvironment (TME). Thus, VM works in a way to enhance the intra-tumoral perfusion network which facilitates the aggressive and invasive behavior of the tumor[143]. Therefore, it is imperative to determine its correlation with established clinical attributes to get a better understating of its role in IDC prognosis. The correlation of VM, phospho-EphA2 and phospho-MET expression with demographic and clinic-pathological data are presented in Table 4. A total of 37 cases (29.83%) were found to be VM positive and 87 cases (70.17%) were VM negative. The presence of VM was significantly higher in cases with higher nodal status ($P < 0.0001$) and poor NPI ($P = 0.005$), even though no significant difference was observed with age ($P = 0.4051$), tumor stage ($P = 0.4402$) and grade ($P = 0.0569$). The positive expression of estrogen receptor (ER) ($P = 0.0002$) and progesterone receptor (PR) ($P = 0.0308$) was negatively correlated with the occurrence of VM, although no significant difference was observed among the HER2-based cohorts. A very interesting finding which corroborates previous studies is the occurrence of VM in higher percentage in the triple-negative breast cancer (TNBC) cohort ($P = 0.0028$) [140], [144]. Similar association was observed in the case of phospho-EphA2 (S897) expression and other established prognostic features of breast cancer like, nodal status ($P < 0.0001$), NPI ($P = 0.0026$) and negatively correlated with ER-positive expression ($P = 0.0252$) with no significant correlation with PR and HER2 status. Also, positive phospho-MET expression was associated with increasing nodal stage ($P = 0.0004$), poor NPI ($P = 0.015$), and negatively associated with ER-positive expression ($P = 0.01$). The positive expression of phospho-EphA2 (S897) ($P = 0.0107$) and also phospho-MET ($P = 0.0001$) were significantly higher in the TNBC patients. All these indicate that VM along with phospho-EphA2 (S897) and phospho-MET positive expression plays a major role in the malignant progression by attributing to aggressive properties in IDC.

Parameters	VM		P values	pEphA2		P values	pc-MET		P values
	Positive	Negative		Positive	Negative		Positive	Negative	
	N (%)	N (%)		N (%)	N (%)		N (%)	N (%)	
Age (years)									
≤ 50	20 (27.03)	54 (72.97)	0.4051	28 (37.84)	46 (62.16)	0.2562	33(44.59)	41(55.40)	0.238
> 50	17 (34)	33 (66)		14 (28)	36 (72)		17(34)	33(66)	
Grades									
1	8 (20)	32 (80)	0.0569	10 (25)	30 (75)	0.1545	12(30)	28(70)	0.0824
2	19 (29.69)	45 (70.31)		22 (34.38)	42 (65.62)		26(40.63)	38(59.37)	
3	10 (50)	10 (50)		10 (50)	10 (50)		12(60)	8(40)	
T stage									
T1	8 (25)	24 (75)	0.4402	7 (21.875)	25 (78.125)	0.1171	10(31.25)	22(68.75)	0.4734
T2	24 (29.63)	57 (70.37)		29 (35.80)	52 (64.20)		35(43.21)	46(56.79)	
T3	5 (45.45)	6 (54.55)		6 (54.55)	5 (45.45)		5(45.45)	6(54.55)	
N stage									
N ₀	7 (14)	43 (86)	<0.0001*	8 (16)	42 (84)	<0.0001*	12(24)	38(76)	0.0004*
N ₁	9 (23.68)	29 (76.32)		14 (36.84)	24 (63.16)		15(39.47)	23(60.53)	
N ₂	14 (53.85)	12 (46.15)		11 (42.31)	15 (57.69)		14(53.85)	12(46.15)	
N ₃	7 (70)	3 (30)		9 (90)	1 (10)		9(90)	1(10)	
NPI									
Good	12 (19.35)	50 (80.65)	0.005*	13 (20.97)	49 (79.03)	0.0026*	18(29.03)	44(70.97)	0.015*
Moderate	21 (36.84)	36 (63.16)		25 (43.86)	32 (56.14)		28(49.12)	29(50.88)	
Poor	4 (80)	1 (20)		4 (80)	1 (20)		4(80)	1(20)	
ER									

Negative	18 (56.25)	14 (43.75)	0.0002*	16 (50)	16 (50)	0.0252*	19(59.37)	13(40.63)	0.01*
Positive	19 (20.65)	73 (79.35)		26 (26.09)	66(73.91)		31(33.70)	61(66.30)	
PR									
Negative	20 (40.82)	29 (49.18)	0.0308*	19 (38.78)	30 (61.22)	0.3509	15(30.61)	34(69.39)	0.535
Positive	17 (22.67)	58 (77.33)		23 (30.67)	52 (69.33)		27(36)	48(64)	
HER2									
Negative	33 (32.35)	69 (67.65)	0.1877	37 (36.27)	65 (63.73)	0.2234	34(33.33)	68(66.67)	0.785
Positive	4 (18.18)	18 (81.82)		5 (22.73)	17 (77.27)		8(36.36)	14(63.64)	
TNBC									
No	28 (25.45)	82 (74.55)	0.0028*	33 (30)	77 (70)	0.0107*	31(28.18)	79(71.81)	0.0001*
Yes	9 (64.29)	5 (35.71)		9 (64.29)	5 (35.71)		11(78.57)	3(21.43)	

Table 4: Relationship of VM, phospho-EphA2, phospho-MET and clinicopathological parameters in invasive ductal carcinoma of breast.

Correlation between VM, phospho-EphA2 (S897) and its effector molecules in invasive breast cancer

The correlation of VM with the relevant molecules (Fig. 8), i.e. phospho-EphA2 (S897) ($r = 0.6193$; $P < 0.001$), phospho-MET ($r = 0.4965$; $P < 0.001$), phospho-ERK 1/2 ($r = 0.4193$; $P < 0.001$) and Laminin 5Y2 ($r = 0.5498$; $P < 0.001$) are depicted in Table 5. Data revealed significant association of the presence of VM with the expression of effector molecules. The markers were significantly correlated with the positive expression status of phospho-EphA2 (S897) as well [phospho-MET ($r = 0.79$; $P < 0.001$), phospho-ERK1/2 ($r = 0.3416$; $P < 0.001$), Laminin 5Y2 ($r = 0.7811$; $P < 0.001$)]. These data indicate that phosphorylation of the EphA2 receptor at S897 residue, phosphorylation of c-MET, along with the downstream effector molecules may act as a deterministic factor in breast cancer progression and VM occurrence.

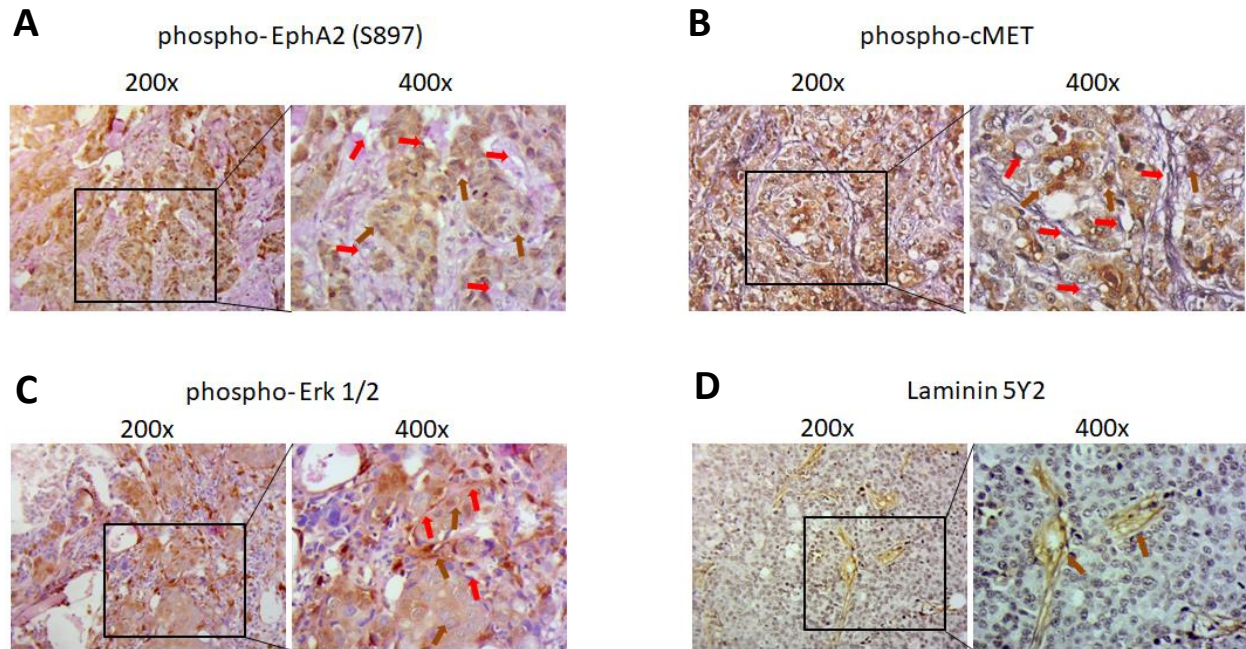


Fig. 8: IHC profile of proteins in the VM-positive breast cancer cohort: Expressional status of **A)** phospho-EphA2 (S897); **B)** phospho-MET; **C)** phospho-ERK 1/2 and **D)** Laminin-5Y2 by immunohistochemical staining. Black arrows indicate positive expression of protein while red arrows exhibit VM.

Variable	pEphA2 (S897)		r	P values	pcMET		r	P values	pERK 1/2		r	P values	Laminin 5Y2		r	P values
	Negative N (%)	Positive N (%)			Negative N (%)	Positive N (%)			Negative N (%)	Positive N (%)			Negative N (%)	Positive N (%)		
VM																
Negative	72 (82.76)	15 (17.24)	0.6764	<0.001	69 (79.31)	18 (20.69)	0.4965	<0.001	54 (62.07)	33 (37.93)	0.4193	<0.001	75 (86.21)	12 (13.79)	0.5498	<0.001
Positive	10 (27.03)	27 (72.97)			5 (13.51)	32 (86.49)			11 (29.73)	26 (70.27)			8 (21.62)	29 (78.38)		
phospho-EphA2																
Negative					73 (89.02)	9 (10.97)	0.79	<0.001	49 (59.76)	33 (40.24)	0.3416	<0.001	68 (82.93)	14 (17.07)	0.7811	<0.001
Positive					1 (2.38)	41 (97.62)			16 (38.10)	26 (61.90)			15 (35.71)	27 (64.29)		

Table 5: Correlation between VM, phospho- EphA2, phospho-MET and relevant proteins in invasive ductal carcinoma of breast.

Association of VM and phospho-EphA2 (S897) double-positive cohort with clinicopathological features

We next wanted to elucidate the clinical impact of expression of VM and phospho-EphA2 dual-positive phenotypes. The relationships between VM/phospho-EphA2 (S897) simultaneous positive, demographic and clinicopathological parameters are listed in Table 6. There were 27 (21.78%) VM and phospho-EphA2 (S897) dual-positive cases, 15(12.10%) VM-negative and phospho-EphA2 (S897)-positive cases, 10 (8.06%) VM-positive and phospho-EphA2 (S897)-negative cases and 72 (58.06%) VM and phospho-EphA2(S897) dual-negative cases. Also, there were 32 (25.81%) VM and phospho-MET dual-positive cases, 18(14.52%) VM-negative and phospho-MET positive cases, 05 (4.03%) VM-positive and phospho-MET negative cases and 69(55.64%) VM and phospho-MET (S897) dual-negative cases. These IHC data together display a spatially defined intra and inter-tumor heterogeneity in different clinical IDC samples. Incidentally, VM and phospho-EphA2 (S897) dual-positive cases were positively correlated with tumor stage ($P = 0.0361$), nodal status ($P < 0.0001$) and NPI ($P < 0.0001$), although there was no significant correlation with age ($P = 0.8869$). In the case of VM and phospho-MET dual-positive cases, they were positively correlated with tumor grade ($P = 0.0073$), nodal status ($P < 0.0001$) and NPI ($P = 0.0004$). These results indicate that there is a strong correlation between VM and phosphorylation of EphA2 receptor at S897 residue and phosphorylation of MET receptor in the pathogenesis of invasive carcinoma of the breast. Notably, the dual positivity of VM and the two receptors is strongly associated with the TNBC subtype of breast cancer.

Parameters	p-EphA2 and VM dual status			p-c-MET and VM dual status		
	Negative N (%)	Positive N (%)	P value	Negative N (%)	Positive N (%)	P value
Age (years)						
≤50	56 (78.38)	16 (21.62)	0.8869	56(75.67)	18(24.32)	0.80
> 50	41 (78)	11 (22)		36(72)	14(28)	
Grades						
1	36 (90)	4 (10)		35(87.5)	5(12.5)	
2	50 (78.13)	14 (21.87)	0.0083*	47(73.43)	17(26.57)	0.0073*
3	11 (55)	9 (45)		10(50)	10(50)	
T stage						
T1	29 (90.63)	3 (9.37)		27(84.38)	5(15.62)	
T2	62 (76.54)	19 (23.46)	0.0368*	59(72.83)	22(27.17)	0.133
T3	6 (54.55)	5 (45.45)		6(54.54)	5(45.45)	
N stage						
N ₀	46 (92)	4 (8)		44(88)	6(12)	
N ₁	32 (84.21)	6 (15.79)				
N ₂	16 (61.54)	10 (38.46)	<0.0001*	31(81.57)	7(18.42)	<0.0001
				14(53.84)	12(46.15)	
N ₃	3 (30)	7 (70)		3(30)	7(70)	
NPI						

Good prognosis	57 (91.94)	5 (8.06)		54(87.09)	8(12.91)	
Moderate prognosis	39 (68.42)	18 (31.58)	<0.0001*	37(64.91)	20(35.08)	0.0004*
Poor prognosis	1 (20)	4 (80)		1(20)	4(80)	
ER						
Positive	79 (85.87)	13 (14.13)		76(82.60)	16(17.39)	
			0.0005*			0.0007*
Negative	18 (56.25)	14 (43.75)		16(50)	16(50)	
PR						
Positive	62 (82.67)	13 (17.33)		59(78.66)	16(17.39)	
			0.1382			0.159
Negative	35 (71.43)	14 (28.57)		33(67.34)	16(32.65)	
HER2						
Positive	18 (81.82)	4 (18.18)		15(68.18)	7(31.82)	
Negative	79 (77.45)	23 (22.55)	0.6526			0.6797
				74(72.55)	28(27.45)	
TNBC						
Yes	8 (57.14)	6 (42.86)		7(50)	7(50)	
No	89 (80.91)	21 (19.09)	0.0424*			0.028*
				85(77.27)	25(22.73)	

Table 6: Relationship of phospho-EphA2, phospho-MET and VM double positive status and clinicopathological parameters in invasive ductal carcinoma of breast.

Correlation between phospho-EphA2(S897), phospho-MET positive expression and VM with survival endpoints

We next sought to elucidate the correlation of VM phenotypes with survival. Survival analysis was conducted using two clinically defined endpoints (i.e. DFS and OS).Kaplan–Meier plots revealed that OS (log rank = 31.257; $P < 0.0001$) and DFS (log rank = 40.562; $P < 0.0001$) of phospho-EphA2 (S897)-positive patients were poorer than phospho-EphA2 (S897)-negative patients (Fig. 11). The same was observed among the VM-positive and VM-negative cohorts for both OS (log rank = 41.158; $P < 0.0001$)and DFS (log rank = 40.544; $P < 0.0001$). Notably, the OS (log rank = 39.810; $P < 0.0001$) and DFS (log rank = 48.456; $P < 0.0001$) of phospho-MET positive patients were also poorer than phospho-MET negative patients. The mean [95% Confidence Interval (CI)] OS time and DFS time of phospho-EphA2 (S897)-positive patients were 62.136(56.284–67.987) months and 53.881 (47.316–60.446)months, respectively, whereas the mean OS and DFS time for phospho-EphA2 (S897)-negative patients were 78.077(76.895–79.260) months and 75.143 (73.325–76.960)months. The median [95% Confidence Interval (CI)] OS and DFS time for phospho-EphA2 (S897)-positive patients were 62 (51.449–72.551) months and 49 (42.758–55.242)months, respectively. In the VM-positive cohort, the mean OS time and the mean DFS time were found to be 60.427(54.234–66.620) months and 52.476 (45.488–59.463)months with the mean OS and DFS time for VM-negative cohort were 77.777 (76.338–79.217) months and 74.220(72.087–76.354) months, respectively. The median OS and DFS time for VM-positive cohort were 62 (55.724–68.276)and 51 (44.209–57.791). The mean [95% Confidence Interval (CI)] OS time and DFS time of phospho-MET-positive patients were 62.746 (57.547–67.946) months and 54.577 (48.691–60.463) months, respectively, whereas the mean

OS and DFS time for phospho-MET-negative patients were 78.885 (78.049–79.721) months and 76.349 (74.940–77.759) months. The patients with both phospho-EphA2 (S897)-positive expression and VM occurrence had the worst survival time both in DFS [log rank = 56.429; $P < 0.0001$; mean time = 48.313 (39.992–56.633) months] and OS [log rank = 49.516; $P < 0.0001$; mean time = 56.692 (49.055–64.328) months] than the negative cohort, who incidentally had the highest survival time in both DFS [mean time = 76.551 (75.204–77.899) months] and OS [mean time = 79.108 (78.388–79.828) months]. The median OS and DFS time for this double-positive cohort was 59 (47.652–70.348) and 46 (39.215–52.785), respectively. Notably, similar findings were observed in case of dual VM and phospho-MET positive cohort. These findings indicate that the coordinated expression of VM, phosphorylation of the EphA2 at the S897 residue and activation of the c-MET receptor is a deterministic factor for survival in breast cancer patients.

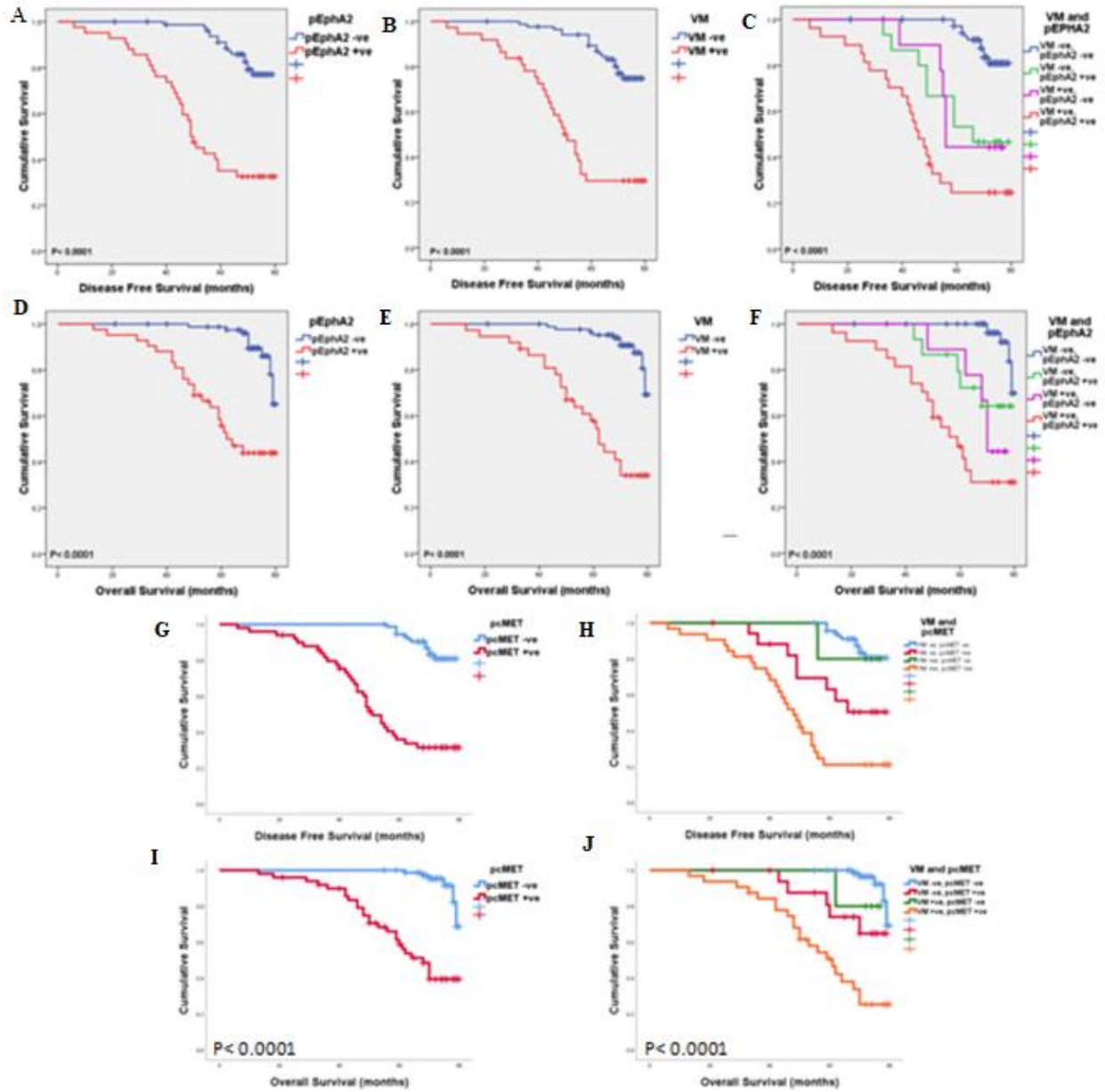


Fig. 9: Kaplan–Meier plots for DFS and OS: Survival curve of DFS in breast cancer patients with A) differential phospho-EphA2 (S897) status; B) VM status; C) VM and phospho-EphA2 (S897) dual status. Survival curve of OS in breast cancer patients with D) differential phospho-EphA2 (S897) status; E) VM status and F) VM and phospho- EphA2 (S897) dual status. Survival curve of DFS in breast cancer patients with G) differential phospho-MET status; H) VM and phospho-MET dual status. Survival curve of OS in breast cancer patients with I) differential phospho-MET status; J) VM and phospho-MET dual status

Risk attributes of phospho-EphA2 (S897) and VMin survival of patients

After performing survival analysis on the stratified cohorts, the risk attributes of phospho-EphA2, phosphor-MET and VM were evaluated. Univariate analysis initially revealed that tumor stage, nodal status, grade, occurrence of VM, phospho-EphA2(S897), phospho-MET,

Parameters	Beta	HR	95% CI		P Values
			Lower	Upper	
Age	-0.224	0.799	0.432	1.477	0.474
T status	0.826	2.284	1.331	3.918	0.003*
N status	0.590	1.804	1.329	2.449	<0.0001*
Grade	0.892	2.440	1.553	3.835	<0.0001*
pEphA2	1.782	5.944	3.194	11.062	<0.0001*
p-cMET	1.768	5.792	3.086	10.292	<0.0001*
VM	1.753	5.773	3.145	10.595	<0.0001*
pEphA2 and VM dual positive	1.839	6.288	3.425	11.545	<0.0001*
pMET and VM dual positive	1.862	6.395	3.581	11.622	<0.0001*

Table 7: Univariate analysis for DFS

VM/phospho-EphA2 (S897) double-positive expressions were significant factors in DFS as well as OS(Tables 7 and 8). Based on these findings, the multivariate Cox regression analysis was performed. Results presented in Table 9unveiled that occurrence of VM [Hazard ratio (HR) 6.005; 95% CI 2.002–18.018; $P = 0.001$], phospho-EphA2 (S897) (HR 4.342; 95% CI 1.717–10.983; $P = 0.002$) and phosphor-MET expression (HR 4.526; 95% CI 1.768–11.235; $P = 0.002$) are independent risk factors for DFS. Similarly, occurrence of VM (HR 11.654; 95% CI 3.195–

42.508; $P < 0.0001$), positive expression of phospho-EphA2 (S897) expression (HR 5.853; 95% CI 1.663–20.602; $P = 0.006$) and positive expression of phosphor-MET (HR 5.961; 95% CI 1.798–20.855; $P = 0.005$) proved to be independent risk factors for OS (Table 10). However, simultaneous VM/phospho- EphA2 (S897) or VM/phosphor-MET double-positive expression did not prove to be an independent survival risk factor for either DFS or OS in the multivariate Cox proportionality hazard regression analysis.

Parameters	Beta	HR	95% CI		P Values
			Lower	Upper	
Age	-0.164	0.849	0.415	1.738	0.654
T status	0.808	2.243	1.177	4.277	0.014*
N status	0.634	1.885	1.329	2.674	<0.0001*
Grade	0.910	2.485	1.471	4.198	0.001*
pEphA2	1.884	6.579	3.085	14.030	<0.0001*
p-cMET	1.805	6.049	3.048	13.894	<0.0001*
VM	2.082	8.021	3.774	17.048	<0.0001*
pEphA2 and VM dual positive	1.967	7.152	3.506	14.588	<0.0001*
pMET and VM dual positive	1.988	7.268	4.547	15.152	<0.0001*

Table 8: Univariate analysis for OS

Disease Free Survival

Variables	HR	P values	95% CI	
			Lower	Upper
Tumour stage	1.043	0.933	0.391	2.781
Nodal status	1.220	0.257	0.865	1.722
Grade	2.493	0.028*	1.102	5.641
VM Only	6.005	0.001*	2.002	18.018
pEphA2 Only	4.342	0.002*	1.717	10.983
pMET Only	4.526	0.002*	1.768	11.235
VM and pEphA2 dual positive	0.365	0.145	0.094	1.414
VM and pMET dual positive	0.415	0.182	0.084	1.318

Table 9: Multivariate Cox proportionality hazard model on DFS

Variables	Overall Survival			
	HR	P values	95% CI	
			Lower	Upper
Tumour Stage	1.149	0.799	0.394	3.347
Nodal status	1.237	0.303	0.825	1.854
Grade	2.418	0.046*	1.017	5.751
VM only	11.654	<0.0001*	3.195	42.508
pEphA2 only	5.853	0.006*	1.663	20.602
pMET only	5.961	0.005*	1.798	20.855
VM and pEphA2 dual positive	0.195	0.052	0.038	1.013
VM and pMET dual positive	0.209	0.065	0.049	1.026

Table 10: Multivariate Cox proportionality hazard model on OS.

Discussion

EphA2 is over-expressed in 60 to 80% of the breast cancer cases[145], [146]. Over-expressed EphA2 receptors physically interact with the epidermal growth factor receptor (EGFR)and ErbB2, resulting in the promotion of RhoA GTPase and ERK activity[146], [147]. This suggests that the EphA2 receptor regulates tumor progression via crosstalk with several other oncogenic pathways most likely via a ligand-independent mechanism [148]. Several reports also implicate EphA2receptor in the promotion of epithelial–mesenchymal transition(EMT) and the stemness of cancer stem-cell-like populations[149]–[151]. EphA2 ligands induce the EphA2 tyrosine kinase activity which in turn inhibits cancer cells, whereas Akt mediates the phosphorylation of EphA2 on Ser-897 ina tyrosine kinase-independent manner in inducing human glioblastoma malignancy [119]. This particular ligand-independent activation of the EphA2 receptor has been exclusively implicated in tumor progression and metastasis[152]. HGF, also known as scatter factor, was first discovered as a fibroblast-derived cell motility factor and a hepatocyte growth factor. 69-kDa alpha-chain and 34-kDa beta-chain subunits of HGF form a heterodimer that is joined by a disulfide bond. HGF can encourage mitosis, cause cell migration and separation, and stimulate the morphogenesis of epithelial cells. Additionally, it can promote the development of vascular endothelial cells and heighten the hydrolysis of extracellular matrix proteins [153]. Cellular MET deregulation is caused by MET-receptor over-expression, chromosomal amplification, mutation, or alternative splicing. Clinical studies on several MET-targeting drugs have shown findings that range from pronounced failure to very good response rates [154]–[157].In our study, we found a strong correlation betweenphospho-EphA2 (S897) and phospho-MET-positive expression with nodal status and poor NPI, indicating the dissemination potential contributed by this particular phosphorylation pattern of theEphA2 and c-MET receptors. There was negative association of

phospho-EphA2 (S897) and phospho-MET with ER status and no significant association between PR and HER2 expression profiles. Incidentally, the positive expressional status of phospho-EphA2 (S897) and phospho-MET were observed significantly higher in the TNBC cohort thus implying important targets for therapy for TNBC cases. Phosphorylation at this S897 residue of the EphA2 receptor and phospho-MET were also observed to be significantly higher in the VM positive cohort indicating a strong correlation of the events with the occurrence of VM. Relevant markers namely, phospho-MET, phospho-ERK 1/2 and Laminin 5Y2 expression were also positively correlated suggesting the regulatory role of this particular phosphorylated EphA2 receptor and its signaling network to influence VM formation. In recent times, anti-cancer therapeutic modalities involving anti-angiogenic drugs are in clinical development [158], [159]. Although patients show clinical benefit from the drugs that target angiogenic proteins like vascular endothelial growth factor, their short-term response and limited efficacy pose a great challenge [159]. This failure of anti-angiogenic therapies is attributed to the occurrence of VM as it provides an alternative intra-tumoral perfusion network which compensates for the lack of angiogenesis and thus promotes tumor aggressiveness even when the tumor is under the pressure of anti-angiogenic drugs. VM has also been found to regulate chemoresistance in various aggressive cancers including cancer of the breast [140]. Breast cancer is known for its diverse histological subtypes having different molecular features and biological behaviors which ultimately impact the response to therapy [160]. Progression of this cancer is influenced by various host and tumor-related factors like tumor grade, size, nodal status and ER, PR and HER2 expression [161]. In spite of these vast arrays of classifications, there is an urgent need to find relevant prognostic markers that might help pave the way for rational treatment regimens at individualized level. Here, we evaluated the implications of VM in association with phospho-

EphA2(S897) and phospho-MET expression with patient survival and prognosis of the disease. We found that the prevalence of VM was significantly higher in the higher lymph node metastasis group and with poor NPI, similar to phospho-EphA2 (S897) expression. VM was also negatively correlated with ER, PR status with no significant difference in the HER2 group. Notably, the occurrence of VM was significantly higher in the triple-negative breast cancer cohort. In case of VM/phospho-EphA2 (S897) and VM/phospho-MET dual-positive cohorts, significant associations with tumor grade, size, lymph node status, NPI and the markers phospho-ERK 1/2 and Laminin 5Y2 were observed. In the survival analysis, both the VM-positive and phospho-EphA2 (S897) and VM-positive and phospho-MET-positive cohorts had lower DFS and OS with the lowest survival time observed in the VM/phospho-EphA2 (S897) or VM/phospho-MET dual-positive cohort. In the multivariate analysis, VM and phospho-EphA2 (S897) and VM and phospho-MET proved to be independent risk factors for DFS and OS. However, the dual-positive cohort was not significant enough to be an independent risk factor. This suggests that the presence of VM and phosphorylation of the S897 residue of EphA2 and phosphorylation of the MET receptor in a spatial setting are detrimental factors in breast cancer patients.



CHAPTER B

To determine the expressional regulation of the c-MET and Ephrin pathways influencing Vasculogenic mimicry in breast cancer.

Introduction:

Breast cancer is currently the most commonly diagnosed cancer worldwide and the 5th leading cause of cancer-related deaths due to cancer[162]. Approximately 10–20% of all breast cancers are found to be triple negative breast cancer (TNBC) subtype, which is often associated with very poor prognosis even at early stages of the disease. Over the last few decades, enormous efforts have been made to understand the underlying molecular mechanisms and improve the clinical scenario, including new molecular subtypes and new generation therapeutic modalities and overall survival remains low[163].

Among the conventional therapies, the National Comprehensive Cancer Network (NCCN) guidelines recommend using combination regimens based on Cyclophosphamide, Anthracycline, Taxane, Fluorouracil and Cisplatin[46]. Unfortunately, all these drugs have severe adverse effects while conferring low and temporary responses. Fluorouracil, despite being an important component of chemotherapy regimens, is more likely to cause nausea, myelosuppression, and ovarian failure[164]. Moreover, not all individual agents in combination chemotherapy uniformly and consistently exert anticancer cytotoxic responses in a synergistic fashion for all patients where regimens show clinical benefits[165], [166]. With these existing challenges, there is an urgent unmet need for the development of more effective drug combinations that have bearable side effects and, at the same time, durable and deep responses against TNBC and other similar molecular subtypes. Elucidation of viable TNBC targets is an obstacle that needs to be overcome. c-MET and EphA2 may be considered viable targets for TNBC, as these RTKs show robust expression in this subset of breast cancer[167]–[169].

The Hepatocyte growth factor receptor (HGFR), also known as c-MET, is a receptor tyrosine kinase (RTK) encoded by c-MET gene. Aberrant c-MET signaling has been mechanistically linked to the promotion of breast cancer, and its perturbation represents an aggressive phenotype[170]. Among all breast cancers, c-MET is overexpressed in 20%–30% of the cases and is more prevalent in TNBC, where 52% of patient tumors express this critical alteration. Drugs that target the oncogenic c-MET pathway are effective against many cancers, including TNBC. Indeed, to maximize anti-c-MET efficacy in personalized settings, further trial designs based on biomarker-guided patient stratification are part of a smart and rational combination selection approach [171], [172]. The downstream effect of c-MET activation relies on canonical signaling modulators that are common in many receptor tyrosine kinases, and mechanistically include activation of the nodal mitogen-activated protein kinase (MAPK) cascades[13], [14], which contextually induces the degradation of matrix proteins, promotion of cell migration, and sustained tumor proliferation [175], [176]. Significant cross-talk exists between the c-MET pathway and other signaling pathways. A key mechanism of tumor development and treatment resistance has been identified as interactions involving members of the MET and HER2 families. Additionally, it has been demonstrated that MET signaling interacts with the VEGF and VEGF receptor (VEGFR) pathways. VEGF-A expression is increased by MET activation to support angiogenesis and endothelial cell development [177].

In a complex RTK network, Ephrin type-A receptor 2 (EphA2) is another complementary onco-protein that is over-expressed in human breast tumors and associated with poor prognosis[178]. From these perspectives, like c-MET, oncogenic EphA2 may underpin critical dysregulation and may act as a clinically actionable driver, influencing the clinical progression of TNBC and may further facilitate angiogenesis, migration, invasion/metastasis, and eventual

treatment resistance. Preclinical evidence supporting this hypothesis revealed that, in MDCK cells, HGF, upon binding to its cognate receptor c-MET, leads to the activation of EphA2 at the S897 residue, which is a non-canonical form of activation for this receptor [132]. Phosphorylation of EphA2 at this specific residue in breast cancer patients leads to reduced overall survival (OS) and disease-free survival (DFS) and has the potential to act as an independent prognostic indicator [179]. Both c-MET and EphA2 receptors respond to HGF-mediated activation and involve the downstream activation of effector molecules, leading to similar phenotypic modulations. In this study, we aimed to delineate the possible crosstalk that occurs between these two signaling axes and evaluate the drugs that can target the perturbation.

Materials and methods:

Patient data and samples

Retrospective clinicopathological and survival data of 135 patients with triple-negative breast cancer (TNBC) were collected from the epidemiology department of the Chittaranjan National Cancer Institute, Kolkata. All relevant patient data were collected and anonymized prior to the analysis. The actual screening method, along with the exclusion and inclusion criteria during patient selection, is shown in Fig. 10. The TNBC patient cohort (Table 11) (N=135) was then stratified into two groups based on the adjuvant therapy they received. One group received 5-Fluorouracil (5FU) containing standard of care (SOC) (5FU, Epirubicin and Cyclophosphamide), and the other group received SOC without 5FU (Doxorubicin, Docetaxel and Cyclophosphamide or Paclitaxel). After a follow-up period of 5 years, cases of recurrence were recorded, and Kaplan-Meier survival plots for disease-free survival (DFS) were prepared. Of the 45 (33.33%) recurrent cases, 35 archived formalin-fixed paraffin-embedded (FFPE) blocks containing

recurrent cancerous tissue were collected for future use. This study was approved by the Institute Ethical Committee and the Declaration of Helsinki ethical standards, and its later amendments were strictly adhered to.)

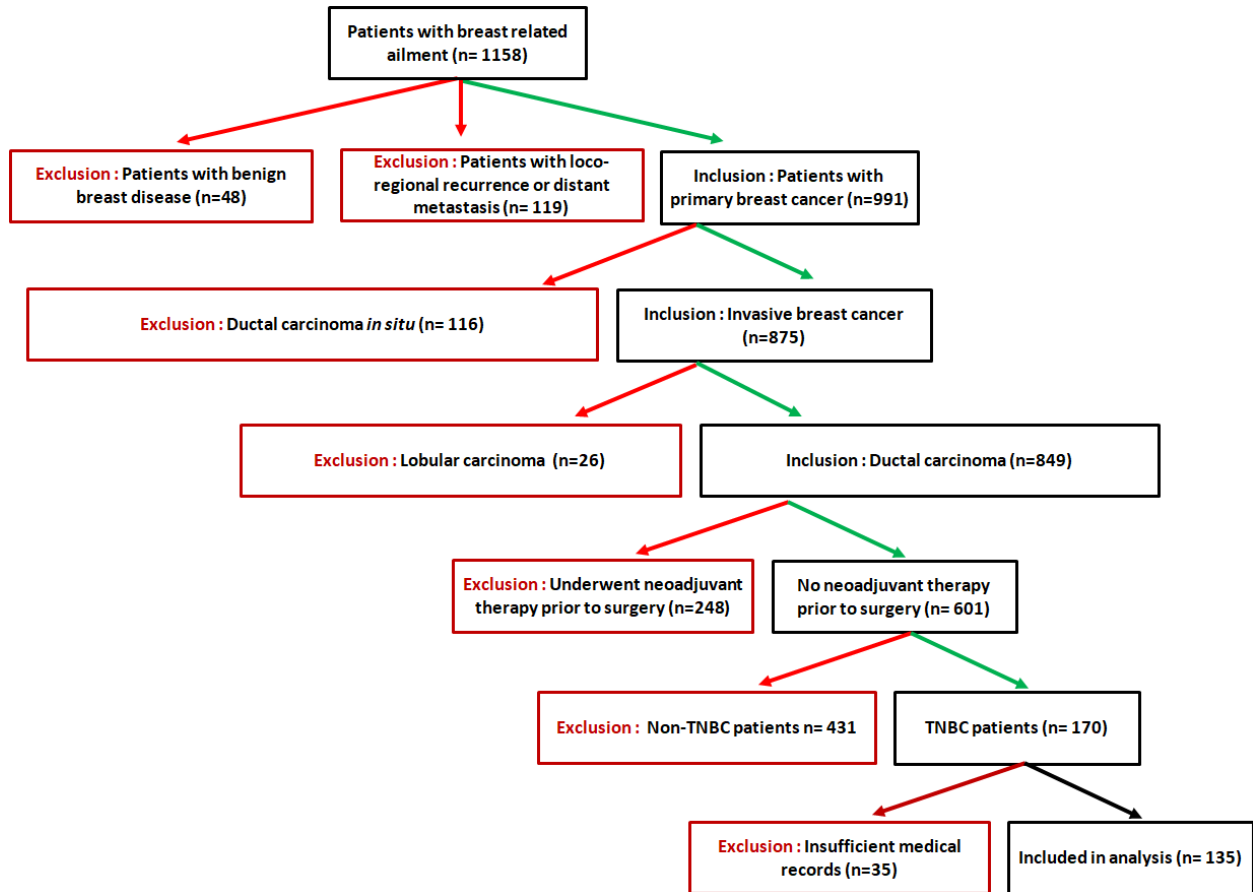


Fig. 10: Flow chart describing the inclusion/exclusion criteria of patients in our study (II)

Parameters	N (%)
Age at diagnosis (years)	
= 50	64 (47.41)
>50	71 (52.59)
T stage	
T1	41 (30.37)
T2	35 (25.92)
T3	25 (18.52)
T4	34 (25.19)
N stage	
N0	64 (47.41)
N1	45 (33.33)
N2	16 (11.85)
N3	10 (7.41)

Table 11: Demographic and pathological profiles of TNBC patients (N=135)

***Ex vivo* tumor fragment culture:**

Fresh TNBC tissues were collected in two phases (N= 15), which were then utilized for patient-derived ex vivo explant cultures. The tissues were sliced into 3 mm³ pieces and cultured in RPMI 1640 medium (Gibco, Life Technologies, USA) containing 8% FBS or HGF and 2% autologous serum. 5FU were added to the treatment arm and incubated for 48 h at 37°C in a 5% CO₂ atmosphere on an orbital shaker at 20 rpm. Each patient’s healthcare records were consulted to gather pertinent clinicopathological and demographic data (Table 12).

Parameters	N (%)
Age at diagnosis (years)	
= 50	6 (40)
>50	9 (60)
T stage	
T1	3 (20)
T2	7 (46.67)
T3	2 (13.33)
T4	3 (20)
N stage	
N0	8 (53.34)
N1	5 (33.33)
N2	2 (13.33)
N3	0 (0)

Table 12: Demographic and pathological profiles of TNBC patients (N=15) used for ex vivo explant culture.

Immunohistochemistry staining:

Tumor slices were fixed in 10% buffered formalin, and formalin-fixed paraffin-embedded (FFPE) blocks were prepared after 24 h of fixation. FFPE blocks were sectioned (4 μ m) and immunohistochemical (IHC) staining was performed using an IHC kit (DAB 150, Merck) following the manufacturer's protocol. The slides were visualized under a bright-field microscope (Carl Zeiss), and images were captured using Zen software. IHC Scoring was performed as previously described [179]. The primary antibodies used are as follows, rabbit polyclonal anti Ki67 (1:100 dilution) and rabbit polyclonal anti cleaved- Caspase3c (Asp175, p17) (1:100 dilution) from Affinity Biosciences, rabbit polyclonal anti MET (clone c28; 1:100 dilution), rabbit polyclonal anti p-Met (Tyr 1349) (1:100 dilution) from Santa Cruz Biotechnology, rabbit monoclonal anti EphA2 (clone D4A2; 1:200 dilution), rabbit monoclonal anti Phospho-EphA2 (Ser897) (clone D9A1; 1:100 dilution) and rabbit monoclonal anti Phospho-p44/42 MAPK (Erk1/2) (Thr202/Tyr204) (clone D13.14.4E; 1:200) from Cell

Signaling Technology, mouse monoclonal anti MMP-2 (clone 8B4; 1:100 dilution; Novus biological), mouse monoclonal anti Laminin- 5 (Y2 chain)(clone D4B5; 1:50 dilution; Merck).

Cell culture and reagents:

The TNBC cell line MDA-MB-231 was procured from NCCS Pune (INDIA). The murine TNBC cell line 4T1 (containing stable expression of the luc2 gene) was a gift from Dr. Rathindranath Baral, Department of Immunoregulation and Immunodiagnostics, Chittaranjan National Cancer Institute, Kolkata. MDA-MB-231 and 4T1 cells were cultured in DMEM containing high glucose and RPMI 1640 media (Gibco, Life Technologies, USA) respectively. The medium was supplemented with 10% FBS (Gibco, Life Technologies, USA) and 1% penicillin-streptomycin (Gibco, Life Technologies, USA) and the cells were maintained in a humidified incubator at 37°C with a constant 5% carbon dioxide environment. Purified Lupeol (S957712), 5-Fluorouracil (5FU) (F6627), human HGF (H9661) from Sigma Aldrich, and recombinant mouse HGF protein (2207-HG-025/CF, R&D Systems) were used for further experiments.

siRNA transfection:

c-MET and EphA2 are overexpressed in both the MDA-MB-231 and 4T1 cells [180]–[185]. siRNAs targeting the human c-MET (ON-TARGET plus Human MET (4233) siRNA-SMARTpool, cat# L-003156-00-0005) and human EphA2 (ON-TARGET plus Human EphA2 (1969) siRNA-SMARTpool, cat# L-003116-00-0005) genes were purchased from Dharmacon (Lafayette, CO, USA). In addition, siRNAs targeting Mouse Met (ON-TARGET plus Mouse Met (17295) siRNA-SMARTpool, cat# L-040878-00-0005) and Mouse EphA2 (ON-TARGET plus Mouse EphA2 (13836) siRNA-SMARTpool, cat# L-040412-00-0005) were obtained. A

non-targeting pool (NTP) (ON-TARGETplus Non-targeting Pool, cat# D-001810-10-05) was used as the negative control. In vitro JetPRIME transfection reagent (Polyplus) was used to transfect these siRNAs individually or simultaneously into MDA-MB-231 and 4T1 cells, according to the manufacturer's protocol[186]. Western blot analysis was performed to confirm the knockdown. Various concentrations of siRNAs were transfected, and the concentration that achieved maximum silencing was used for further experiments.

In vivo intratumoral knockdown was performed by combining siRNAs (10µg) targeting murine EphA2 and MET with in vivo-jet PEI (1.2µl) and 5% solution of Sucrose (50µl) [187]. Initial delivery was performed when the tumor volume reached approximately 40-60 mm². Four doses of siRNAs were given to each mouse every other day and were sacrificed 3 days after the last injection.

Pharmacological regulation:

ALW-II-41-27 (Cayman) (0.5µM)[188] and Cabozantinib (Apexbio) (2 µM) [189] was used as specific pharmacological phosphorylation inhibitors targeting EphA2 and c-MET respectively. HGF (100ng/ml)[190] was applied to cells for 15 min prior to the experimental endpoint. Western blot analysis was performed to confirm inhibition/activation.

Western blotting:

Western blotting was performed as previously described [191]. The primary antibodies used are as follows: rabbit polyclonal anti MET (clone c28; 1:200 dilution) and rabbit polyclonal anti p-Met (Tyr 1349) (1:200), rabbit polyclonal anti E-cadherin (clone H-108; 1:200), mouse monoclonal anti Vimentin (clone V9; 1:200) from Santa Cruz Biotechnology, rabbit monoclonal anti EphA2 (clone D4A2; 1:1000), rabbit monoclonal anti Phospho-EphA2 (Ser897) (clone

D9A1; 1:1000), rabbit monoclonal anti Phospho-p44/42 MAPK (Erk1/2) (Thr202/Tyr204) (clone D13.14.4E; 1:2000) from Cell signaling Technology, rabbit polyclonal anti- ERK1+ERK2 antibody (1:1000; Abcam), mouse monoclonal anti MMP-2 (clone 8B4; 1:1000), mouse monoclonal anti Twist-1 (clone 10E4E6; 1:1000), mouse monoclonal anti slug (clone 4B6D5; 1:1000) and mouse monoclonal anti Snai1 (clone 20C8; 1:1000) from Novus Biological, mouse monoclonal anti Laminin- 5 (Y2 chain)(clone D4B5; 1:500; Merck). The secondary antibodies used for western blotting were goat anti-rabbit polyclonal IgG (1:20000) and rabbit anti-mouse polyclonal IgG (1:40000) from Sigma. The protein bands were visualized using ECL (BIO-RAD) and captured in a ChemiDoc XRS (BIO-RAD), followed by analysis using ImageJ software.

Transwell invasion and migration:

Transwell inserts (Corning) with a pore size of 8 μm were used in this experiment. The inserts were coated with growth factor-reduced Matrigel (Corning) for the invasion assays. Transfected and knocked down MDA-MB-231 cells (1×10^5) were initially seeded into Transwell inserts containing serum-free media. Pharmacological inhibitors, Lupeol, 5FU or both were also added to the respective inserts. The lower chamber contained media containing HGF (100 ng/ml), which acts as a chemotactic factor. After incubation for 48 h, the inserts were collected. The migrated and invaded cells present on the lower side of the insert were fixed in methanol, stained with crystal violet, and visualized using a bright-field microscope (Carl Zeiss).

Mammosphere formation assay:

MDA-MB-231 cells (1×10^3) were seeded into each well of ultra-low attachment 96 well plates in mammosphere forming media (serum-free DMEM high glucose media with 100 ng/ml HGF, 1X

B27 supplement and 5 µg/ml Insulin). Post-transfection and knockdown with pharmacological inhibitors, single agent Lupeol, 5FU or both in combination were added. The plates were incubated for 7 days without any disturbance, and the formed mammospheres were observed. The primary mammospheres were dissociated, and single cells were subsequently seeded for evaluation of secondary mammosphere formation and further incubated for a week. Images were obtained using an inverted light microscope (Olympus).

Tube formation assay:

Each well of a 96 well plate was coated with growth factor-reduced Matrigel. 1×10^3 transfected and knocked down MDA-MB-231 cells were seeded in each coated well. HGF, pharmacological inhibitors, Lupeol, 5FU, or both were added to the respective wells and incubated for 3 days to observe their effect on the tube-forming capability of the cells. The tubes were then visualized under an inverted light microscope (Olympus). AngioTool v0.6a software was used to quantify the total vessel length and number of junctions in the tubes formed in various groups.

In vivo experiments

Initially, siRNA-mediated c-MET, EphA2, or dual knockdown 4T1 cells (1×10^6) were injected into the abdominal mammary fat pads of BALB/c mice, following a previously described protocol [192]. Tumor growth was observed every other day by injecting the mice with XenoLight D-Luciferin, Potassium salt (Product no.:122799, Perkin Elmer). In vivo live animal imaging was performed using an IVIS Lumina in vivo imaging system (PerkinElmer). From the 5th day, the mice in all groups except the control group were treated with mouse HGF (10 µg/g/week)[193]. At ethical endpoints, the mice were sacrificed and the tumors were harvested. Similar regimens were followed for combinatorial studies, with Lupeol (20 mg/kg/2

days) (intraperitoneal)[194] and/or 5FU (10 mg/kg/2 days)[195] (intraperitoneal), as well as mouse HGF. In addition, initial cytotoxicity studies with the above-mentioned treatment regimens were conducted in non-tumor-bearing BALB/c mice.

Statistical analysis:

Each experiment was performed in triplicate. GraphPad Prism software version 7.0 was used for all statistical analyses, and data are represented as mean \pm SD (Intuitive Software for Science, San Diego, CA, USA). Chi-square test and one- or two-way ANOVA ($p < 0.05$) were used to compare all of the studies, followed by post-tests using Bonferroni or Tukey's test. Survival curves were computed by the Kaplan–Meier method and the differences in survival time (months) was compared using the Log-rank test. These statistical analyses were conducted using the SPSS 17 software (SPSS Inc, Chicago, IL, USA). P value less than 0.05 was considered to be significant.

Results:

5- Fluorouracil non-response and delineation of its underlying mechanism

From our follow up study and the Kaplan-Meier plot for disease-free survival (Fig. 11A), it was observed that there was a significant difference (log rank [Mantel-Cox] = 4.405; $P = 0.036$) in disease-free survival between the cohort that received 5FU containing SOC and the cohort that received other SOC not containing 5FU. The mean (95% Confidence Interval [CI]) DFS time of patients who received 5FU SOC was 49.517 ± 3.302 months (43.045-55.988) and that of other SOC was 58.982 ± 3.210 months (52.690-65.274). Archived tumor blocks of recurrent tissues were collected and probed for the phosphorylation status of EphA2 and c-MET (Fig. 11B), these two RTKs have been extensively implicated in drug resistance, poor patient prognosis, and

survival in various cancer models, including TNBC [167], [169], [178], [179], [196]–[198]. Notably, both EphA2 (P=0.001) and c-MET (P=0.032) were significantly more phosphorylated in the 5FU based SOC treated cohort (Tables 13 and 14). Next, fresh TNBC samples were collected and cultured for 48 h under sterile conditions, and the samples were exposed to 5FU in the presence of HGF (Fig. 11C). Subsequently, tumor blocks were prepared by probing for Ki67 and Caspase 3c revealed two distinct cohorts. The cohort where there was a significant difference in the expression patterns of Ki67/Caspase 3c among the various treatment arms were designated as the “responders” (Fig. 11D) and where there was no significant difference were the “non-responders” (Fig. 11E). Graphs representing the IHC scores vs. the various treatment arms are shown in Fig. 12. Furthermore, we checked for the phosphorylation status of EphA2 and c-MET and found that they were significantly more phosphorylated in the non-responders even after exposing the tissue to 5FU (Fig. 11F) (Tables 15 and 16). This sheds light on the underlying mechanism of treatment failure and non-response to 5FU containing SOC, and the activated status of EphA2 and c-MET in the presence of HGF may be implicated in the same

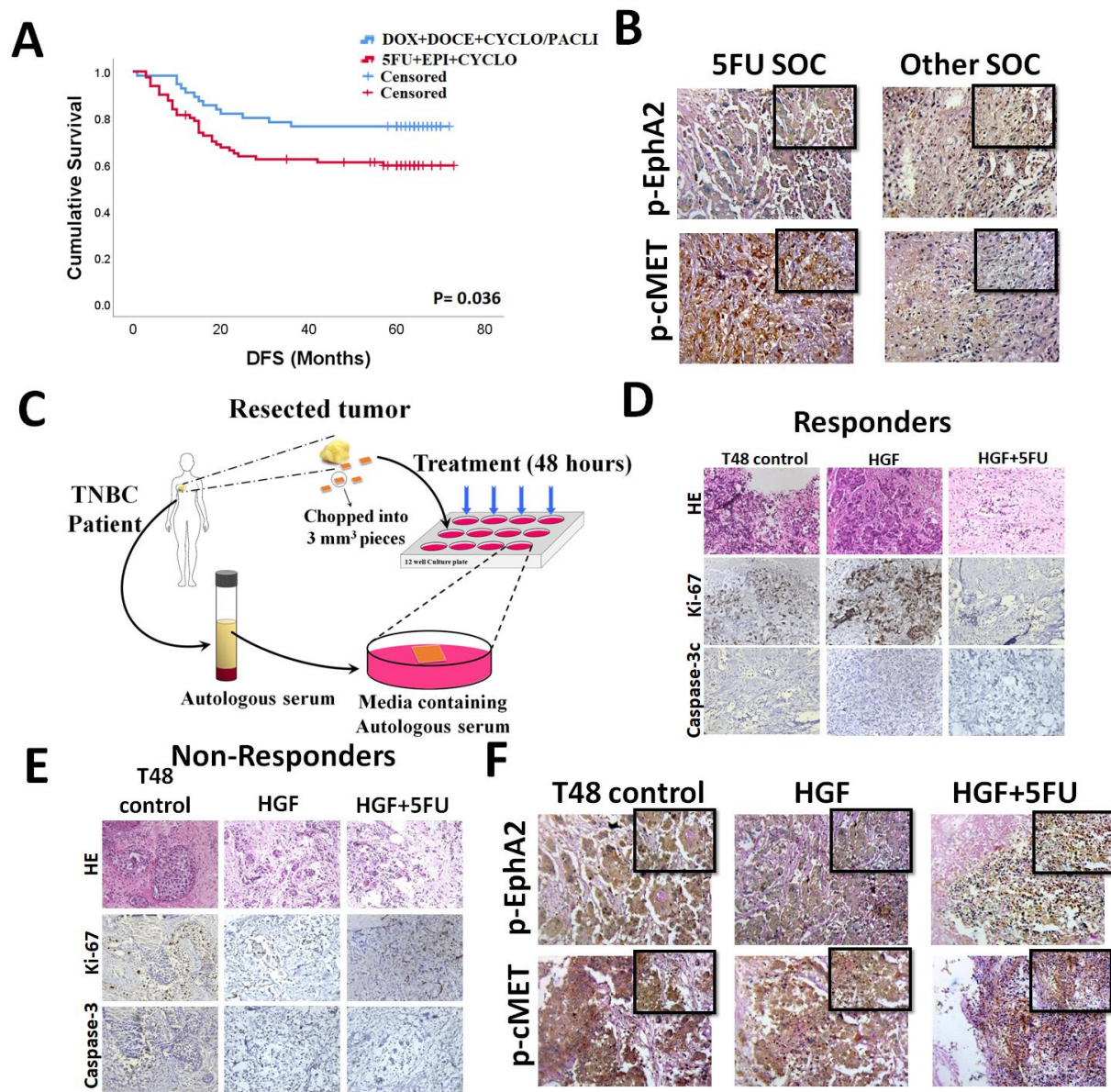


Fig. 11: Treatment failure and evaluation of the underlying mechanism of non- response in TNBC recurrence, post treatment with 5FU. (A) Survival curve of DFS in TNBC patients with differential treatment regimens, one SOC containing 5FU and the other cohort received SOC without 5FU. (B) Differential expression of phospho-EphA2 and phospho-c-MET in recurrent TNBC tissue. (C) Schematic representation of ex vivo explants culture (D and E) Differential expression of Ki67 and Caspase 3c in TNBC patient derived ex vivo explants cultures, stratifying the cohort into responders and non- responder population. (F) Expressional status of phospho- EphA2 and phospho-MET in the non-responder population from explants cultured tissues. All images were captured at 200X magnification (400X magnification in inset). Data are representative of triplicate experiments. * $p < 0.05$ represents statistically significant difference.

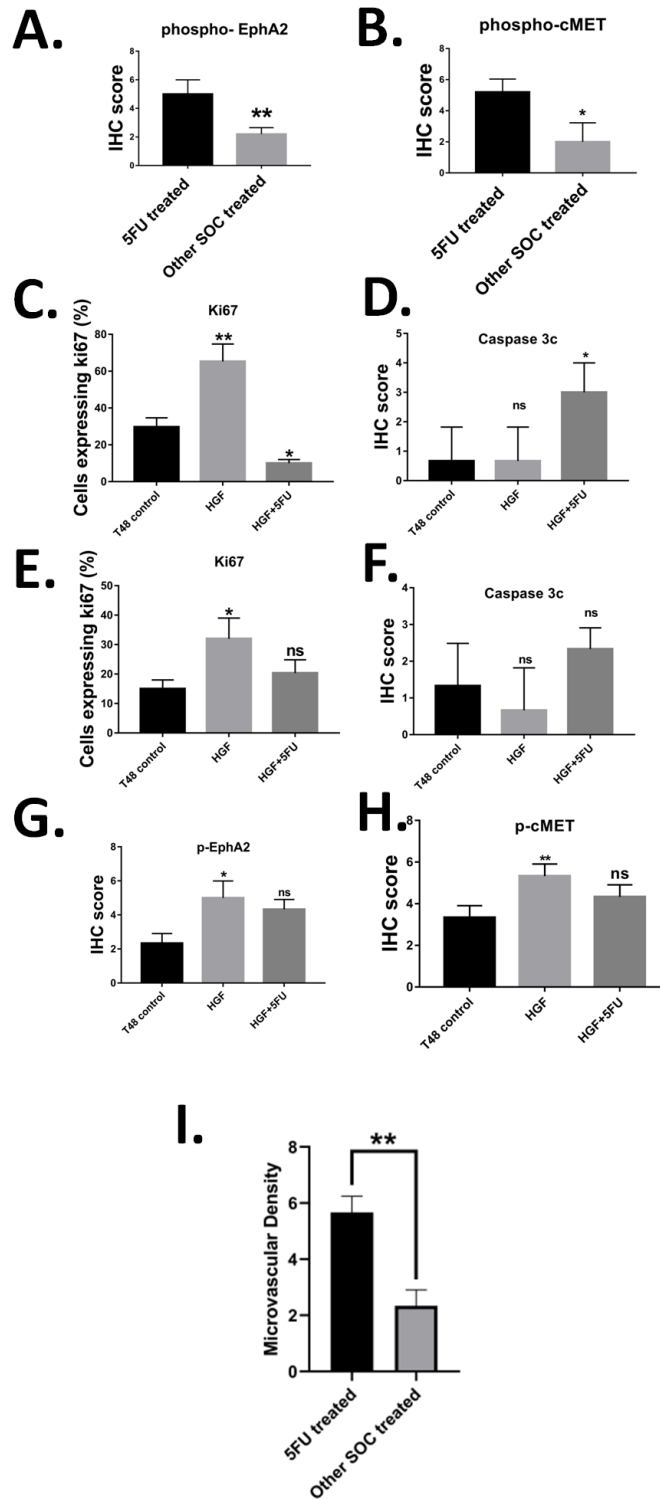


Fig. 12: Graphs representing the IHC scores vs various treatment arms and also microvascular density. A) and B) Graphs representing the differential IHC score of phospho-EphA2 and phospho-c-MET respectively in the 5FU treated and other SOC treated group. C) Ki67 in responders, D) Caspase 3c in responders, E) Ki67 in non-responders, F) Caspase 3c in non-responders, G) and H) phospho-EphA2 and phospho-c-MET in non-responders. I) Microvascular density

	pEphA2 positive	pEphA2 negative	P value
5FU treated [N (%)]	24 (75)	8 (25)	
Other SOC [N (%)]	3 (23.08)	10 (76.92)	0.001271*

Table 13: Association between the differential expressional status of phospho-EphA2 in the 5FU/Other SOC treated cohort. *p<0.05 was considered to be statistically significant.

	p-cMET positive	p-cMET negative	P value
5FU treated [N (%)]	21 (75)	11 (25)	
Other SOC [N (%)]	4 (23.08)	9 (76.92)	0.032944*

Table 14: Association between the differential expressional status of phospho-c-MET in the 5FU/Other SOC treated cohort. *p<0.05 was considered to be statistically significant.

	Non- responder	responder	P value
pEphA2 levels not changed [N (%)]	7 (75)	1 (25)	
pEphA2 levels decreased [N (%)]	2 (23.08)	5(76.92)	0.020*

Table 15: Association between the differential expressional status of phospho-EphA2 levels in the responder and non-responder groups. *p<0.05 was considered to be statistically significant.

	Non- responder	responder	P value
pMET levels not changed [N (%)]	8 (80)	2 (20)	
pMET levels decreased [N (%)]	1 (25)	4(75)	0.025*

Table 16: Association between the differential expressional status of phospho-c-MET levels in the responder and non-responder groups. *p<0.05 was considered to be statistically significant.

Dual knockdown of c-MET and EphA2 signaling exhibits reversal of aggressive phenotype in TNBC cells

Prior evidence highlighting that both c-MET and EphA2 surface receptors are upregulated in TNBC cells provides a suitable model for evaluating the potential crosstalk between these receptor signaling pathways [180]–[182]. To investigate the possible crosstalk between the c-MET and EphA2 signaling axes in TNBC cells, we utilized siRNA-mediated silencing of targets in both MDA-MB-231 and 4T1 cell lines. Upon transfecting the cells with various concentrations of the siRNA, maximum inhibition of protein expression was demonstrated at 150 nM concentration of both c-MET and EphA2 siRNAs in both cell lines (Fig. 13). Additionally, specific phospho-c-MET inhibitors (cabozantinib) and phospho-EphA2 inhibitors (ALW-II-41-27) were used as pharmacological antagonists. A dual silencing strategy was adopted in which the cells were subjected to concurrent knockdown of c-MET and EphA2. In parallel, cells were treated with c-MET and EphA2 inhibitors together in a separate group. All groups, apart from the control groups (vehicle control and NTP as negative control), were subsequently treated with HGF (100 ng/ml) for 15 min prior to cell lysate preparation. Western blot analysis revealed that HGF induced phosphorylation of both c-MET and EphA2 receptors and resulted in the upregulation/activation of key downstream molecules, namely, phospho-ERK1/2, MMP2 and Laminin-5Y2 (Fig. 14A). Notably, phosphorylation of EphA2 was specifically detected at S897, a selective kinase active site that has been implicated in promoting tumorigenic activity and activation of the ERK1/2 cascade, leading to increased cellular plasticity, ECM remodeling, and evasion of apoptosis [132], [199]. Upon individual knockdown of either c-MET or EphA2 in the presence of HGF, the residual constitutive expression of downstream molecules was observed. This tonic signal was entirely abolished in the dual knockdown and inhibitor groups, suggesting

the presence of a compensatory downstream cascade. Further ascertaining the functional consequences of this perturbation, dual knockdown groups displayed maximum potency in preventing cellular migration and invasion when compared to individual knockdown groups in the presence of HGF (Fig. 14B, Fig. 14C) (Fig. 15 A and B). A schematic diagram of the mammosphere formation assay is shown in Fig. 16D. Similar effects were observed in the mammosphere and Matrigel tube formation assays upon HGF treatment in cells with complete knockdown or inhibition (Fig. 14E and F) (Fig. 15 C and D). The relative mammosphere formation efficiency was compromised in the dual knockdown groups, indicating that inhibiting only the c-MET or EphA2 axis in the presence of HGF is not sufficient to completely abrogate sphere formation. Similarly, the total number of intracellular junctions and the total vessel length drastically reduced as the cells were impaired to form proper tube-like structures in Matrigel in the dual knockdown groups, compared to individual knockdown groups (Fig. 15 E and F).

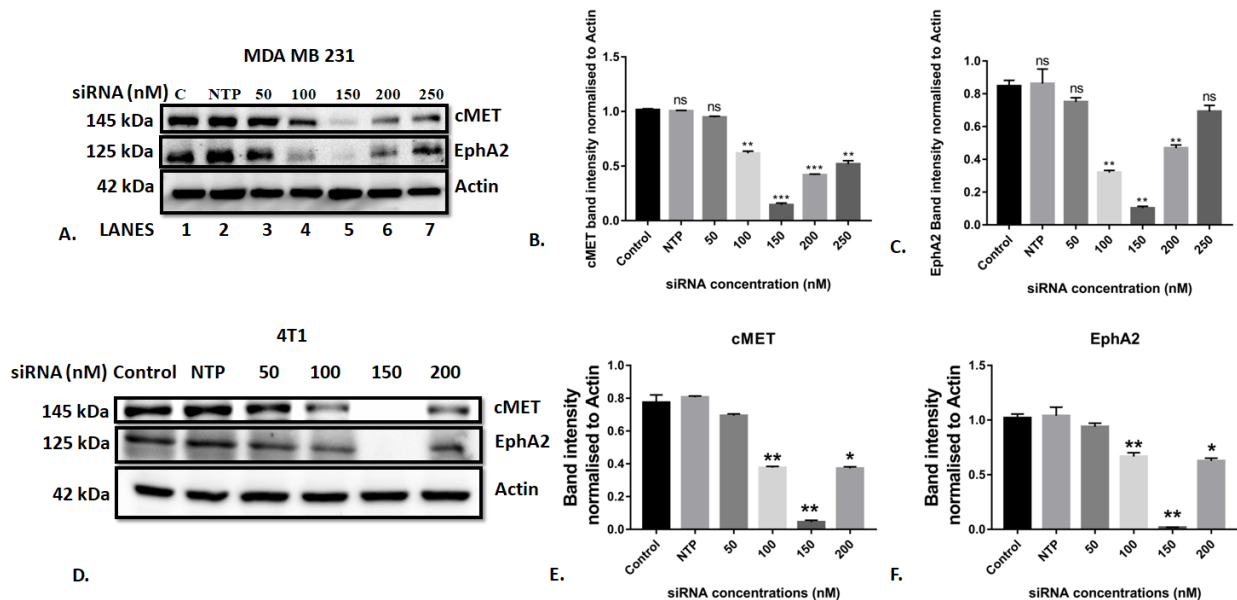


Fig. 13: Representative image depicting evaluation of siRNA mediated silencing by Western blot post-transfection. A) Western blot bands of c-MET and EphA2 post-silencing at various concentrations on MDA MB 231 cells. B) and C) Graph depicting normalised band intensity of c-MET and EphA2, respectively, post-transfection with siRNA at various concentrations. Actin was used as loading control. D) Western blot bands of c-

MET and EphA2 post-silencing at various concentrations on 4T1 cells. E) and F) Graph depicting normalised band intensity of c-MET and EphA2, respectively, post-transfection with siRNA at various concentrations. Actin was used as loading control. Data are representative of triplicate experiments (mean \pm SD). *p<0.05, **p<0.02 and ***p<0.001 statistically significant difference compared to corresponding control.

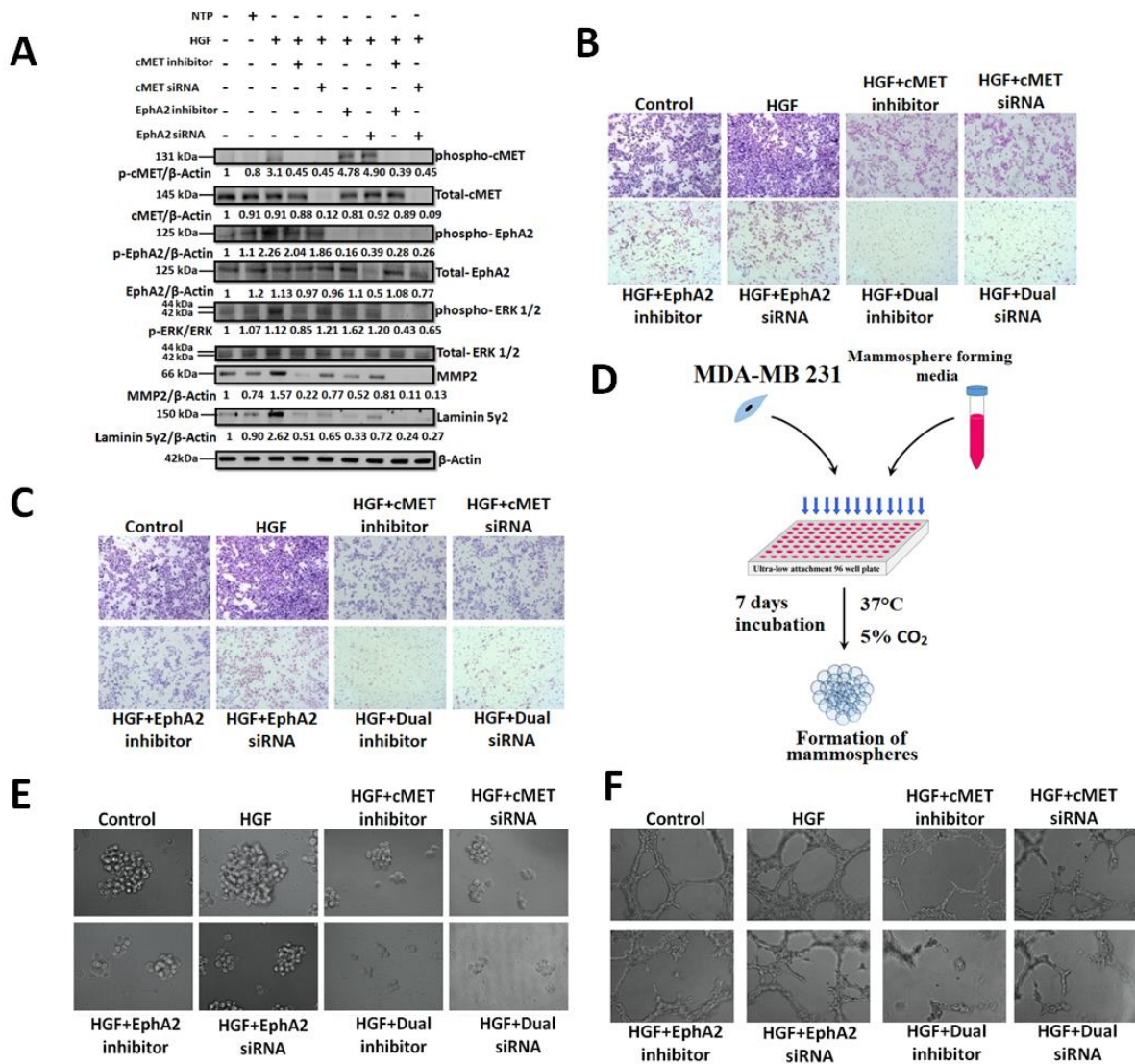


Fig. 14: Evaluation of the effect of individual and dual knock down of c-MET and EphA2 genes on MDA MB 231 in the presence of HGF (A) c-MET and EphA2 knockdown/inhibition and its effect on downstream effectors on MDA-MB-231 cells was analysed by western blot. (B) Transwell migration assay post knockdown/inhibition of c-MET or EphA2 or both and HGF as a chemotactic factor on MDA-MB-231 cells. (C) Transwell invasion assay post knockdown/inhibition of EphA2 and c-MET or both and HGF as a chemotactic factor on MDA-MB-231 cells. (D) A schematic representation of the mammosphere formation assay. (E) Mammosphere formation assay post knockdown/inhibition of c-MET or EphA2 or both in the presence of HGF. (F) Matrigel tube formation assay post knockdown/inhibition of c-MET or EphA2 or both in the presence of HGF. All images were captured at 100X

magnification. Data are representative of triplicate experiments (mean±SD). *p<0.05 statistically significant difference compared to corresponding control.

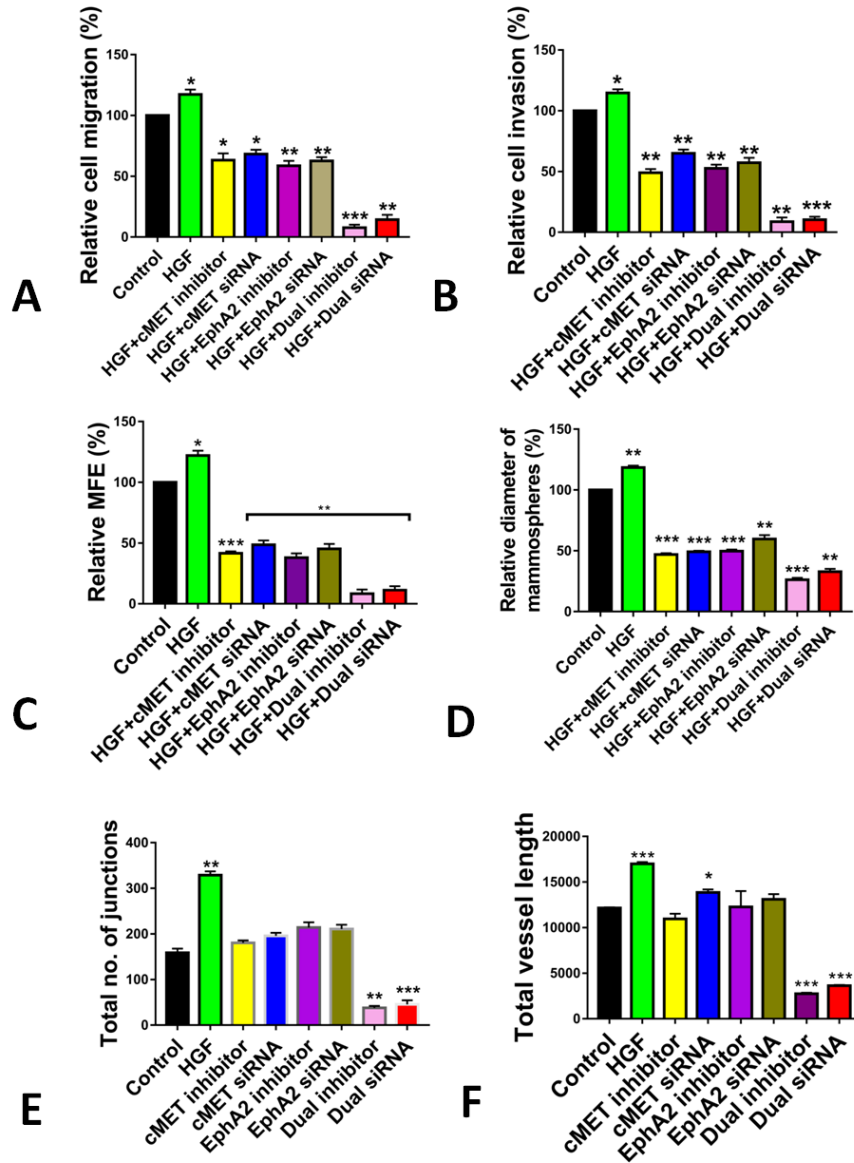


Fig. 15: Graphs pertaining to Fig. 16. A) and B) Graphs representing the differential relative cell migration and invasion respectively in various groups C) Graph depicting the differential relative mammosphere forming efficiency (%) of MDA-MB-231 cells in various groups. D) Graph depicting the differential relative diameter of mammosphere (%) of MDA MB cells in various groups. E) Graph depicting the differential number of junctions in the tube formation assay. F) Graph depicting the differential number of vessel lengths. Data are representative of triplicate experiments (mean±SD). *p<0.05, **p<0.02 and ***p<0.001 statistically significant difference compared to corresponding control.

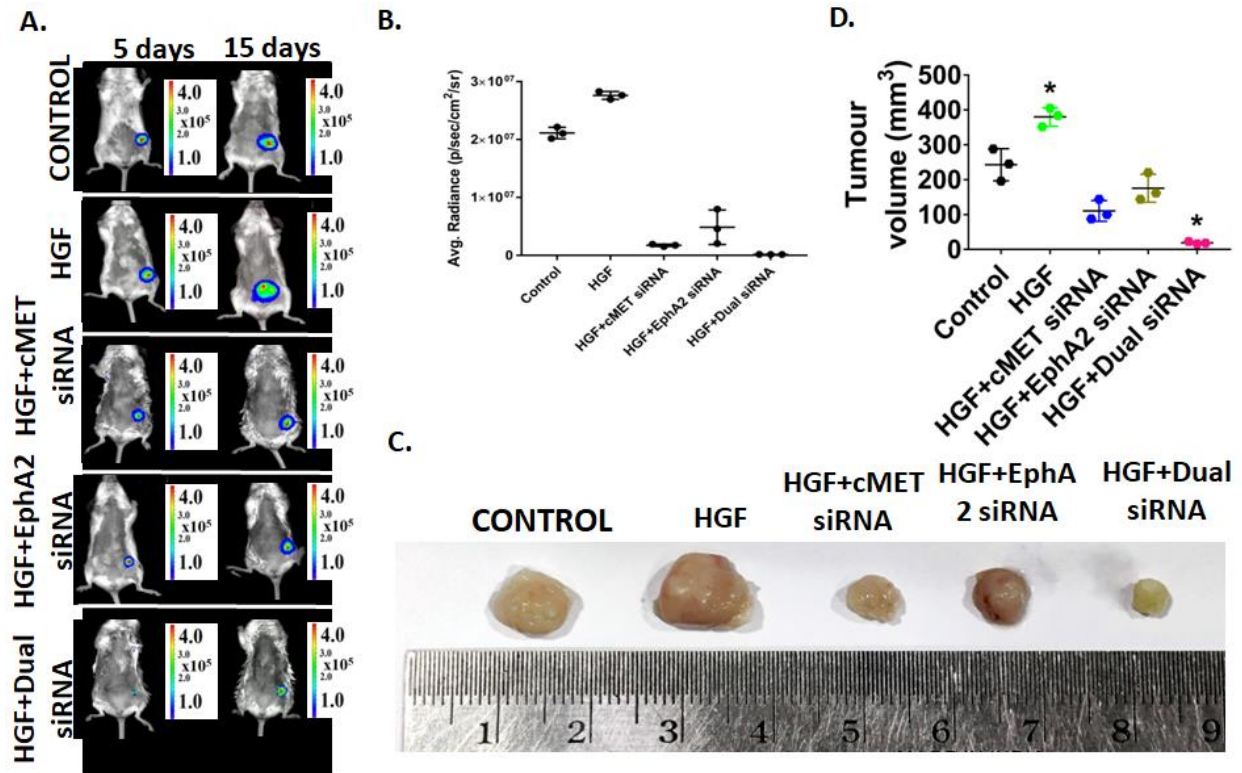


Fig: 16: in vivo evaluation of the effect of individual/dual silencing of c-MET and EphA2 in the presence of HGF. A) Live animal imaging of 4T1^{luc2} induced breast tumors in BALB/c mice undergoing various silencing modalities. B) Graph representing the average radiance of the luminescence exhibited by the 4T1^{luc2} induced tumors. C) Harvested tumors post silencing. D) Graph representing the tumor volume of various silenced groups in the presence of HGF.

These findings were further validated in a TNBC syngeneic mouse model, wherein c-MET, EphA2, or dual knockdown 4T1 cells were injected into the mammary fat pads of BALB/c mice. Subsequently, the mice were exposed to HGF. The tumor volume was significantly lower in the dual knockdown group (Fig.16), thus confirming that simultaneous dual targeting of c-MET and EphA2 has a more significant impact on abrogating tumorigenesis in TNBC cell populations.

Discussion:

ER-negative, PR-negative, HER2 negative breast cancer, commonly known as TNBC[48], is one of the most challenging breast cancer molecular subtypes, and achieving durable therapeutic success using current treatment paradigms is far from our expectations. Due to its special phenotypic status, TNBC does not respond to molecular-targeted therapy, even to endocrine therapy. Therefore, chemotherapy is the only systemic treatment option. Unfortunately, the prognosis of TNBC patients undergoing conventional postoperative adjuvant chemo-radiotherapy is poor. Tumor recurrence and metastatic progression eventually occur due to residual lesions that persist and often disseminate as drug-tolerant cells [201], [202]. One of the potential drivers of this frequent treatment failure is the perturbation of multiple oncogenic RTK signaling axes. Aberrant c-Met signaling has been reported in various cancer types and is regarded as a novel therapeutic target [203]. High levels of c-MET and its phosphorylated form have been observed in all breast cancer subtypes, and are correlated with poor prognosis [204]. The similar mechanistic underpinnings of EphA2 lend credence to this pathway as a promising therapeutic (druggable) target for breast cancer because its deactivation/downregulation can be actionable and therefore inhibited by multiple regimens for restoring sensitivity to drugs[178]. Here, we evaluated the underlying downstream molecular mechanism and subsequent phenotypic modulation of TNBC in the presence of HGF in a model system in which c-MET, EphA2, or both were silenced. The following two strategies were implemented: 1. Silencing with specific siRNAs and, 2. Specific inhibitors of receptor phosphorylation. Both strategies yielded similar results. Treating known TNBC cell lines, such as MDA-MB-231, with HGF increased the phosphorylation of both EphA2 and c-MET receptors. This prospectively resulted in the increased phosphorylation of ERK 1/2 which cascaded to the increased expression

of potent extracellular matrix remodeling factors like MMP-2 and ultimately Laminin-5Y2. Notably, the individual knockdown of these receptors diminished the expression of these effector molecules. Indeed, some cells were able to evade this strategy and successfully retain their migratory and invasive potential. Single knockdown also failed to prevent TNBC cells from forming mammospheres or tubes in the presence of Matrigel. This observation indicates that single-target knockdown or pharmacological inhibition might decrease the aggressiveness of the cells but fail to abrogate their various characteristics completely as one of the signaling axes compensates for the other in a context when one remains largely unperturbed. This prompted us to adopt a dual knockdown/inhibition strategy, which was more effective in downregulating the expression of effector molecules even in the presence of HGF. In addition, the migratory, invasive, mammosphere formation, and matrigel tube formation potential of MDA-MB-231 cells were successfully inhibited by this dual knockdown/inhibition strategy. We further validated these findings using a TNBC syngeneic mouse model. Consistent with our in vitro findings, the in vivo tumorigenic potential of 4T1 cells was most significantly abrogated in the dual-silenced group.



CHAPTER C

To demonstrate the potential synergistic effect of the phytochemical Lupeol along with chemotherapeutic drugs in regulation of vasculogenic mimicry.

Introduction:

Plant-derived small molecules are used in many clinical indications, including cancer. Lupeol, a pentacyclic triterpenoid, is a natural product that exhibits biological activity against cancer [110], [205]–[209].

In recent years, extensive studies have shown that phytochemicals can emerge as powerful remedy for various cancers and expectedly involve low cost and reduced toxicity. These agents have versatile pharmacological properties conferring antioxidative, hepatoprotective, antimutagenic, anti-inflammatory, antiarthritic, and antitumorigenic effects[89], [210]–[215]. Triterpene group of phytochemicals are hydrocarbons formed by the condensation of six isoprene units and represent important structural components of plant membranes. Lupeol (Lup-20(29)-en-3h-ol) is a naturally occurring and pharmacologically active triterpene (phytosterol) found in various fruits (e.g., olive, mango, strawberry, and grapes), vegetables, and in several medicinal plants [216]. Induction of tumor differentiation and inhibition of tumor growth has been reported following Lupeol treatment in mouse melanoma and human leukemia cells[217]. Studies have also shown that Lupeol inhibits the growth of hepatocellular carcinoma cells by downregulating the expression of ATP-binding cassette sub-family G member 2 (ABCG2) through interfering with the Phosphatase and tensin homolog (PTEN)-AKT signaling network[212].

From the huge number of studies focusing on phytochemicals exhibiting cytotoxic effects on most cancer cells, it appears that some of these agents are able to kill CSCs. Curcumin [218],

Genistein [219], Resveratrol [220] have shown to lower the CSC pool either by induction of apoptosis or by decreasing the number of CD 133+ve cells. Lupeol, a well-known triterpene, found in various fruits (e.g. olive, mango, strawberry and grapes), vegetables and several medicinal plants, has been reported for its potent anti-cancer activity in different cell lines [206], [207], [221]. The phytochemical has shown major to mild cytotoxicity against different types of melanoma cells[211]. The modes of action documented till date are the inhibition of angiogenesis [222], cytoskeletal remodeling[210]and induction of the intrinsic pathway of apoptosis for both human as well as murine melanoma model. Despite these novel properties, Lupeol's effect on VM and angiogenesis in breast cancer is still largely not elucidated. Based on these findings, we tried to decipher the role of Lupeol alone and in combination with 5FU in controlling CSC mediated VM in various types of breast cancer. The cytotoxicity of both chemotherapeutic agents were first determined in vitro and then on solid tumor focusing on the understanding the complex balance between VM, the mode of action of Lupeol to compensate 5FU resistance, the inhibitory role of Lupeol on CD 133+ve CSC pool, reversal of EMT etc.

Therefore, the present study aimed to delineate thecombinatorial effect of Lupeol and the clinically approved chemotherapeutic drug 5-Fluorouracil (5FU) on breast cancer.

Materials and Methods

Cytotoxicity assay:

Cellular cytotoxicity was evaluated by the MTT colorimetric assay after 24 hours of treatment. MCF-7 and MDA-MB-231 cells (1×10^3) per well were plated in 96 well plates containing complete medium and allowed to adhere for 24 hours. Subsequently, the media was changed with fresh complete media containing various doses of 5FU and Lupeol. After 24 hours of

incubation, 10µl of MTT (stock concentration:2mg/ml) was added to each well. The plates were incubated at 37°C for 4 hours. The formazan crystals formed were solubilised in 100% DMSO. The absorbance was measured on a multi-mode plate reader at 570nm. GraphPad Prism 7.0 software was used to calculate the IC₅₀value of each compound. Based on these values, further MTT assay was performed to evaluate the combinatorial effect of Lupeol and 5FU using sub-IC₅₀ doses of both the compounds. In order to check Lupeol's possible off-target effect on normal human cells, we performed the cytotoxicity assay on WRL-68 human hepatic cells over 24 and 48 hours.

Colony formation assay:

MCF-7 and MDA-MB-231 cells were plated in 6 well plates at low densities (500 and 250 cells/well, respectively) and incubated at 37°C overnight. The cells were then treated with Lupeol or 5FU alone or in combination in serum containing media (for MCF-7 cells) and with HGF, Lupeol or 5FU alone or in combination in serum free media (for MDA-MB-231 cells). The cells were incubated for 24 hours, then the media was changed, and the cells were incubated for further 5 days. The colonies that formed (>50 cells) were fixed in 100% cold methanol and stained with 0.5% crystal violet.

Wound healing assay:

MCF-7 and MDA-MB-231 cells were plated in 6 well plates in serum containing media and monitored till they reached more than 80% confluency. A scratch was made using a 200 µl sterile tip and the media was replaced by serum (1%) containing media having Lupeol, 5FU alone or both for MCF-7 cells and serum free media for MDA-MB-231 cells containing HGF, Lupeol, 5FU alone or in combination. The cellular wound healing capacity was monitored every

24 hours. The end point for this experiment was when the cells completely healed the inflicted wound. Imaging was done using an inverted light microscope (Olympus). The total wound area was quantified using ImageJ software.

Determination of combination index (CI):

The Combination index (CI) was determined according to the previously described method by Chou and Talalay. Briefly, MCF-7 and MDA-MB-231 cells (1×10^3) were plated and subsequently treated for 24 hours in media in presence or absence of : 1) Lupeol (MCF-7: 0-240 μM and MDA-MB-231: 0-180 μM); 2) 5FU (MCF-7: 0-22 μM and MDA-MB-231: 0-170 μM) or finally; 3) 5FU, 3 μM for MCF-7 cells or 10 μM for MDA-MB-231 (30% of its IC₅₀ for each cell line) + Lupeol (0-20 μM for MDA-MB-231 or 0-100 μM for MCF-7 cells). MTT assay was performed and IC₅₀ values for various treatments were calculated as described previously. The concentration of each component required to reduce viability to 50% was then used to compute the CI (Supplementary table 1). For the effect of combination of two drugs, the CI values of 0.9 were judged to be synergistic, CI between 0.9-1.1 considered to be additive, and >1.1 to be antagonistic [223], [224].

Apoptosis assay:

MCF-7 and MDA-MB-231 cells were plated in 6 well plates in serum containing media and allowed to adhere overnight. Then, for MDA-MB-231 cells, the media was replaced with serum free media. MCF-7 cells were treated with 5FU, Lupeol alone or in combination. MDA-MB-231 cells were treated with HGF, 5FU, Lupeol alone or in combination. After 24 hours of treatment, the cells were used for performing the apoptosis assay using the Annexin V/PI kit (Santa Cruz Biotechnology Inc) following the manufacturer's protocol. Briefly, the cells were washed with

PBS and 5 μ l of FITC tagged Annexin V and 3 μ l of PI was added and incubated in dark conditions at room temperature (RT) for 15 minutes. The cells acquired immediately by flow cytometry using FACSCalibur instrument (BD). Data was analysed using FlowJoTMv10 software.

Immunofluorescence staining:

Immunofluorescence staining was performed as previously described [207]. MCF7 and MDA-MB-231 cells were seeded in 6 well plates onto sterile glass cover slips in serum containing media and allowed to adhere overnight. Then, the cells were exposed to either HGF, 5FU, Lupeol alone or in combination and allowed to incubate for 24 hours. Afterwards, the cells were washed with PBS and fixed using 100% methanol. The cells were permeabilised by washing with 0.1% Triton X-100 in 1X Phosphate Buffered Saline (PBS). Blocking was done by 2% Bovine Serum Albumin (BSA) in PBS for 1 hour at room temperature. The desired antibodies (Bax, CD133, E-cadherin and Vimentin) were added to each well and incubated at room temperature for 2 hours, followed by washing with 1X PBS. Appropriate fluorescence-dye tagged secondary antibodies were added for another hour in room temperature. After 2 washes with 1X PBS, 4',6-diamidino-2-phenylindole (DAPI) was applied to the cells as nuclear counterstain, followed by mounting the cover slips onto glass slides using glycerol. The cells were visualised by using a fluorescence microscope (OLYMPUS). ImageJ software was used to calculate the corrected total cell fluorescence. The primary antibodies used were mouse monoclonal anti Bax (clone B-9; 1:200; Santa Cruz biotechnology), rabbit polyclonal anti E-cadherin (clone H-108; 1:200 dilution; Santa Cruz biotechnology), mouse monoclonal anti Vimentin (clone V9; 1:200; Santa Cruz biotechnology), rabbit polyclonal anti CD133 (1:500; Novus biologicals). The secondary antibodies involved in this experiment were Goat anti-Rabbit

IgG F(ab')₂ secondary antibody with FITC conjugate (1:500 dilution) and F(ab')₂ Goat anti-mouse IgG (H+L) secondary antibody with PE conjugate (1:500 dilution).

Western blotting:

Initially, post knock down by siRNA and specific pharmacological inhibition in the presence/absence of HGF, the cells were lysed in ice cold lysis buffer (15 mM Tris, 2 mM ethylene-diamine-tetraacetic acid, 50 mM β -mercaptoethanol, 0.1% Triton X-100, 20% glycerol, 1 mM sodium orthovanadate, 1 mM sodium fluoride, 1 mM phenylmethylsulphonyl fluoride, 1 μ g/mL leupeptin, 1 μ g/mL aprotinin and 1 μ g/mL pepstatin), sonicated and the cell debris were separated by centrifugation. The resultant supernatant contained the total protein from the cells and was quantified by BCA protein assay kit (Thermo scientific) following manufacturer's protocol. Subsequently, 50 μ g of total protein per lane of denaturing polyacrylamide gel was loaded and resolved. The resolved proteins were then electro-blotted onto an activated and equilibrated PVDF membrane (Merck) using a semi-dry electro-blotting apparatus (Bio-RAD). Non-specific proteins were blocked by using 5% non-fat dry milk (Amresco) in TBST for 1 hour at room temperature. Then, the membranes were incubated overnight with the primary antibody at 4°C. The same method was used while performing western blots for cells treated with Lupeol, 5-FU or both, in the presence/absence of HGF. β -Actin was used as loading control in all the cases. The primary antibodies used are as follows: rabbit polyclonal anti MET (clone c28; 1: 200 dilution; Santa Cruz Biotechnology), rabbit polyclonal anti p-Met (Tyr 1349) (1:200 dilution; Santa Cruz Biotechnology), rabbit monoclonal anti EphA2 (clone D4A2; 1:1000 dilution; Cell signalling Technology), rabbit monoclonal anti Phospho-EphA2 (Ser897) (clone D9A1; 1:1000 dilution; Cell signalling Technology), rabbit monoclonal anti Phospho-p44/42 MAPK (Erk1/2) (Thr202/Tyr204) (clone D13.14.4E; 1:2000; Cell signalling Technology), rabbit

polyclonal anti- ERK1+ERK2 antibody (1:1000 dilution; Abcam), mouse monoclonal anti MMP-2 (clone 8B4; 1:1000 dilution; Novus Biological), mouse monoclonal anti Laminin- 5 (Y2 chain)(clone D4B5; 1:500 dilution; Merck), mouse monoclonal anti Bax (clone B-9; 1:200; Santa Cruz Biotechnology), rabbit monoclonal anti Bcl-2 (Clone JF104-8; 1:1000 dilution; Novus Biological), rabbit polyclonal anti E-cadherin (clone H-108; 1:200 dilution; Santa Cruz Biotechnology), mouse monoclonal anti Vimentin (clone V9; 1:200; Santa Cruz Biotechnology), rabbit polyclonal anti CD133 (1:500; Novus Biological), mouse monoclonal anti Twist-1 (clone 10E4E6; 1:1000; Novus Biological); mouse monoclonal anti slug (clone 4B6D5; 1:1000; Novus biological); mouse monoclonal anti Snail (clone 20C8; 1: 1000; Novus Biological). Next day, the membrane was washed in TBST, thrice for 5 minutes each and then probed with appropriate secondary antibody for 1 hour at room temperature, followed by washing with TBST. The secondary antibodies used for western blot are as follows: Goat anti-rabbit polyclonal IgG (1:20000 dilution; Sigma), Rabbit anti-mouse polyclonal IgG (1:40000 dilution; Sigma). The protein bands were visualised by using clarity western ECL (BIO-RAD) and captured in a ChemiDoc XRS (BIO-RAD).

Flow cytometry:

Initially, MDA-MB-231 cells were seeded in 6 well plates and allowed to adhere overnight. Subsequently, HGF, 5FU, Lupeol alone or in combination was added to the cells and incubated overnight. The cells were then scraped, fixed and permeabilised and stained with anti-CD133 antibody. Then, FITC tagged appropriate secondary antibody was applied. Flow cytometric analysis was performed using FACSCalibur instrument (BD). The primary antibody used was rabbit polyclonal anti CD133 (1:500; Novus biological) and the secondary antibody was Goat anti-Rabbit IgG F(ab')₂ secondary antibody with FITC conjugate (1:500 dilution).

Transwell invasion and migration:

Transwell inserts (Corning) with a pore size of 8 μm were used in this experiment. The inserts were coated with growth factor-reduced Matrigel (Corning) for the invasion assays. Transfected and knocked down MDA-MB-231 cells (1×10^5) were initially seeded into Transwell inserts containing serum-free media. Pharmacological inhibitors, Lupeol, 5FU or both were also added to the respective inserts. The lower chamber contained media containing HGF (100 ng/ml), which acts as a chemotactic factor. After incubation for 48 h, the inserts were collected. The migrated and invaded cells present on the lower side of the insert were fixed in methanol, stained with crystal violet, and visualized using a bright-field microscope (Carl Zeiss).

Mammosphere formation assay:

MDA-MB-231 cells (1×10^3) were seeded into each well of ultra-low attachment 96 well plates in mammosphere forming media (serum-free DMEM high glucose media with 100 ng/ml HGF, 1X B27 supplement and 5 $\mu\text{g/ml}$ Insulin). Post-transfection and knockdown with pharmacological inhibitors, single agent Lupeol, 5FU or both in combination were added. The plates were incubated for 7 days without any disturbance, and the formed mammospheres were observed. The primary mammospheres were dissociated, and single cells were subsequently seeded for evaluation of secondary mammosphere formation and further incubated for a week. Images were obtained using an inverted light microscope (Olympus).

Tube formation assay:

Each well of a 96 well plate was coated with growth factor-reduced matrigel. 1×10^3 transfected and knocked down MDA-MB-231 cells were seeded in each coated well. HGF, pharmacological inhibitors, Lupeol, 5FU, or both were added to the respective wells and incubated for 3 days to

observe their effect on the tube-forming capability of the cells. The tubes were then visualized under an inverted light microscope (Olympus). AngioTool v0.6a software was used to quantify the total vessel length and number of junctions in the tubes formed in various groups.

Protein-protein interaction (PPI) analysis and network modeling:

All input markers were chosen from the current study and queried using STRING protein-protein interaction (PPI) network analysis (<https://string-db.org>) *in silico* using a combination of text mining, databases, experiments, co-expression, neighborhood, gene fusion, co-occurrence, full network (type), confidence (edge meaning), and multiple active interaction sources and channels. A high-confidence (edge) interaction score of 0.700 was chosen as the minimum requirement, and edges with a confidence of 0.700 or above were considered as the highest. No additional layer or second shell was created. Instead, we confined the maximum number of interaction scores to only the input proteins whose roles were elucidated and profiled within the framework of the present study.

In vivo experiments

Initially, 4T1 cells (1×10^6) were injected into the abdominal mammary fat pads of BALB/c mice, following a previously described protocol [192]. Tumor growth was observed every other day by injecting the mice with XenoLight D-Luciferin, Potassium salt (Product no.:122799, Perkin Elmer). In vivo live animal imaging was performed using an IVIS Lumina in vivo imaging system (PerkinElmer). From the 5th day, the mice in all groups except the control group were treated with mouse HGF (10 μ g/g/week) [193]. At ethical endpoints, the mice were sacrificed and the tumors were harvested. Similar regimens were followed for combinatorial studies, with Lupeol (20 mg/kg/2 days) (intraperitoneal) [194] and/or 5FU (10 mg/kg/2 days) [195]

(intraperitoneal), as well as mouse HGF. In addition, initial cytotoxicity studies with the above-mentioned treatment regimens were conducted in non-tumor-bearing BALB/c mice.

***Ex vivo* tumor fragment culture:**

Fresh TNBC tissues were collected in two phases (N=10), which were then utilized for patient-derived ex vivo explant cultures. The tissues were sliced into 3 mm³ pieces and cultured in RPMI 1640 medium (Gibco, Life Technologies, USA) containing 8% FBS or HGF and 2% autologous serum. 5FU and, Lupeol alone or in combination were added to the treatment arms and incubated for 48 h at 37°C in a 5% CO₂ atmosphere on an orbital shaker at 20 rpm. Each patient's healthcare records were consulted to gather pertinent clinicopathological and demographic data

Immunohistochemistry staining:

Tumor slices were fixed in 10% buffered formalin and Formalin fixed paraffin embedded (FFPE) blocks were prepared after 24 hours of fixation. The FFPE blocks were sectioned using a microtome (Leica), with each section being 4µm thick. Thereafter, immuno-histochemical (IHC) staining was performed using the IHC kit (Merck) following manufacturer's protocol. After the application of DAB and subsequent development of immunogenic colour on the tissue sections, PAS staining was performed to detect the ECM remodelling in the tissues. The stained tissue sections were mounted on clean glass slides using DPX as a mounting agent. The slides were visualised under a bright field microscope (Carl Zeiss) and the images were captured using Zen software. IHC Scoring was done as previously described [179]. The staining index, which was utilised to determine the final outcome for each sample, was calculated by adding the stain intensity and positive cell score. The primary antibodies used are as follows, rabbit polyclonal anti Ki67 (1:100 dilution) and rabbit polyclonal anti cleaved- Caspase3c (Asp175, p17) (1:100

dilution) from Affinity Biosciences, rabbit polyclonal anti MET (clone c28; 1:100 dilution), rabbit polyclonal anti p-Met (Tyr 1349) (1:100 dilution) from Santa Cruz Biotechnology, rabbit monoclonal anti EphA2 (clone D4A2; 1:200 dilution), rabbit monoclonal anti Phospho-EphA2 (Ser897) (clone D9A1; 1:100 dilution) from Cell Signaling Technology

Results:

Lupeol and 5FU treatments synergize to impart cytotoxic effect and abrogate wound healing

To evaluate the cytotoxic effects of the combined treatment of 5FU and Lupeol on different types of breast cancer cells in an *in-vitro* setting, the IC₅₀ of Lupeol and 5FU was determined by performing the MTT cell viability assay of MCF-7 and MDA-MB-231 cells (Table 17). The percentage of viability of MCF-7 (Fig. 17A) and MDA-MB-231 cells (Fig. 18 A) upon treatment with various doses of Lupeol and 5FU was determined. The IC₅₀ of Lupeol was 76.68 µM and 5FU was 10.06 µM for MCF-7 cells. The IC₅₀ of Lupeol was 29.54 µM and that of 5FU was 37.13 µM for MDA-MB-231 cells. In case of MCF-7, the combination treatment resulted in the IC₅₀ of Lupeol as 40.75 µM when the cells were treated with 3 µM and, in the case of MDA-MB-231, the IC₅₀ of Lupeol was 8.651 µM and 10 µM for 5FU. The combination Index (CI) for MCF-7 and MDA-MB-231 was calculated to be 0.829 and 0.562, respectively. In both the cases, the CI is less than 0.9, suggesting that the combination regimen is synergistic in nature [223], [224]. Notably, the dose reduction index (DRI) for 5FU in combination with Lupeol was observed to be 3.35 in case of MCF-7 and 3.71 for MDA-MB-231 cells. The colony formation assay confirmed that the combination of Lupeol and 5FU is the most effective in reducing the cell plating efficiency and subsequent colony formation potential of MCF 7 (Fig. 17B and C) and

MDA-MB-231 even under the influence of HGF (Fig. 18B and C). Similar trend was observed in wound healing assay where the combination of Lupeol and 5FU was found to be most efficient in diminishing the wound healing potential of MCF-7 cells (Fig. 17D and E) and MDA-MB-231 cells (Fig. 18D and E) than the individual compounds even in the presence of HGF, over a period of 48 hours. Also, no significant differences in cellular viability was observed upon treating WRL-68 cells with Lupeol, over 24 and 48 hours (Fig. 19)

	<u>MCF-7</u>	<u>MDA-MB 231</u>
Factors	Lupeol+ 5FU (C1)	Lupeol+ 5FU (C2)
Dose selection (μM)	Lupeol: 20, 40, 60, 80, 100 5FU: 1, 3, 5	Lupeol: 2,4,8,10,15,20 5FU:5, 10, 15
IC 50 for individual compound treatment (μM)	Lupeol: 76.68 5FU: 10.06	Lupeol: 29.54 5FU: 37.13
IC 50 for combined treatment (μM) (Effective Dose)	Lupeol: 40.75 when 5FU 3	Lupeol: 8.651 when 5FU 10
Combination Index (CI) (5FU: 3 μM) $CI = (D_{Lupeol, Comb}) / (D_{Lupeol}) + (D_{5FU, Comb}) / (D_{5FU})$	C1= (40.75/76.68)+ (3/10.06) = 0.829	C2= (8.651/29.54)+ (10/37.13) = 0.562
Dose reduction Index (DRI) $D_{Drug} / D_{Drug, Comb}$	Lupeol: (76.68/40.75)= 1.88 5FU: (10.06/3)= 3.35	Lupeol: (29.54/8.651)= 3.41 5FU= (37.13/10)= 3.71
Combination effect	Synergistic	Synergistic

Table 17: Determination of effective dose and combination effect. IC 50= 50% cell growth inhibition after treatment with certain drug. $D_{Lupeol} (\mu M)$ = Dose of Lupeol to affect cell growth inhibition when treated individually. $D_{5FU, Comb} (\mu M)$ = Dose of 5FU to affect cell growth inhibition when treated in combination with Lupeol.

$D_{Lupeol, Comb} (\mu M)$ =Dose of Lupeol to affect cell growth inhibition when treated in combination with 5FU. $D_{5FU} (\mu M)$ =Dose of 5FU to affect cell growth inhibition when treated individually.

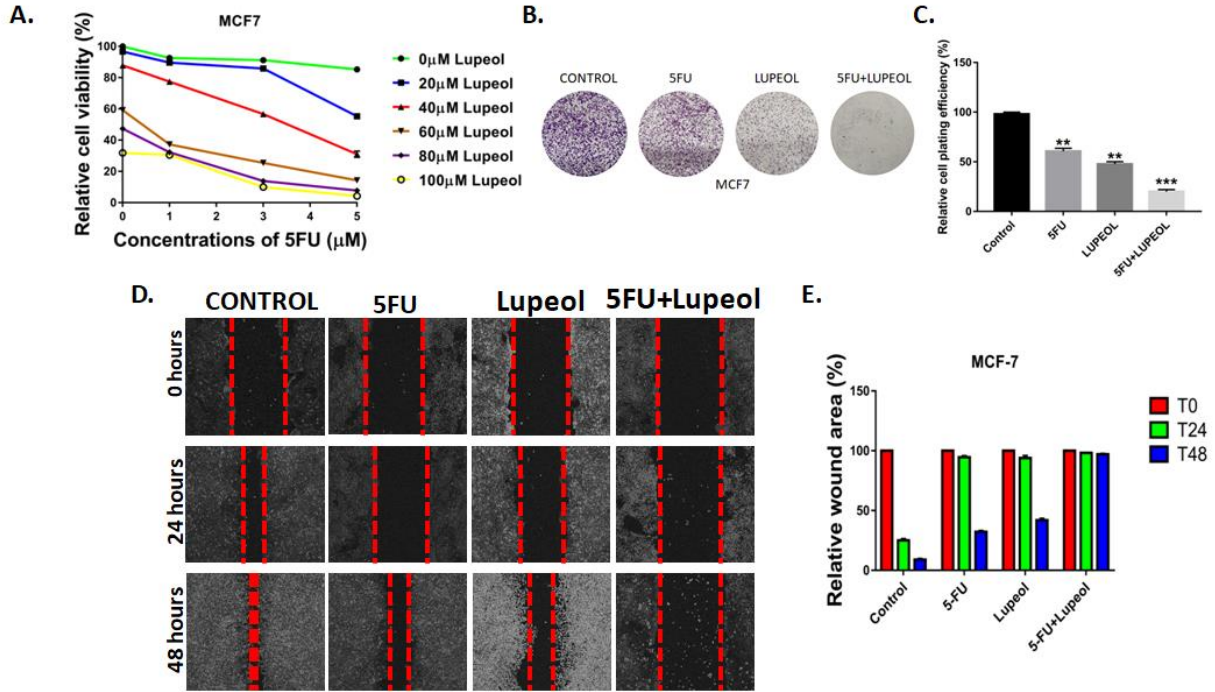


Fig. 17: Combination of Lupeol and 5FU induces cytotoxicity on MCF-7 cells and also reduces their wound healing potential. a) Percentage cell viability graph depicting the various Combination treatment of MCF cells with Lupeol (0-100 μM) and 5FU (0, 1, 3, 5 μM). b) Relative cell plating efficiency of MCF 7 cells upon treatment with 5FU, Lupeol individually or in combination as compared to control. c) The graph representing the relative cell plating efficiency of MDA-MB-231 cells upon treatment with Lupeol and 5FU in the presence of HGF d) Wound healing assay post treatment with Lupeol or 5FU or both on MCF-7 cells (40X magnification). Data are representative of triplicate experiments (mean \pm SD). * $p < 0.05$ statistically significant difference compared to corresponding control.

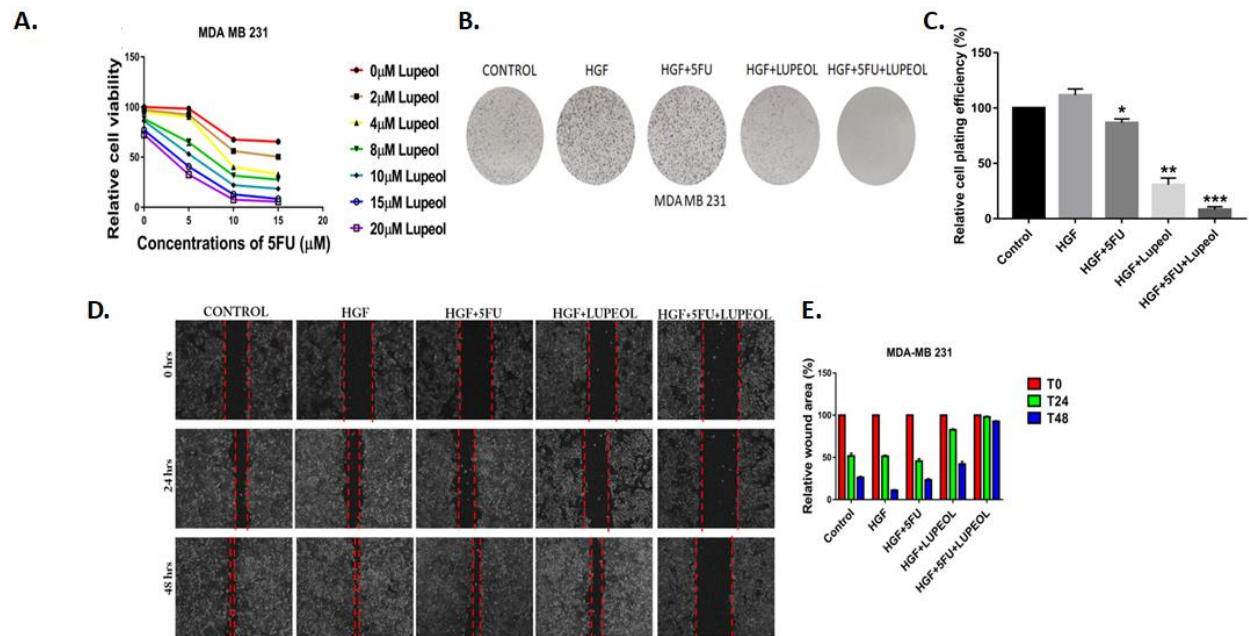


Fig. 18: Combination of Lupeol and 5FU induces cytotoxicity on MDA-MB-231 cells and reduces their wound healing potential. (a) Percentage cell viability graph depicting the various combination treatment of MDA-MB-231 cells with Lupeol (0-20 μM) and 5FU (0, 5, 10, 15 μM). (b) Colony formation assay post treatment with Lupeol or 5FU or both (in the presence of HGF) on MDA-MB-231 cells, respectively. (c) Wound healing assay post treatment with Lupeol or 5FU or both on MDA-MB-231 cells in the presence of HGF (image magnification:40X) (left) and their corresponding graph of relative wound area (%) (right). Data are representative of triplicate experiments (mean \pm SD). * p <0.05, ** p <0.01, *** p <0.001 statistically significant difference compared to corresponding control.

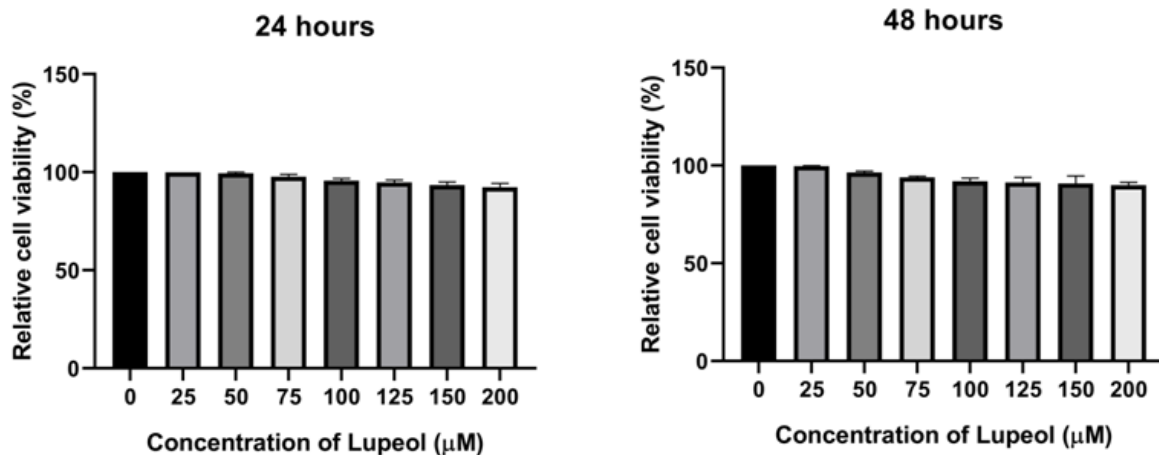


Fig.19: Graphs representing the relative cell viability of WRL-68 cells after treatment with various doses of Lupeol for 24 and 48 hours.

Combination of Lupeol and 5FU induces apoptosis in breast cancer cells *in vitro* and *ex vivo*

In order to evaluate the potential of the combination of inducing apoptosis in breast cancer cells, the Annexin V/PI apoptosis assay was performed in MCF-7 (Fig. 20A and B) and MDA-MB-231 (Fig. 21A and B) cells. Notably, the combination induced apoptosis in both the cell lines compared to the individually treated arms when exogenous HGF was present in the milieu in MDA-MB-231 cells. The subsequent expression of the pro-apoptotic protein Bax was evaluated by immuno-fluorescence staining in both MCF-7 (Fig. 20C and D) and MDA-MB-231 cells (Fig. 21 C and D). Similar effect was observed as combination showed the most corrected total cell fluorescence (CTCF) indicating the maximum expression of Bax. Western blot analysis confirmed this elevated expression of Bax in the combination arm in both the MCF-7 (Fig. 20E and F) and MDA-MB-231 cells (Fig. 21E and F). Concomitantly, there was a significant decrease in the expression of the anti-apoptotic protein Bcl2 in the combination arm in both MCF-7 cells (Fig. 20 E and G) and MDA-MB-231 (Fig. 21 E and G).

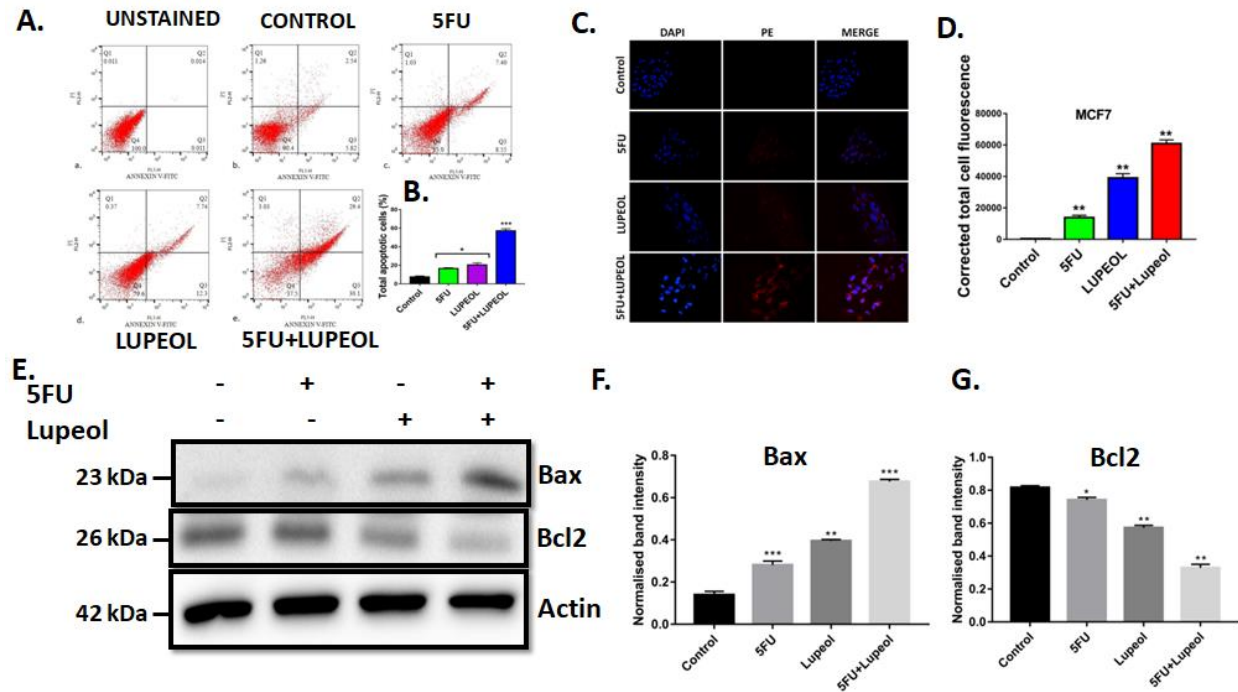


Fig. 20: Induction of apoptosis by the combination regimen of Lupeol and 5FU on MCF-7 cells. A) Annexin V/PI apoptosis assay by flow cytometry post treatment with Lupeol or 5FU or both on MCF-7 cells. Annexin V on x-axis and PI on y-axis B) Immunofluorescence staining to detect Bax protein (exhibiting red fluorescence) post treatment with Lupeol and 5FU or both on MCF-7 cells (400X magnification). C) Western blot analysis probed for Bax and Bcl2 proteins post treatment with Lupeol or 5FU or both on MCF-7 cells. Data are representative of triplicate experiments (mean \pm SD). * $p < 0.05$ statistically significant difference compared to corresponding control.

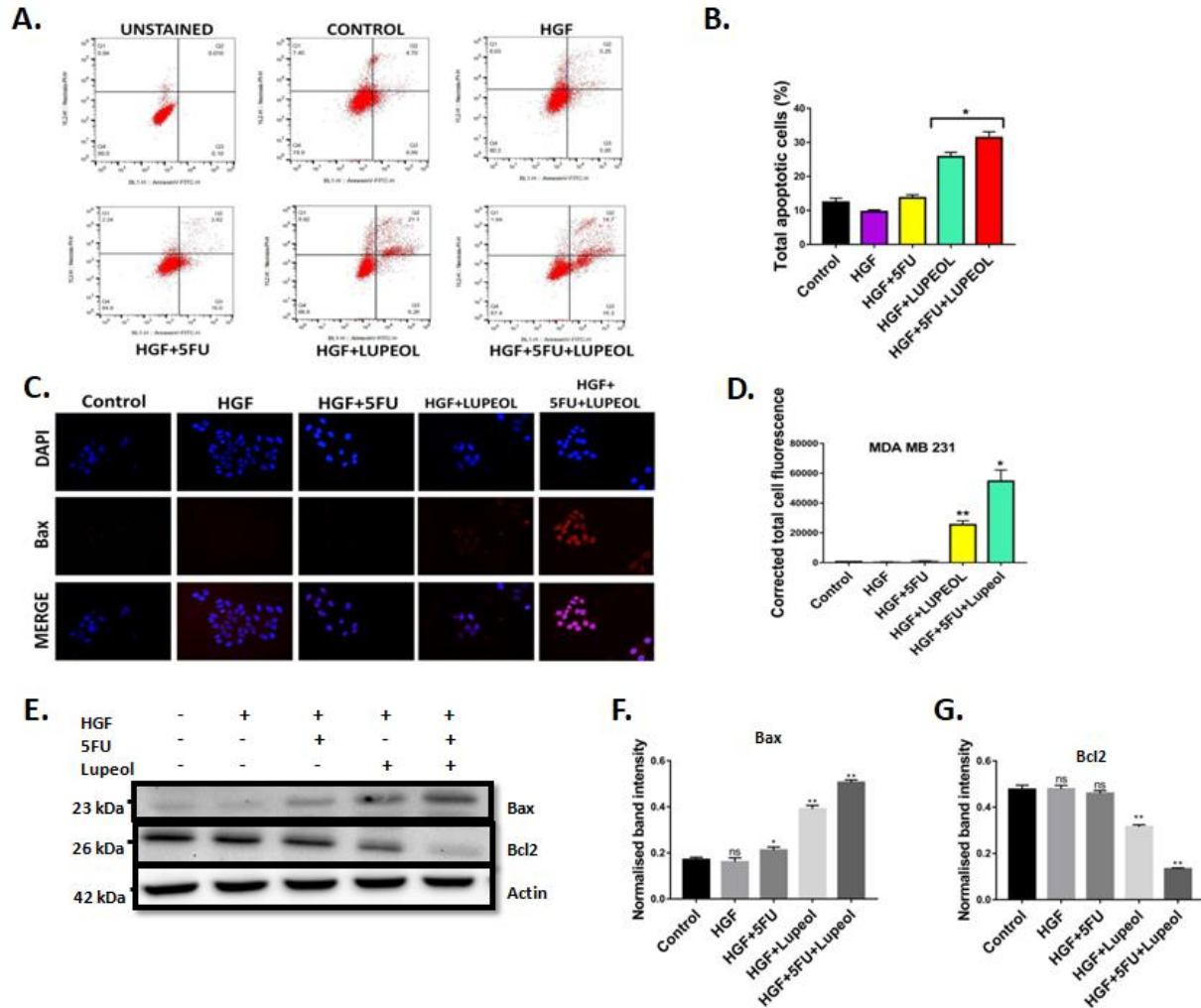


Fig. 21: Induction of apoptosis by the combination regimen of Lupeol and 5FU on MDA-MB-231 cells. A) Annexin V/PI apoptosis assay by flow cytometry, post treatment with Lupeol or 5FU or both on MDA-MB-231 cells in the presence of HGF (left) and the respective graph of total apoptotic cells in various treatment arms (right). Annexin V on x-axis and PI on y-axis B) Immunofluorescence staining detecting Bax protein (red fluorescence) post treatment with Lupeol and 5FU or both on MDA-MB-231 cells in the presence of HGF (image magnification: 400X) (right) and their corresponding graph of corrected total cell fluorescence (left). C) Western blot analysis detecting Bax and Bcl2 proteins post treatment with Lupeol or 5FU or both on MDA-MB-231 cells in the presence of HGF (top), graph representing the normalised band intensities of Bax (bottom left) and Bcl2 (bottom right). D) Work flow diagram of patient derived ex vivo explants culture E) Immunohistochemical staining of live breast cancer tissue treated with Lupeol or 5FU or both, in the presence of HGF and cultured for 48 hours (image magnification: 200X), graph representing the cells expressing ki67 (top right) and IHC score of Caspase 3c (bottom right) . Data are representative of triplicate experiments (mean \pm SD). * p <0.05, ** p <0.01, *** p <0.001 statistically significant difference compared to corresponding control.

Lupeol and 5FU treatments synergize to downregulate critical protein involved in VM formation and also induce reversal of EMT on MDA-MB- 231 cells

Upon evaluation of the modulation of critical proteins involved in VM formation, it was observed that the combination arm was most efficacious in significantly downregulating the phosphorylation of both c-MET and EphA2 and the downstream molecules (Fig. 22A). *in silico* protein-protein interaction (PPI) network simulation revealed significant interactions with several molecules involved in the modulation of EMT (Fig. 22B). Since preclinical data from the present study identified the critical mechanistic connections of multiple EMT and CSC related markers in a perturbed c-MET and EphA2 pathway cross talk and Lupeol in combination with 5FU showed differentiated reversal effects, we next attempted to analyze the network of all the functionally evaluated markers implicated in our assays. Using STRING PPI analysis platform, we look into the functional relationship between the differentially expressed proteins in the proposed network. In our study, the STRING analysis identified a number of high confidence interactive edges in the primary network associated with cellular proliferation, extracellular matrix remodeling, EMT, CSC phenotype, and apoptosis. The different degrees of association were denoted by the confidence level (low-0.150, medium-0.400, high-0.700, highest-0.900), One of our key network proteins, c-MET exhibited highest degree of association with HGF (0.999) and E-cadherin (CDH1) (0.999), followed by Erk1 (MAPK3) (0.936), Erk2 (MAPK1) (0.925) and Laminin 5Y2 (LAMC2) (0.916). Whereas, EphA2 showed highest degree of association with E-cadherin (0.969) followed by HGF (0.746). MDA-MB-231 cells, representing the TNBC subtype, display a mesenchymal phenotype with high migratory and invasive potential. HGF further enhanced the mesenchymal characteristics. However, subsequent treatment with Lupeol and 5FU in combination reduced the migratory and invasive potential of

MDA-MB-231 cells when HGF acted as a chemotactic factor, as is evident from the transwell migration and invasion assays (Fig. 22C and D). To delineate the impact of Lupeol and 5FU in the context of invasive properties, we profiled vasculogenic mimicry using the Matrigel tube formation assay in MDA-MB-231 cells *in vitro* upon subsequent treatment with HGF, Lupeol and 5FU alone or in combination (Fig. 22E). The combination group showed tubes with the least number of intercellular junctions and minimum vessel length among all groups. In parallel, upon treatment with HGF, MDA-MB-231 cells tended to form increased numbers of mammospheres with significantly larger diameters, when compared to the control arm. Subsequent treatment with Lupeol and 5FU alone or in combination most significantly abrogated the mammosphere-forming capability of the cells. Notably, this effect was sustained even in the secondary mammosphere-forming potential of the MDA-MB-231 cells originating from the treatment arms, even when the treatment stress was relieved (Fig. 22F). Dual immunofluorescence staining of MDA-MB-231 cells for epithelial marker E-cadherin and mesenchymal marker vimentin revealed that the combination regimen of Lupeol and 5FU resulted in a reversal of epithelial mesenchymal transition (EMT) (Fig. 22G). The maximum expression of E-cadherin and minimum expression of vimentin were observed in the combined treatment group. Subsequently, the differential expression of critical markers implicated in the induction of EMT, such as SNAI1, SLUG, and TWIST, was also evaluated by western blotting, which further confirmed the significantly diminished expression of these positive EMT regulators in the combination arm compared to the individually treated arms (Fig. 22H). All relevant graphs pertaining to Fig. 22 are represented in Fig. 23.

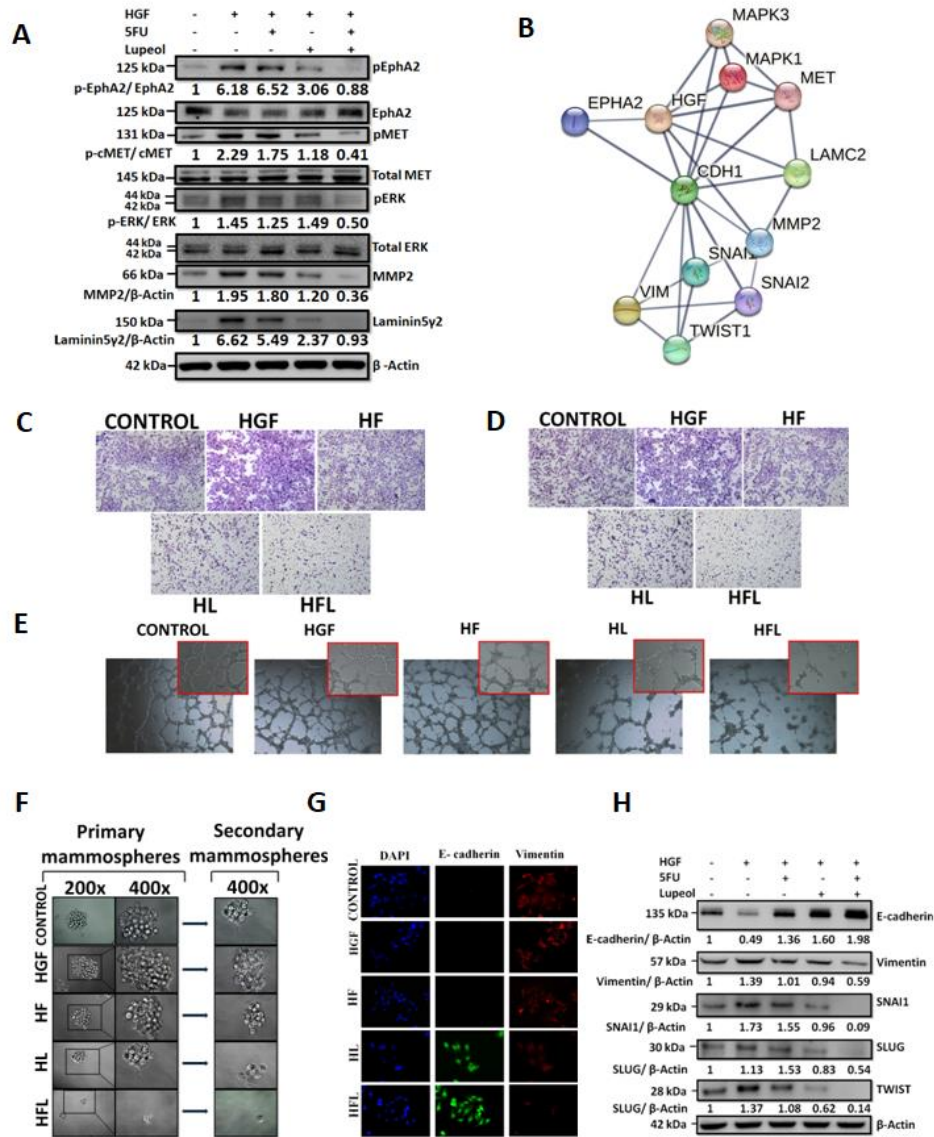


Fig. 22: Evaluation of the combinatorial effect of 5FU and Lupeol on MDA-MB 231 cells. (A) Western blot analysis of MDA-MB-231 cells treated with 5FU, Lupeol or both in the presence of HGF and probed for phospho-EphA2 (S897), EphA2, phospho-c-MET, total c-MET, pERK1/2, total ERK1/2, MMP2 and Laminin-5Y2 protein expression. β - Actin was used as a loading control. (B) Protein-protein interaction (PPI) network analysis using input proteins from the present study using STRING platform showing interacting molecules and edge confidence levels in the network. (C) and (D) Transwell migration and invasion of MDA-MB-231 cells upon treatment with Lupeol, 5FU or both, while HGF was used as a chemotactic factor (image magnification:100X). (E) Matrigel tube formation of MDA-MB-231 cells upon treatment with Lupeol, 5FU or both in the presence of HGF (40X and 100X magnification in inset). (F) Primary and secondary Mammosphere formation of MDA-MB-231 cells in the presence of HGF and treated with 5FU, Lupeol or both (200X and 400X magnification). (G) Immunofluorescence staining of MDA-MB-231 cells for the detection of E- cadherin (green) and Vimentin (red) post treatment with Lupeol or 5FU or both in the presence of HGF (image magnification: 400X) (H) Western blot analysis of MDA-MB-231 cells treated with Lupeol, 5FU or both in the presence of HGF and probed for E-cadherin, Vimentin, Snai1, Slug, Twist. HGF= Hepatocyte Growth Factor; HF= HGF+5FU; HL= HGF+Lupeol; HFL= HGF+5FU+Lupeol.

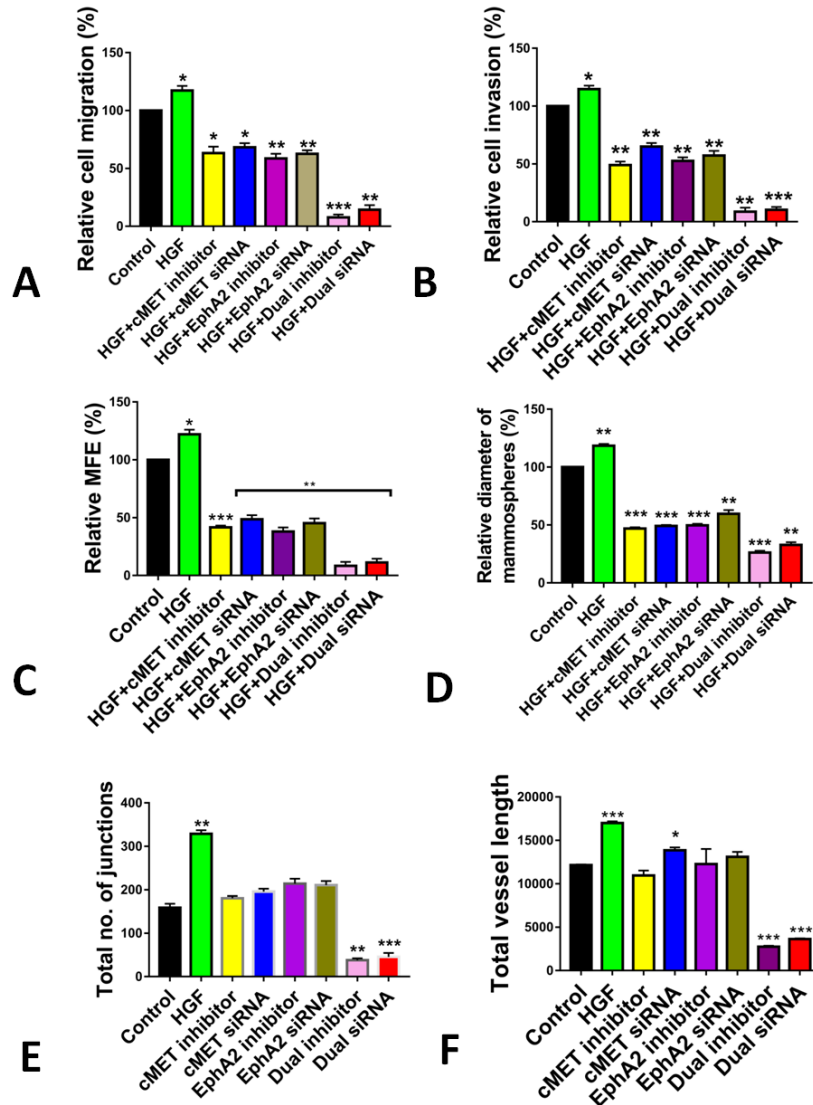


Fig. 23: Graphs pertaining to Fig. 24. A) and B) Graphs representing the differential relative cell migration and invasion respectively in various groups C) Graph depicting the differential relative mammosphere forming efficiency (%) of MDA-MB-231 cells in various groups. D) Graph depicting the differential relative diameter of mammosphere (%) of MDA MB cells in various groups. E) Graph depicting the differential number of junctions in the tube formation assay. F) Graph depicting the differential number of vessel lengths. Data are representative of triplicate experiments (mean+SD). * $p < 0.05$, ** $p < 0.02$ and *** $p < 0.001$ statistically significant difference compared to corresponding control.

Combined regimen of Lupeol and 5FU decreases the stemness of TNBC cells *in vitro*

Immuno-fluorescence staining delineating the expression of established cancer stem cell marker, CD133 (Fig. 24A and B). It revealed that HGF treatment increased the expression of CD133 in MDA-MB-231 cells. The combined regimen of Lupeol and 5FU resulted in significant reduction of the expression of CD133 compared to the individually treated groups. These results were confirmed by the flow cytometry analysis of MDA-MB-231 cells where the highest number of cells expressing CD133 marker were detected in the HGF treated group, whereas a significant reduction in CD133 expression was observed in the combined treatment arm (Fig. 24C and D). Similar expression status of CD133 was also demonstrated by Western blot analysis of cells under identical treatment conditions (Fig. 24E and F).

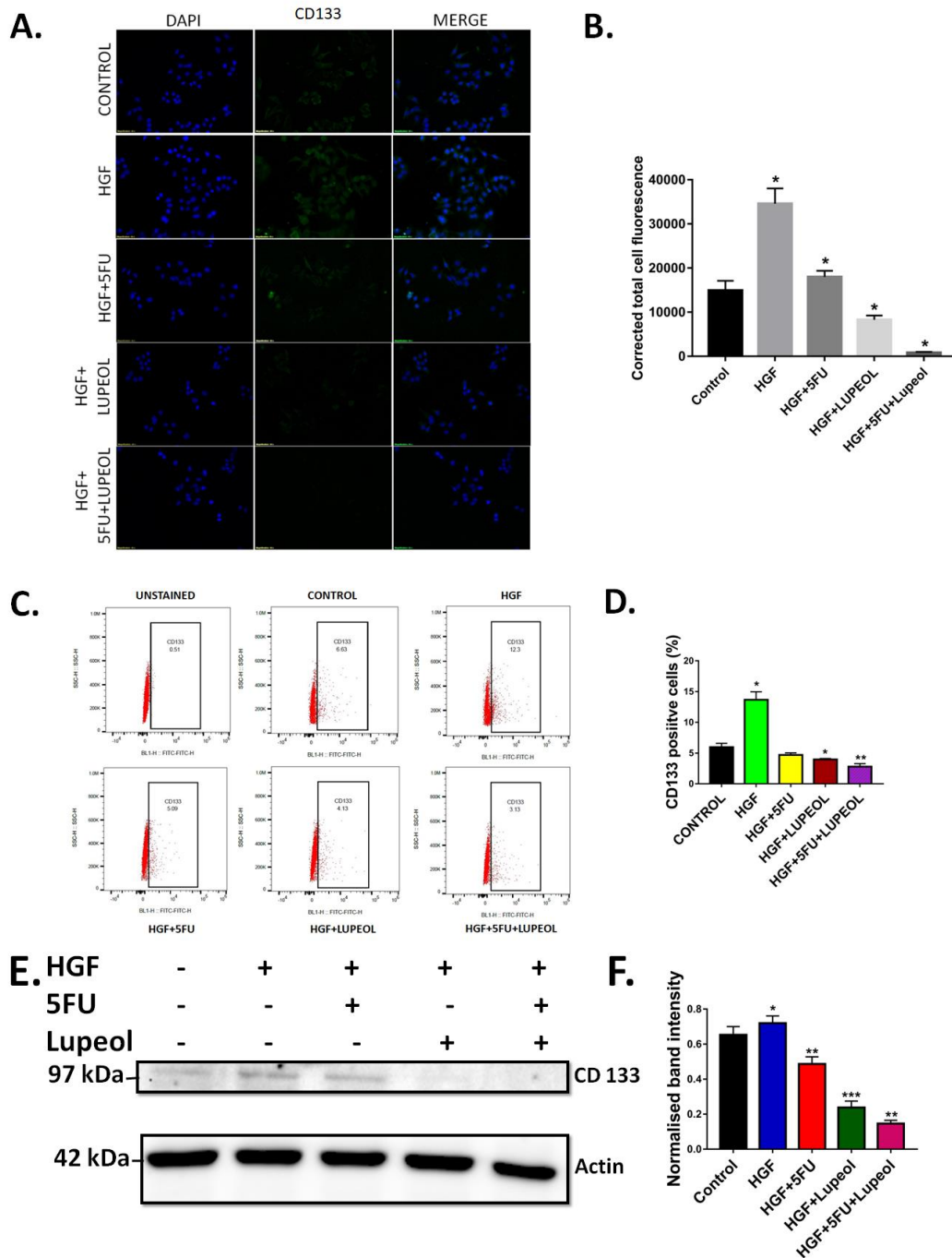


Fig. 24: Evaluation of the effect of the combination of Lupeol and 5FU on the stemness of TNBC cells. A) Immunofluorescence staining of MDA-MB-231 cells [probing for CD133: green], B) Graph representing the CTCF values of various treatment arms, C) Dot plots representing the flow cytometric analysis of MDA MB cells and the modulation of CD133 expression in various treatment arms. D) Graph representing the CD133 positive population in various treatment arms, E) Western blot analysis to quantify the modulation of expression of CD133 protein in MDA-MB-231 cells in various treatment arms while beta-actin was used as a loading control, F) Graph representing the normalized band intensity of CD133 expression in various treatment arms. Data are representative of triplicate

experiments (mean+SD). * $p < 0.05$, ** $p < 0.02$ and *** $p < 0.001$ statistically significant difference compared to corresponding control.

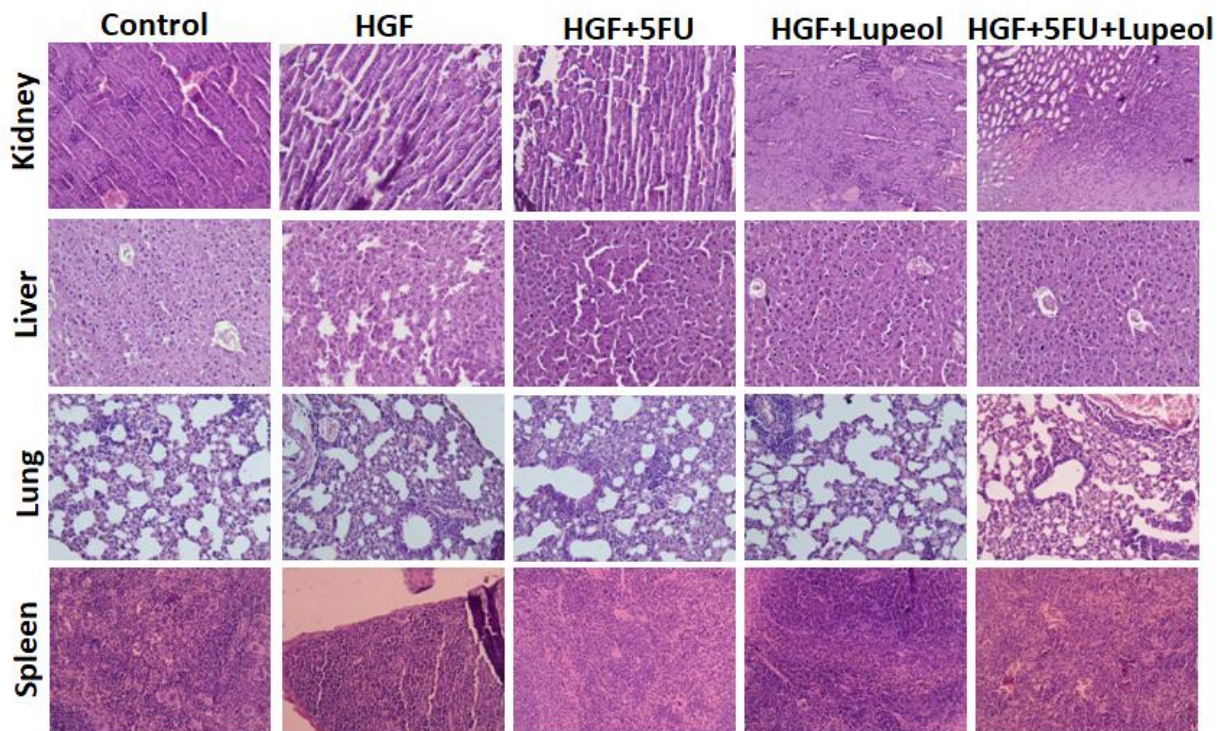


Fig. 25: Histopathological evaluation of the effect of the various treatment arms by haematoxyline and Eosin staining of Kidney, liver, lung and Spleen of mice after they were treated with HGF, 5FU and Lupeol, alone or in combination.

Parameters	Untreated Control	Vehicle Control	HGF	HF	HL	HFL
UR(mg/dL)	37.84±3.42	38.12±4.25	38.72±5.28	39.55±3.56	37.52±4.23	38.29±2.15
UA (mg/dL)	3.01±0.18	3.25±0.12	3.16±0.22	3.56±0.45	3.23±0.18	3.38±0.19
GLB (g/dL)	3.82±1.62	3.75±0.81	3.77±1.26	3.96±1.36	3.80±1.02	3.78±1.19
TP (g/dL)	5.45±1.85	5.51±1.95	5.59±2.05	5.32±2.20	5.41±0.98	5.61±1.58
ALB (g/dL)	1.82±0.55	1.85±0.61	1.90±0.58	1.95±0.91	1.86±0.68	1.88±0.69
CHL (mg/dL)	80.18±30.29	81.28±26.38	82.15±32.58	78.29±45.41	81.45±32.84	79.12±20.58
TG (mg/dL)	72.58±28.25	71.26±25.58	72.42±21.98	71.59±36.15	73.61±29.54	71.22±26.24
GLC (mg/dL)	152±21.97	150.24±18.65	151.29±26.57	154.48±20.35	153.68±20.02	156.41±23.68
AP (U/L)	384±48.21	386±56.21	381±42.38	376±56.28	385±35.85	383±38.69
AST (U/L)	162±33.50	162±31.29	164±26.21	169±30.18	159.25±18.68	160±25.98
ALT (U/L)	245.96±38.94	250.31±40.18	257±32.04	262.91±39.12	249.21±35.06	256.28±42.12

Table 18: Various serum parameters of mice after treatment with HGF, 5FU or Lupeol, alone or in combination. Abbreviations: **ALB**= albumin; **ALT**= alanine transaminase; **AP**= Alkaline phosphatase; **AST**= aspartate transaminase; **CHL**= cholesterol; **GLB**= globulin; **GLC**= glucose; **TG**= triglycerides; **TP**= total protein; **UA**= uric acid; **UR**= urea.

Systemic evaluation of the combinatorial effect of 5FU and Lupeol

Initially, the chosen doses were evaluated on a separate group of non-tumor-bearing mice. They were administered the same treatment regimens to check for impending off-target toxicity. No significant alterations were observed in the major organs (pathology) or biochemical parameters in the blood [225] of the exposed mice (Fig. 25 and Table 18). 4T1 TNBC cells derived from BALB/c mice were used to induce syngeneic TNBC tumors in female BALB/c mice. After tumor induction (5 days after the injection of 4T1 cells into abdominal mammary fat pads), when the tumor reached a dimension of 5 × 5 mm, the mice were treated with 5FU and/or Lupeol

along with HGF (Fig. 26A). In this live animal model, tumor growth was monitored by in vivo animal imaging using IVIS, which detects bioluminescence as a measure of viable tumor cell density (Fig. 26B). It was observed that there was a significant inhibition of tumor growth in the combination arm, even in the presence of HGF, compared to the other groups (Fig 26C, D, and E). IHC staining of the harvested tumors revealed a marked reduction in the expression of Ki-67 and an increase in caspase 3c expression (Fig. 26F). Notably, the phosphorylation of EphA2, c-MET, and their downstream molecules was significantly reduced in the combination arm, thus confirming the efficacy of the combination regimen (Fig. 26G).

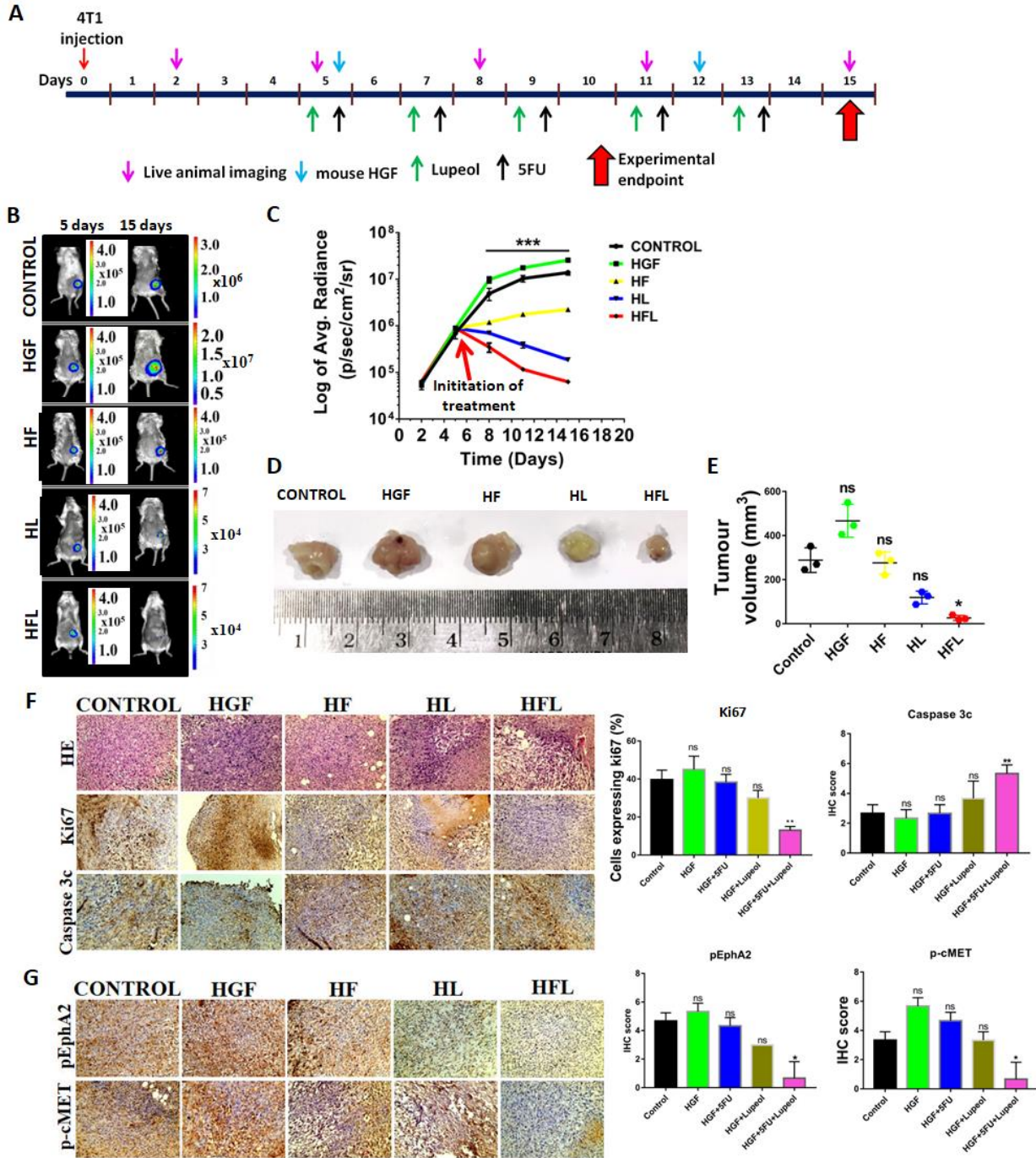


Fig. 26: In vivo evaluation of the combinatorial effect of 5FU and Lupeol in a TNBC syngeneic mice model. (A) Schematic representation of dosing schedule (B) in vivo live animal images of the 4T1^{luc2} induced tumors in various treatment arms in BALB/c mice at day 5 (initiation of treatment) and at day 15 (experimentation endpoint). (C) Graph representing the Log of average radiance vs. Time of the tumor growth. (D) Representative photomicrograph of freshly harvested breast tumors with a ruler (below) for scale. (E) Graph representing the tumor volume vs the various treatment arms. (F) Representative images of Haematoxyline and Eosin stain followed by IHC staining for Ki67 and Caspase 3c in the sections of harvested tumors developed in BALB/c mice. (G) Representative images of the IHC staining to evaluate the differential expression of phospho-EphA2, phosphor-c-

MET, phospho-Erk 1/2 and Laminin 5 γ 2 in the tumors of the various treatment arms.*p<0.05 and ***p<0.001 statistically significant difference compared to corresponding control. HGF= Hepatocyte Growth Factor; HF= HGF+5FU; HL= HGF+Lupeol; HFL= HGF+5FU+Lupeol.

Perturbation of the c-MET and EphA2 activation upon combined exposure to 5FU and Lupeol in patient tumor derived ex vivo model.

To demonstrate the mechanistic regulation of c-MET and EphA2 signaling axes by Lupeol and 5FU, an *ex vivo* explant culture was performed in freshly acquired breast cancer tissues (N=10), and their nodal status (N) and tumor size distribution (T) are shown in Fig 27A. Upon probing the tissue sections for Ki67 and Caspase 3c (Fig. 27B), we observed that the expression of Ki67 in the combination arm was significantly reduced (Fig. 27C). Concomitant induction of caspase 3c was also observed (Fig 27D). IHC profiling of serial tissue sections for the activation status of c-MET and EphA2 (Fig. 27E) revealed that the phosphorylation of EphA2 (Fig. 27F) and c-MET (Fig. 27G) was significantly abrogated in the combination-treated group.

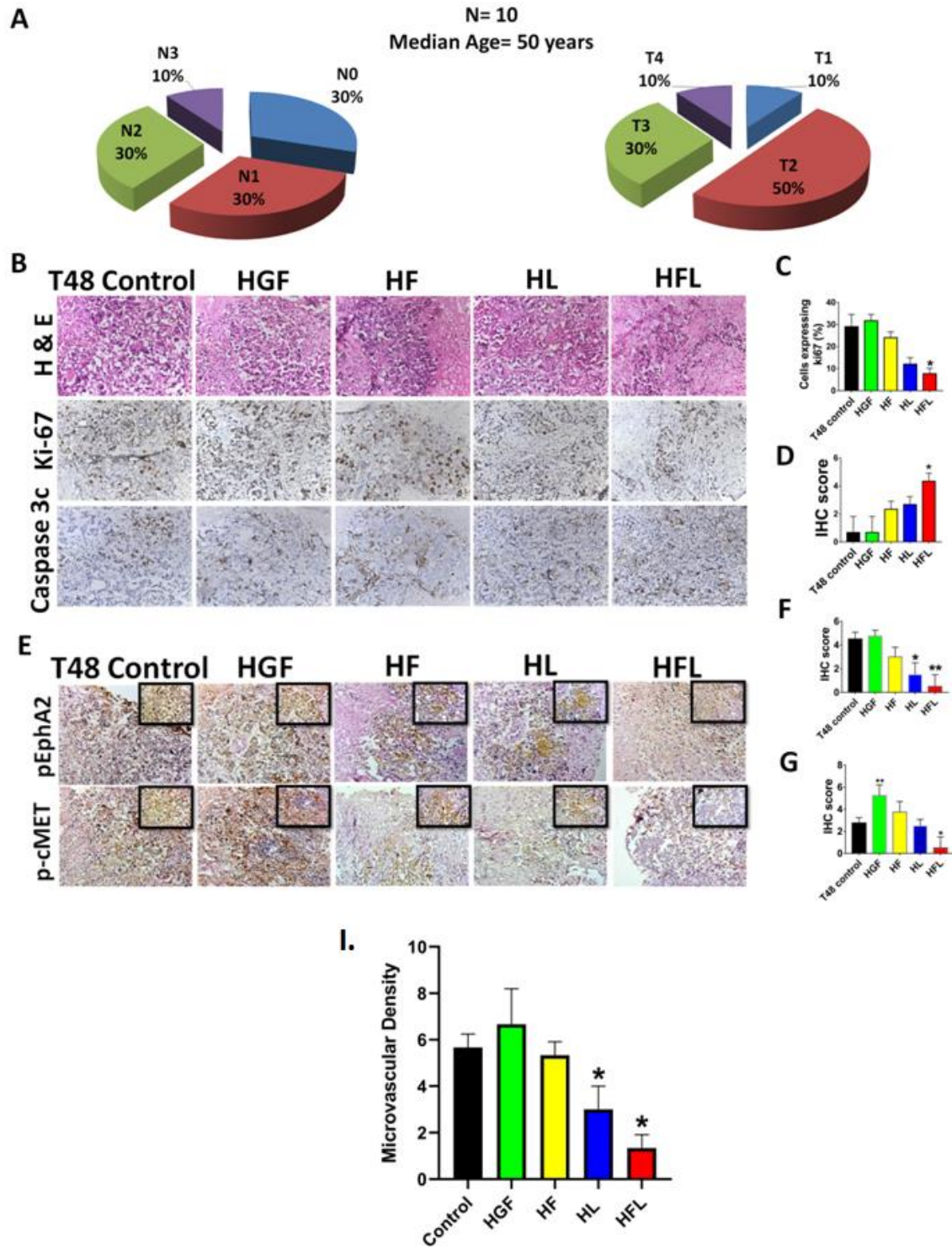


Fig. 27: Evaluation of the combinatorial effect of 5FU and Lupeol in ex vivo explant culture model (A) Graphical representation of the patient data used in this experiment, pertaining to the Nodal status and Tumor size (B) representative images of IHC staining of TNBC tissue fragments, post exposure to HGF, 5FU, Lupeol alone or in combination cells for the detection of Ki67 and Caspase 3c protein expression (200X magnification). (C) Graph representing the percentage of cells expressing Ki67 vs the various treatment arms (D) Graph representing the IHC

score of Caspase 3c vs. various treatment arms (E) representative images of IHC staining for the evaluation of phospho-EphA2 and phospho-c-MET in various treatment arms. (F) Graph representing the various IHC scores of phospho-EphA2 in various treatment arms (G) graph representing the various IHC scores of phospho-c-MET in various treatment arms. Data are representative of triplicate experiments (mean±SD). *p<0.05 statistically significant difference compared to corresponding control. HGF= Hepatocyte Growth Factor; HF= HGF+5FU; HL= HGF+Lupeol; HFL= HGF+5FU+Lupeol.

Discussion:

Chemotherapy remains the mainstay of treatment for TNBC and 5FU is one of a critical agent in the NCCN-approved regimen. However, in addition to the limited response rate, between 31% and 34% of individuals receiving 5-FU exhibit dose-limiting toxicities [226]. Fluoro-nucleotide incorporation into RNA and DNA, as well as the direct inhibition of thymidylate synthase, have been identified as the main mechanisms of cytotoxicity caused by 5-FU[227]. Hematological and gastrointestinal adverse effects are more frequent in patients receiving 5-FU [68]. As mono-therapy generally does not maximize chemo-drug efficacy, 5-FU is co-administered with other substances to boost its effectiveness [228]. Lupeol is a natural phytochemical that has shown cytotoxic effects on cancer cells and is highly effective in inducing apoptosis [206], [207]. This paves the way for investigating the therapeutic cooperation of these two drugs in our study. The synergistic effect of the combinatorial strategy of Lupeol and 5FU that we adopted was tested on breast cancer cell lines, MCF-7 and MDA-MB-231, which proved to be effective in reducing the proliferation and wound healing potential while inducing apoptosis. In addition, MDA-MB-231 cells are phenotypically mesenchymal, and thus notorious owing to their multidrug resistance [229],[230]. As MDA-MB-231 cells contextually preserve a mesenchymal phenotype, we evaluated the effect of the combination regimen on these cells. There was a marked change in the migratory and invasive potentials of the cells. This can be attributed to a mechanistic shift in which the mesenchymal characteristics of the cells

decrease and the epithelial characteristics become more pronounced. In other words, the combination of 5FU and Lupeol orchestrated the EMT reversal. To substantiate this response, we selectively profiled the expression of mesenchymal markers (Vimentin, TWIST, SNAIL and SLUG) and observed augmented expression when cells were exposed to HGF. However, upon subsequent treatment, expression was significantly reduced in the combination arm. In contrast, the combination resulted in increased expression of E-cadherin, despite the active engagement of HGF in the milieu. Furthermore, the data obtained from the cell line require further validation using more complex and clinically relevant systems to ascertain a better translational impact. To bridge this gap, we used an *in vivo* syngeneic mouse model and an *ex vivo* patient tumor-derived live tumor slice culture model that maintains the key phenotypes and heterogeneity of the original patient tumor microenvironment in short-term culture and therefore provides a suitable context for delineating the mechanistic underpinnings of signaling crosstalk and reliably modeling drug effects. Indeed, both of these models confirmed that the combination regimen reduced the proliferative potential of breast cancer cells and induced apoptosis in a ligand (HGF)-complemented niche.



CHAPTER 3

Conclusion

These findings elucidated that phosphorylation of the EphA2 receptor at the S897 residue, phosphorylation of c-MET and occurrence of VM are independent prognostic factors in breast cancer and are responsible for the aggressiveness and progression of the disease. We successfully delineated a viable target for more rationally defined therapy selection. This study presented initial data and warrants further validation in multiple independent cohorts which may lead to define better patient survival. Endothelia- independent networks is associated with highly aggressive metastatic tumors and poor patient survival [49], [65], [231]. It was elucidated site-specific phosphorylation of the EphA2 receptor in conjunction with vasculogenic mimicry as an indicator of poor prognosis in breast cancer patients [179]. It was observed that in the presence of HGF, the MDA-MB-231 cell line phenocopying TNBC formed more robust tubes in Matrigel. Notably, these tubes were disrupted or failed to assume a mature architecture upon subjecting them to the combination of Lupeol and 5FU. Subsequently, it was revealed that the combination regimen significantly downregulated both c-MET and EphA2 signaling axes, as well as their downstream effector molecules. We hypothesize that this receptor inhibition of Lupeol might be the cause of its anti- cancer effect and paves the way for more elaborate studies to leverage its role as a novel anticancer therapeutic (Fig. 28). To the best of our knowledge, this is the first study to elucidate the effect of a combination regimen consisting of Lupeol and 5FU in breast cancer in vitro, in vivo, and ex vivo models. Taken together, our results suggest that this combination has the capacity to comprehensively inhibit the diverse phenotypic modalities of breast cancer cells, especially the clinically elusive TNBC subtype. We did not observe any clinical signs or symptoms of toxicity in the combinational group of mice. However, further toxicity studies are required in larger animals prior to clinical studies. Our data suggest that this

combination can prevent tumor recurrence, increase survival, and enhance the quality of life of patients with TNBC.

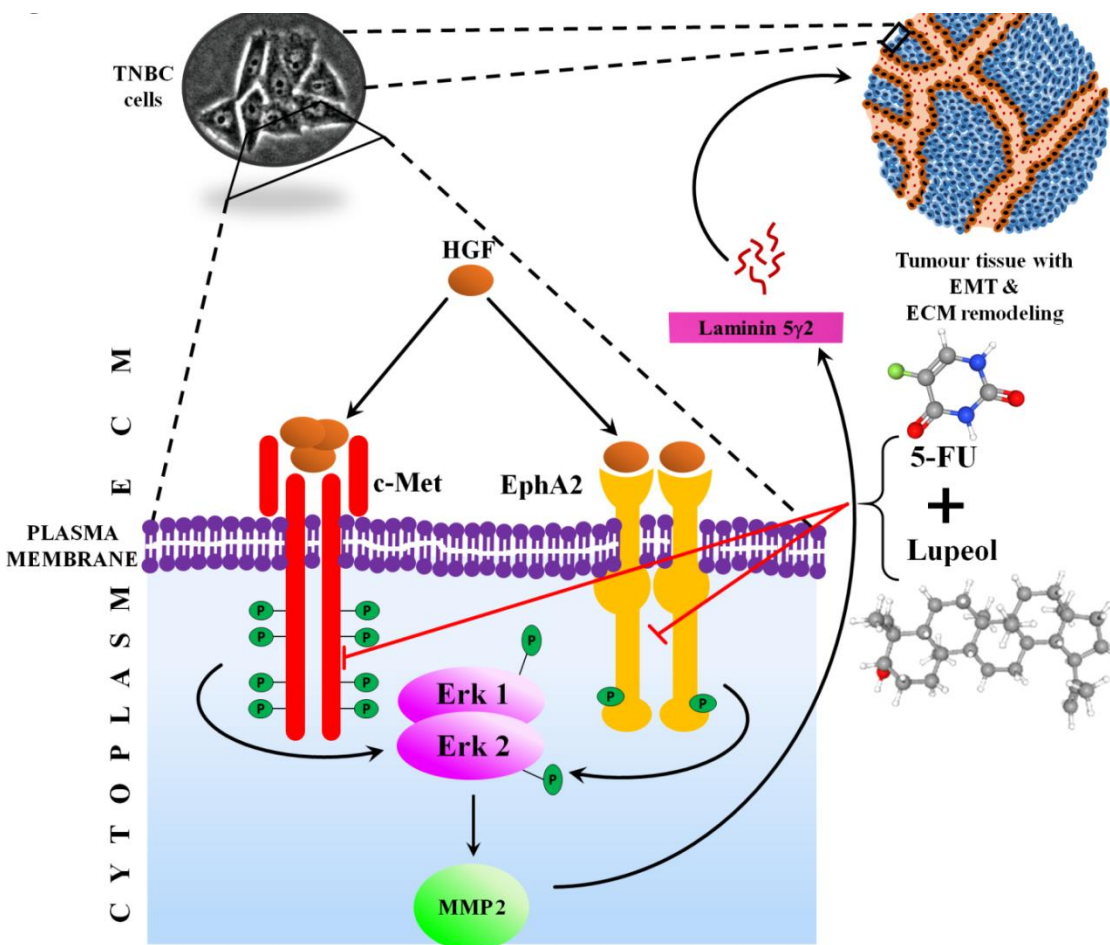


Fig. 28: Schematic representation of the synergistic effect of Lupeol and 5FU in regulating the cross talk between c-MET and EphA2 highlighting the therapeutic opportunities of combining these two drugs in oncogenic RTK pathway perturbation in TNBC model. The structures of 5FU (PubChem ID: 3385) and Lupeol (PubChem ID: 259846) from <https://pubchem.ncbi.nlm.nih.gov>.



CHAPTER 4

Bibliography

- [1] G. M. Cooper, "The Development and Causes of Cancer," in *The Cell: A Molecular Approach. 2nd edition*, Sinauer Associates, 2000. Accessed: Jun. 12, 2023. [Online]. Available: <https://www.ncbi.nlm.nih.gov/books/NBK9963/>
- [2] A. I. Baba and C. Câtoi, "CARCINOGENESIS," in *Comparative Oncology*, The Publishing House of the Romanian Academy, 2007. Accessed: Jun. 12, 2023. [Online]. Available: <https://www.ncbi.nlm.nih.gov/books/NBK9552/>
- [3] "Environmental Factors Inducing Human Cancers - PMC." <https://www.ncbi.nlm.nih.gov/pmc/articles/PMC3521879/> (accessed Jun. 12, 2023).
- [4] "The Genetics of Cancer - NCI," Apr. 22, 2015. <https://www.cancer.gov/about-cancer/causes-prevention/genetics> (accessed Jun. 12, 2023).
- [5] "Cancer Classification | SEER Training." <https://training.seer.cancer.gov/disease/categories/classification.html> (accessed Jun. 12, 2023).
- [6] D. Hanahan and R. A. Weinberg, "Hallmarks of cancer: the next generation," *Cell*, vol. 144, no. 5, pp. 646–674, Mar. 2011, doi: 10.1016/j.cell.2011.02.013.
- [7] "Proto-Oncogenes - an overview | ScienceDirect Topics." <https://www.sciencedirect.com/topics/agricultural-and-biological-sciences/proto-oncogenes> (accessed Jun. 12, 2023).
- [8] G. M. Cooper, "Tumor Suppressor Genes," in *The Cell: A Molecular Approach. 2nd edition*, Sinauer Associates, 2000. Accessed: Jun. 12, 2023. [Online]. Available: <https://www.ncbi.nlm.nih.gov/books/NBK9894/>
- [9] "Types of cancer | Cancer Research UK." <https://www.cancerresearchuk.org/what-is-cancer/how-cancer-starts/types-of-cancer> (accessed Jun. 12, 2023).
- [10] A. I. Baba and C. Câtoi, "TUMOR CELL MORPHOLOGY," in *Comparative Oncology*, The Publishing House of the Romanian Academy, 2007. Accessed: Jun. 12, 2023. [Online]. Available: <https://www.ncbi.nlm.nih.gov/books/NBK9553/>
- [11] T. Kawamata, Y. Kamada, Y. Kabeya, T. Sekito, and Y. Ohsumi, "Organization of the pre-autophagosomal structure responsible for autophagosome formation," *Mol Biol Cell*, vol. 19, no. 5, pp. 2039–2050, May 2008, doi: 10.1091/mbc.e07-10-1048.
- [12] "Definition of metastasis - NCI Dictionary of Cancer Terms - NCI," Feb. 02, 2011. <https://www.cancer.gov/publications/dictionaries/cancer-terms/def/metastasis> (accessed Jun. 12, 2023).
- [13] T. J. Key, P. K. Verkasalo, and E. Banks, "Epidemiology of breast cancer," *Lancet Oncol*, vol. 2, no. 3, pp. 133–140, Mar. 2001, doi: 10.1016/S1470-2045(00)00254-0.
- [14] Y. S. Khan and H. Sajjad, "Anatomy, Thorax, Mammary Gland," in *StatPearls*, Treasure Island (FL): StatPearls Publishing, 2023. Accessed: Jun. 12, 2023. [Online]. Available: <http://www.ncbi.nlm.nih.gov/books/NBK547666/>
- [15] A. Stachs, J. Stubert, T. Reimer, and S. Hartmann, "Benign Breast Disease in Women," *Dtsch Arztebl Int*, vol. 116, no. 33–34, pp. 565–574, Aug. 2019, doi: 10.3238/arztebl.2019.0565.
- [16] "Menarche, menopause, and breast cancer risk: individual participant meta-analysis, including 118 964 women with breast cancer from 117 epidemiological studies," *Lancet Oncol*, vol. 13, no. 11, pp. 1141–1151, Nov. 2012, doi: 10.1016/S1470-2045(12)70425-4.
- [17] T. R. Lyons, P. J. Schedin, and V. F. Borges, "Pregnancy and Breast Cancer: when They Collide," *J Mammary Gland Biol Neoplasia*, vol. 14, no. 2, pp. 87–98, Jun. 2009, doi: 10.1007/s10911-009-9119-7.
- [18] V. W. Lim *et al.*, "Serum estrogen receptor bioactivity and breast cancer risk among postmenopausal women," *Endocr Relat Cancer*, vol. 21, no. 2, pp. 263–273, Apr. 2014, doi: 10.1530/ERC-13-0233.
- [19] N. D. White, "Hormonal Contraception and Breast Cancer Risk," *Am J Lifestyle Med*, vol. 12, no. 3, pp. 224–226, Jan. 2018, doi: 10.1177/1559827618754833.

- [20] X. Liu, J. Yue, R. Pervaiz, H. Zhang, and L. Wang, "Association between fertility treatments and breast cancer risk in women with a family history or BRCA mutations: a systematic review and meta-analysis," *Front Endocrinol (Lausanne)*, vol. 13, p. 986477, Sep. 2022, doi: 10.3389/fendo.2022.986477.
- [21] "Family history of breast cancer and inherited genes." <https://www.cancerresearchuk.org/about-cancer/breast-cancer/risks-causes/family-history-and-inherited-genes> (accessed Jun. 12, 2023).
- [22] N. Petrucelli, M. B. Daly, and T. Pal, "BRCA1- and BRCA2-Associated Hereditary Breast and Ovarian Cancer," in *GeneReviews*[®], M. P. Adam, G. M. Mirzaa, R. A. Pagon, S. E. Wallace, L. J. Bean, K. W. Gripp, and A. Amemiya, Eds., Seattle (WA): University of Washington, Seattle, 1993. Accessed: Jun. 12, 2023. [Online]. Available: <http://www.ncbi.nlm.nih.gov/books/NBK1247/>
- [23] J. A. McDonald, A. Goyal, and M. B. Terry, "Alcohol Intake and Breast Cancer Risk: Weighing the Overall Evidence," *Curr Breast Cancer Rep*, vol. 5, no. 3, p. 10.1007/s12609-013-0114-z, Sep. 2013, doi: 10.1007/s12609-013-0114-z.
- [24] J. Makki, "Diversity of Breast Carcinoma: Histological Subtypes and Clinical Relevance," *Clin Med Insights Pathol*, vol. 8, pp. 23–31, Dec. 2015, doi: 10.4137/CPath.S31563.
- [25] G. N. Sharma, R. Dave, J. Sanadya, P. Sharma, and K. K. Sharma, "VARIOUS TYPES AND MANAGEMENT OF BREAST CANCER: AN OVERVIEW," *J Adv Pharm Technol Res*, vol. 1, no. 2, pp. 109–126, 2010.
- [26] H. Y. Wen and E. Brogi, "Lobular Carcinoma in Situ," *Surg Pathol Clin*, vol. 11, no. 1, pp. 123–145, Mar. 2018, doi: 10.1016/j.path.2017.09.009.
- [27] S. Tomlinson-Hansen, M. Khan, and S. Cassaro, "Breast Ductal Carcinoma in Situ," in *StatPearls*, Treasure Island (FL): StatPearls Publishing, 2023. Accessed: Jun. 12, 2023. [Online]. Available: <http://www.ncbi.nlm.nih.gov/books/NBK567766/>
- [28] "Invasive Lobular Carcinoma (ILC)." <https://www.breastcancer.org/types/invasive-lobular-carcinoma> (accessed Jun. 12, 2023).
- [29] Y. Feng *et al.*, "Breast cancer development and progression: Risk factors, cancer stem cells, signaling pathways, genomics, and molecular pathogenesis," *Genes Dis*, vol. 5, no. 2, pp. 77–106, May 2018, doi: 10.1016/j.gendis.2018.05.001.
- [30] F. Limaiem and M. Mlika, "Medullary Breast Carcinoma," in *StatPearls*, Treasure Island (FL): StatPearls Publishing, 2023. Accessed: Jun. 12, 2023. [Online]. Available: <http://www.ncbi.nlm.nih.gov/books/NBK542292/>
- [31] F. Limaiem and M. Mlika, "Tubular Breast Carcinoma," in *StatPearls*, Treasure Island (FL): StatPearls Publishing, 2023. Accessed: Jun. 12, 2023. [Online]. Available: <http://www.ncbi.nlm.nih.gov/books/NBK542223/>
- [32] M. Akram, M. Iqbal, M. Daniyal, and A. U. Khan, "Awareness and current knowledge of breast cancer," *Biol Res*, vol. 50, p. 33, Oct. 2017, doi: 10.1186/s40659-017-0140-9.
- [33] C. Karakas, "Paget's disease of the breast," *J Carcinog*, vol. 10, p. 31, Dec. 2011, doi: 10.4103/1477-3163.90676.
- [34] C. Daly and Y. Puckett, "New Breast Mass," in *StatPearls*, Treasure Island (FL): StatPearls Publishing, 2023. Accessed: Jun. 12, 2023. [Online]. Available: <http://www.ncbi.nlm.nih.gov/books/NBK560757/>
- [35] "What Is Breast Cancer Screening?," *Centers for Disease Control and Prevention*, Nov. 17, 2022. https://www.cdc.gov/cancer/breast/basic_info/screening.htm (accessed Jun. 12, 2023).
- [36] "Breast Magnetic Resonance Imaging (MRI)," Aug. 08, 2021. <https://www.hopkinsmedicine.org/health/treatment-tests-and-therapies/breast-mri> (accessed Jun. 12, 2023).
- [37] "Breast Cancer: Stages | Cancer.Net." <https://www.cancer.net/cancer-types/breast-cancer/stages> (accessed Jun. 12, 2023).

- [38] M. L. Czajka and C. Pfeifer, "Breast Cancer Surgery," in *StatPearls*, Treasure Island (FL): StatPearls Publishing, 2023. Accessed: Jun. 12, 2023. [Online]. Available: <http://www.ncbi.nlm.nih.gov/books/NBK553076/>
- [39] R. Baskar, K. A. Lee, R. Yeo, and K.-W. Yeoh, "Cancer and Radiation Therapy: Current Advances and Future Directions," *Int J Med Sci*, vol. 9, no. 3, pp. 193–199, Feb. 2012, doi: 10.7150/ijms.3635.
- [40] L. N. Chaudhary, K. H. Wilkinson, and A. Kong, "Triple-Negative Breast Cancer: Who Should Receive Neoadjuvant Chemotherapy?," *Surg Oncol Clin N Am*, vol. 27, no. 1, pp. 141–153, Jan. 2018, doi: 10.1016/j.soc.2017.08.004.
- [41] F. C. Geyer *et al.*, "The Spectrum of Triple-Negative Breast Disease," *Am J Pathol*, vol. 187, no. 10, pp. 2139–2151, Oct. 2017, doi: 10.1016/j.ajpath.2017.03.016.
- [42] J. D. C. Hon *et al.*, "Breast cancer molecular subtypes: from TNBC to QNBC," *Am J Cancer Res*, vol. 6, no. 9, pp. 1864–1872, Sep. 2016.
- [43] S. G. Ahn, S. J. Kim, C. Kim, and J. Jeong, "Molecular Classification of Triple-Negative Breast Cancer," *J Breast Cancer*, vol. 19, no. 3, pp. 223–230, Sep. 2016, doi: 10.4048/jbc.2016.19.3.223.
- [44] A. M. Badowska-Kozakiewicz and M. P. Budzik, "Immunohistochemical characteristics of basal-like breast cancer," *Contemp Oncol (Pozn)*, vol. 20, no. 6, pp. 436–443, 2016, doi: 10.5114/wo.2016.56938.
- [45] H. A. Wahba and H. A. El-Hadaad, "Current approaches in treatment of triple-negative breast cancer," *Cancer Biol Med*, vol. 12, no. 2, pp. 106–116, Jun. 2015, doi: 10.7497/j.issn.2095-3941.2015.0030.
- [46] L. Yin, J.-J. Duan, X.-W. Bian, and S. Yu, "Triple-negative breast cancer molecular subtyping and treatment progress," *Breast Cancer Research*, vol. 22, no. 1, p. 61, Jun. 2020, doi: 10.1186/s13058-020-01296-5.
- [47] R. Salgado *et al.*, "The evaluation of tumor-infiltrating lymphocytes (TILs) in breast cancer: recommendations by an International TILs Working Group 2014," *Ann Oncol*, vol. 26, no. 2, pp. 259–271, Feb. 2015, doi: 10.1093/annonc/mdu450.
- [48] M. Holanek *et al.*, "Neoadjuvant Chemotherapy of Triple-Negative Breast Cancer: Evaluation of Early Clinical Response, Pathological Complete Response Rates, and Addition of Platinum Salts Benefit Based on Real-World Evidence," *Cancers (Basel)*, vol. 13, no. 7, p. 1586, Mar. 2021, doi: 10.3390/cancers13071586.
- [49] A. J. Maniotis *et al.*, "Vascular Channel Formation by Human Melanoma Cells in Vivo and in Vitro: Vasculogenic Mimicry," *Am J Pathol*, vol. 155, no. 3, pp. 739–752, Sep. 1999.
- [50] R. Folberg, M. J. Hendrix, and A. J. Maniotis, "Vasculogenic mimicry and tumor angiogenesis," *Am J Pathol*, vol. 156, no. 2, pp. 361–381, Feb. 2000, doi: 10.1016/S0002-9440(10)64739-6.
- [51] D. M. McDonald, L. Munn, and R. K. Jain, "Vasculogenic Mimicry: How Convincing, How Novel, and How Significant?," *Am J Pathol*, vol. 156, no. 2, pp. 383–388, Feb. 2000.
- [52] X. Chen, A. J. Maniotis, D. Majumdar, J. Pe'er, and R. Folberg, "Uveal melanoma cell staining for CD34 and assessment of tumor vascularity," *Invest Ophthalmol Vis Sci*, vol. 43, no. 8, pp. 2533–2539, Aug. 2002.
- [53] V. Rummelt *et al.*, "Microcirculation architecture of melanocytic nevi and malignant melanomas of the ciliary body and choroid. A comparative histopathologic and ultrastructural study," *Ophthalmology*, vol. 101, no. 4, pp. 718–727, Apr. 1994, doi: 10.1016/s0161-6420(94)31273-5.
- [54] F. Pezzella *et al.*, "Non-small-cell lung carcinoma tumor growth without morphological evidence of neo-angiogenesis.," *The American Journal of Pathology*, vol. 151, no. 5, p. 1417, Nov. 1997.
- [55] E. Passalidou *et al.*, "Vascular phenotype in angiogenic and non-angiogenic lung non-small cell carcinomas," *Br J Cancer*, vol. 86, no. 2, pp. 244–249, Jan. 2002, doi: 10.1038/sj.bjc.6600015.

- [56] M. J. C. Hendrix, E. A. Seftor, A. R. Hess, and R. E. B. Seftor, "Vasculogenic mimicry and tumour-cell plasticity: lessons from melanoma," *Nat Rev Cancer*, vol. 3, no. 6, pp. 411–421, Jun. 2003, doi: 10.1038/nrc1092.
- [57] J. Folkman, "Can mosaic tumor vessels facilitate molecular diagnosis of cancer?," *Proc Natl Acad Sci U S A*, vol. 98, no. 2, pp. 398–400, Jan. 2001, doi: 10.1073/pnas.98.2.398.
- [58] A. J. Maniotis *et al.*, "Control of melanoma morphogenesis, endothelial survival, and perfusion by extracellular matrix," *Lab Invest*, vol. 82, no. 8, pp. 1031–1043, Aug. 2002, doi: 10.1097/01.lab.0000024362.12721.67.
- [59] L. Sanz, M. Feijóo, B. Blanco, A. Serrano, and L. Alvarez-Vallina, "Generation of non-permissive basement membranes by anti-laminin antibody fragments produced by matrix-embedded gene-modified cells," *Cancer Immunol Immunother*, vol. 52, no. 10, pp. 643–647, Oct. 2003, doi: 10.1007/s00262-003-0400-0.
- [60] C. Liu *et al.*, "Prostate-specific membrane antigen directed selective thrombotic infarction of tumors," *Cancer Res*, vol. 62, no. 19, pp. 5470–5475, Oct. 2002.
- [61] K. Shirakawa *et al.*, "Absence of endothelial cells, central necrosis, and fibrosis are associated with aggressive inflammatory breast cancer," *Cancer Res*, vol. 61, no. 2, pp. 445–451, Jan. 2001.
- [62] K. Shirakawa *et al.*, "Vasculogenic mimicry and pseudo-comedo formation in breast cancer," *Int J Cancer*, vol. 99, no. 6, pp. 821–828, Jun. 2002, doi: 10.1002/ijc.10423.
- [63] K. Shirakawa *et al.*, "Hemodynamics in vasculogenic mimicry and angiogenesis of inflammatory breast cancer xenograft," *Cancer Res*, vol. 62, no. 2, pp. 560–566, Jan. 2002.
- [64] V. L. Silvestri, E. Henriët, R. M. Linville, A. D. Wong, P. C. Searson, and A. J. Ewald, "A Tissue-Engineered 3D Microvessel Model Reveals the Dynamics of Mosaic Vessel Formation in Breast Cancer," *Cancer Res*, vol. 80, no. 19, pp. 4288–4301, Oct. 2020, doi: 10.1158/0008-5472.CAN-19-1564.
- [65] Y. Xu, Q. Li, X.-Y. Li, Q.-Y. Yang, W.-W. Xu, and G.-L. Liu, "Short-term anti-vascular endothelial growth factor treatment elicits vasculogenic mimicry formation of tumors to accelerate metastasis," *J Exp Clin Cancer Res*, vol. 31, p. 16, Feb. 2012, doi: 10.1186/1756-9966-31-16.
- [66] P. Kumar and R. Aggarwal, "An overview of triple-negative breast cancer," *Arch Gynecol Obstet*, vol. 293, no. 2, pp. 247–269, Feb. 2016, doi: 10.1007/s00404-015-3859-y.
- [67] N. Zhang, Y. Yin, S.-J. Xu, and W.-S. Chen, "5-Fluorouracil: Mechanisms of Resistance and Reversal Strategies," *Molecules*, vol. 13, no. 8, pp. 1551–1569, Aug. 2008, doi: 10.3390/molecules13081551.
- [68] U. Amstutz, T. K. Froehlich, and C. R. Largiadèr, "Dihydropyrimidine dehydrogenase gene as a major predictor of severe 5-fluorouracil toxicity," *Pharmacogenomics*, vol. 12, no. 9, pp. 1321–1336, Sep. 2011, doi: 10.2217/pgs.11.72.
- [69] M. A. García *et al.*, "The chemotherapeutic drug 5-fluorouracil promotes PKR-mediated apoptosis in a p53-independent manner in colon and breast cancer cells," *PLoS One*, vol. 6, no. 8, p. e23887, 2011, doi: 10.1371/journal.pone.0023887.
- [70] K. Miura *et al.*, "5-FU Metabolism in Cancer and Orally-Administrable 5-FU Drugs," *Cancers (Basel)*, vol. 2, no. 3, pp. 1717–1730, Sep. 2010, doi: 10.3390/cancers2031717.
- [71] "Purine and Pyrimidine Nucleotide Synthesis and Metabolism - PMC." <https://www.ncbi.nlm.nih.gov/pmc/articles/PMC3243375/> (accessed Jun. 12, 2023).
- [72] F. Michailidou, T. Lebl, A. M. Z. Slawin, S. V. Sharma, M. J. B. Brown, and R. J. M. Goss, "Synthesis and Conformational Analysis of Fluorinated Uridine Analogues Provide Insight into a Neighbouring-Group Participation Mechanism," *Molecules*, vol. 25, no. 23, p. 5513, Nov. 2020, doi: 10.3390/molecules25235513.
- [73] R. Duschinsky, E. Plevin, and C. Heidelberger, "THE SYNTHESIS OF 5-FLUOROPYRIMIDINES," *J. Am. Chem. Soc.*, vol. 79, no. 16, pp. 4559–4560, Aug. 1957, doi: 10.1021/ja01573a087.

- [74] D. M. Volochnyuk, O. O. Grygorenko, and A. O. Gorlova, "Fluorine-Containing Diazines in Medicinal Chemistry and Agrochemistry," *Fluorine in Heterocyclic Chemistry Volume 2*, pp. 577–672, Jun. 2014, doi: 10.1007/978-3-319-04435-4_7.
- [75] E. G. Sander and C. L. Deyrup, "The effect of bisulfite on the dehalogenation of 5-chloro-, 5-bromo-, and 5-iodouracil," *Archives of Biochemistry and Biophysics*, vol. 150, no. 2, pp. 600–605, Jun. 1972, doi: 10.1016/0003-9861(72)90079-3.
- [76] "Discovery of 5'-Substituted 5-Fluoro-2'-deoxyuridine Monophosphate Analogs: A Novel Class of Thymidylate Synthase Inhibitors | ACS Pharmacology & Translational Science." <https://pubs.acs.org/doi/10.1021/acsptsci.2c00252> (accessed Jun. 12, 2023).
- [77] S. S. Fidai, A. E. Sharma, D. N. Johnson, J. P. Segal, and R. R. Lastra, "Dihydropyrimidine dehydrogenase deficiency as a cause of fatal 5-Fluorouracil toxicity," *Autops Case Rep*, vol. 8, no. 4, p. e2018049, Nov. 2018, doi: 10.4322/acr.2018.049.
- [78] C. Kaehler, J. Isensee, T. Hucho, H. Lehrach, and S. Krobitsch, "5-Fluorouracil affects assembly of stress granules based on RNA incorporation," *Nucleic Acids Res*, vol. 42, no. 10, pp. 6436–6447, Jun. 2014, doi: 10.1093/nar/gku264.
- [79] T. J. Wigle, E. V. Tsvetkova, S. A. Welch, and R. B. Kim, "DPYD and Fluorouracil-Based Chemotherapy: Mini Review and Case Report," *Pharmaceutics*, vol. 11, no. 5, p. 199, May 2019, doi: 10.3390/pharmaceutics11050199.
- [80] J. S. Lee, S. E. Yost, and Y. Yuan, "Neoadjuvant Treatment for Triple Negative Breast Cancer: Recent Progresses and Challenges," *Cancers (Basel)*, vol. 12, no. 6, p. 1404, May 2020, doi: 10.3390/cancers12061404.
- [81] M. Saleem, "Lupeol, A Novel Anti-inflammatory and Anti-cancer Dietary Triterpene," *Cancer Lett*, vol. 285, no. 2, pp. 109–115, Nov. 2009, doi: 10.1016/j.canlet.2009.04.033.
- [82] "(1) (PDF) A review on Lupeol: Superficial triterpenoid from horticulture crops." https://www.researchgate.net/publication/351351029_A_review_on_Lupeol_Superficial_triterpenoid_from_horticulture_crops (accessed Jun. 12, 2023).
- [83] M. Martelanc, I. Vovk, and B. Simonovska, "Determination of three major triterpenoids in epicuticular wax of cabbage (*Brassica oleracea* L.) by high-performance liquid chromatography with UV and mass spectrometric detection," *Journal of chromatography. A*, vol. 1164, pp. 145–52, Oct. 2007, doi: 10.1016/j.chroma.2007.06.062.
- [84] M. S. Donaldson, "Nutrition and cancer: A review of the evidence for an anti-cancer diet," *Nutr J*, vol. 3, p. 19, Oct. 2004, doi: 10.1186/1475-2891-3-19.
- [85] P. G. Bradford and A. B. Awad, "Phytosterols as anticancer compounds," *Mol Nutr Food Res*, vol. 51, no. 2, pp. 161–170, Feb. 2007, doi: 10.1002/mnfr.200600164.
- [86] W. N. Setzer and M. C. Setzer, "Plant-derived triterpenoids as potential antineoplastic agents," *Mini Rev Med Chem*, vol. 3, no. 6, pp. 540–556, Sep. 2003, doi: 10.2174/1389557033487854.
- [87] R. S. Tarapore, I. A. Siddiqui, and H. Mukhtar, "Modulation of Wnt/ β -catenin signaling pathway by bioactive food components," *Carcinogenesis*, vol. 33, no. 3, pp. 483–491, Mar. 2012, doi: 10.1093/carcin/bgr305.
- [88] N. Nigam, S. Prasad, and Y. Shukla, "Preventive effects of lupeol on DMBA induced DNA alkylation damage in mouse skin," *Food Chem Toxicol*, vol. 45, no. 11, pp. 2331–2335, Nov. 2007, doi: 10.1016/j.fct.2007.06.002.
- [89] S. Prasad, V. Kumar Yadav, S. Srivastava, and Y. Shukla, "Protective effects of lupeol against benzo[a]pyrene induced clastogenicity in mouse bone marrow cells," *Mol Nutr Food Res*, vol. 52, no. 10, pp. 1117–1120, Oct. 2008, doi: 10.1002/mnfr.200700420.
- [90] M. Saleem, F. Afaq, V. M. Adhami, and H. Mukhtar, "Lupeol modulates NF-kappaB and PI3K/Akt pathways and inhibits skin cancer in CD-1 mice," *Oncogene*, vol. 23, no. 30, pp. 5203–5214, Jul. 2004, doi: 10.1038/sj.onc.1207641.

- [91] T. M. Kolb and M. A. Davis, "The tumor promoter 12-O-tetradecanoylphorbol 13-acetate (TPA) provokes a prolonged morphologic response and ERK activation in Tsc2-null renal tumor cells," *Toxicol Sci*, vol. 81, no. 1, pp. 233–242, Sep. 2004, doi: 10.1093/toxsci/kfh183.
- [92] C. Sorina *et al.*, "Lupeol, a pentacyclic triterpene that reduces the lesions and irritability on murine skin and is effective on in vitro tumor models," *Journal of Agroalimentary Processes and Technologies Journal of Agroalimentary Processes and Technologies*, vol. 16, pp. 427–432, Jan. 2010.
- [93] F. Bociort *et al.*, "Investigation of Lupeol as Anti-Melanoma Agent: An In Vitro-In Ovo Perspective," *Curr Oncol*, vol. 28, no. 6, pp. 5054–5066, Dec. 2021, doi: 10.3390/currenol28060425.
- [94] T. A. Martin, L. Ye, A. J. Sanders, J. Lane, and W. G. Jiang, "Cancer Invasion and Metastasis: Molecular and Cellular Perspective," in *Madame Curie Bioscience Database [Internet]*, Landes Bioscience, 2013. Accessed: Jun. 12, 2023. [Online]. Available: <https://www.ncbi.nlm.nih.gov/books/NBK164700/>
- [95] G.-Y. Liou and P. Storz, "Reactive oxygen species in cancer," *Free Radic Res*, vol. 44, no. 5, pp. 479–496, May 2010, doi: 10.3109/10715761003667554.
- [96] M. Saleem *et al.*, "Lupeol inhibits proliferation of human prostate cancer cells by targeting β -catenin signaling," *Carcinogenesis*, vol. 30, no. 5, pp. 808–817, May 2009, doi: 10.1093/carcin/bgp044.
- [97] "(1) (PDF) Lupeol, A Novel Anti-inflammatory and Anti-cancer Dietary Triterpene." https://www.researchgate.net/publication/26236400_Lupeol_A_Novel_Anti-inflammatory_and_Anti-cancer_Dietary_Triterpene (accessed Jun. 12, 2023).
- [98] H. R. Siddique, S. K. Mishra, R. J. Karnes, and M. Saleem, "Lupeol, a Novel Androgen Receptor Inhibitor: Implications in Prostate Cancer Therapy," *Clin Cancer Res*, vol. 17, no. 16, pp. 5379–5391, Aug. 2011, doi: 10.1158/1078-0432.CCR-11-0916.
- [99] F. Bray, J. Ferlay, I. Soerjomataram, R. L. Siegel, L. A. Torre, and A. Jemal, "Global cancer statistics 2018: GLOBOCAN estimates of incidence and mortality worldwide for 36 cancers in 185 countries," *CA Cancer J Clin*, vol. 68, no. 6, pp. 394–424, Nov. 2018, doi: 10.3322/caac.21492.
- [100] C. Yam, S. A. Mani, and S. L. Moulder, "Targeting the Molecular Subtypes of Triple Negative Breast Cancer: Understanding the Diversity to Progress the Field," *Oncologist*, vol. 22, no. 9, pp. 1086–1093, Sep. 2017, doi: 10.1634/theoncologist.2017-0095.
- [101] B. Janic and A. S. Arbab, "The role and therapeutic potential of endothelial progenitor cells in tumor neovascularization," *ScientificWorldJournal*, vol. 10, pp. 1088–1099, Jun. 2010, doi: 10.1100/tsw.2010.100.
- [102] K. Servick, "Breast cancer. Breast cancer: a world of differences," *Science*, vol. 343, no. 6178, pp. 1452–1453, Mar. 2014, doi: 10.1126/science.343.6178.1452.
- [103] N. Kumar *et al.*, "cAMP regulated EPAC1 supports microvascular density, angiogenic and metastatic properties in a model of triple negative breast cancer," *Carcinogenesis*, vol. 39, no. 10, pp. 1245–1253, Oct. 2018, doi: 10.1093/carcin/bgy090.
- [104] Y. A. Fouad and C. Aanei, "Revisiting the hallmarks of cancer," *Am J Cancer Res*, vol. 7, no. 5, pp. 1016–1036, 2017.
- [105] N. J. Robert *et al.*, "RIBBON-1: randomized, double-blind, placebo-controlled, phase III trial of chemotherapy with or without bevacizumab for first-line treatment of human epidermal growth factor receptor 2-negative, locally recurrent or metastatic breast cancer," *J Clin Oncol*, vol. 29, no. 10, pp. 1252–1260, Apr. 2011, doi: 10.1200/JCO.2010.28.0982.
- [106] C. Rochlitz *et al.*, "SAKK 24/09: safety and tolerability of bevacizumab plus paclitaxel vs. bevacizumab plus metronomic cyclophosphamide and capecitabine as first-line therapy in patients with HER2-negative advanced stage breast cancer - a multicenter, randomized phase III trial," *BMC Cancer*, vol. 16, no. 1, p. 780, Oct. 2016, doi: 10.1186/s12885-016-2823-y.
- [107] M. N. Dickler *et al.*, "Phase III Trial Evaluating Letrozole As First-Line Endocrine Therapy With or Without Bevacizumab for the Treatment of Postmenopausal Women With Hormone Receptor-

- Positive Advanced-Stage Breast Cancer: CALGB 40503 (Alliance),” *J Clin Oncol*, vol. 34, no. 22, pp. 2602–2609, Aug. 2016, doi: 10.1200/JCO.2015.66.1595.
- [108] H. Ge and H. Luo, “Overview of advances in vasculogenic mimicry - a potential target for tumor therapy,” *Cancer Manag Res*, vol. 10, pp. 2429–2437, 2018, doi: 10.2147/CMAR.S164675.
- [109] Q. Li *et al.*, “A phase II study of capecitabine plus cisplatin in metastatic triple-negative breast cancer patients pretreated with anthracyclines and taxanes,” *Cancer Biol Ther*, vol. 16, no. 12, pp. 1746–1753, Oct. 2015, doi: 10.1080/15384047.2015.1095400.
- [110] S. Bhattacharyya *et al.*, “Reversing effect of Lupeol on vasculogenic mimicry in murine melanoma progression,” *Microvasc Res*, vol. 121, pp. 52–62, Jan. 2019, doi: 10.1016/j.mvr.2018.10.008.
- [111] S. Wu, L. Yu, Z. Cheng, W. Song, L. Zhou, and Y. Tao, “Expression of maspin in non-small cell lung cancer and its relationship to vasculogenic mimicry,” *J Huazhong Univ Sci Technolog Med Sci*, vol. 32, no. 3, pp. 346–352, Jun. 2012, doi: 10.1007/s11596-012-0060-4.
- [112] W. Liu *et al.*, “Prognostic significance and mechanisms of patterned matrix vasculogenic mimicry in hepatocellular carcinoma,” *Med Oncol*, vol. 28 Suppl 1, pp. S228-238, Dec. 2011, doi: 10.1007/s12032-010-9706-x.
- [113] M. Li *et al.*, “Vasculogenic mimicry: a new prognostic sign of gastric adenocarcinoma,” *Pathol Oncol Res*, vol. 16, no. 2, pp. 259–266, Jun. 2010, doi: 10.1007/s12253-009-9220-7.
- [114] Q. Sun, X. Zou, T. Zhang, J. Shen, Y. Yin, and J. Xiang, “The role of miR-200a in vasculogenic mimicry and its clinical significance in ovarian cancer,” *Gynecol Oncol*, vol. 132, no. 3, pp. 730–738, Mar. 2014, doi: 10.1016/j.ygyno.2014.01.047.
- [115] W. Gong *et al.*, “Nodal signaling promotes vasculogenic mimicry formation in breast cancer via the Smad2/3 pathway,” *Oncotarget*, vol. 7, no. 43, pp. 70152–70167, Oct. 2016, doi: 10.18632/oncotarget.12161.
- [116] Y. Liu *et al.*, “Function of AURKA protein kinase in the formation of vasculogenic mimicry in triple-negative breast cancer stem cells,” *Onco Targets Ther*, vol. 9, pp. 3473–3484, 2016, doi: 10.2147/OTT.S93015.
- [117] R. Liu, K. Yang, C. Meng, Z. Zhang, and Y. Xu, “Vasculogenic mimicry is a marker of poor prognosis in prostate cancer,” *Cancer Biol Ther*, vol. 13, no. 7, pp. 527–533, May 2012, doi: 10.4161/cbt.19602.
- [118] A. W. Boyd, P. F. Bartlett, and M. Lackmann, “Therapeutic targeting of Eph receptors and their ligands,” *Nat Rev Drug Discov*, vol. 13, no. 1, pp. 39–62, Jan. 2014, doi: 10.1038/nrd4175.
- [119] H. Miao *et al.*, “EphA2 mediates ligand-dependent inhibition and ligand-independent promotion of cell migration and invasion via a reciprocal regulatory loop with Akt,” *Cancer Cell*, vol. 16, no. 1, pp. 9–20, Jul. 2009, doi: 10.1016/j.ccr.2009.04.009.
- [120] A. Barquilla and E. B. Pasquale, “Eph receptors and ephrins: therapeutic opportunities,” *Annu Rev Pharmacol Toxicol*, vol. 55, pp. 465–487, 2015, doi: 10.1146/annurev-pharmtox-011112-140226.
- [121] E. B. Pasquale, “Eph receptors and ephrins in cancer: bidirectional signalling and beyond,” *Nat Rev Cancer*, vol. 10, no. 3, pp. 165–180, Mar. 2010, doi: 10.1038/nrc2806.
- [122] E. B. Pasquale, “Eph-ephrin bidirectional signaling in physiology and disease,” *Cell*, vol. 133, no. 1, pp. 38–52, Apr. 2008, doi: 10.1016/j.cell.2008.03.011.
- [123] R. C. Ireton and J. Chen, “EphA2 receptor tyrosine kinase as a promising target for cancer therapeutics,” *Curr Cancer Drug Targets*, vol. 5, no. 3, pp. 149–157, May 2005, doi: 10.2174/1568009053765780.
- [124] A. Barquilla, I. Lamberto, R. Noberini, S. Heynen-Genel, L. M. Brill, and E. B. Pasquale, “Protein kinase A can block EphA2 receptor-mediated cell repulsion by increasing EphA2 S897

- phosphorylation," *Mol Biol Cell*, vol. 27, no. 17, pp. 2757–2770, Sep. 2016, doi: 10.1091/mbc.E16-01-0048.
- [125] Y. Zhou *et al.*, "Crucial roles of RSK in cell motility by catalysing serine phosphorylation of EphA2," *Nat Commun*, vol. 6, p. 7679, Jul. 2015, doi: 10.1038/ncomms8679.
- [126] D. M. Brantley-Sieders *et al.*, "Eph/ephrin profiling in human breast cancer reveals significant associations between expression level and clinical outcome," *PLoS One*, vol. 6, no. 9, p. e24426, 2011, doi: 10.1371/journal.pone.0024426.
- [127] A. R. Hess, E. A. Seftor, L. M. Gruman, M. S. Kinch, R. E. B. Seftor, and M. J. C. Hendrix, "VE-cadherin regulates EphA2 in aggressive melanoma cells through a novel signaling pathway: implications for vasculogenic mimicry," *Cancer Biol Ther*, vol. 5, no. 2, pp. 228–233, Feb. 2006, doi: 10.4161/cbt.5.2.2510.
- [128] H. Wang *et al.*, "Vasculogenic Mimicry in Prostate Cancer: The Roles of EphA2 and PI3K," *J Cancer*, vol. 7, no. 9, pp. 1114–1124, 2016, doi: 10.7150/jca.14120.
- [129] W. Wang *et al.*, "Epithelial-mesenchymal transition regulated by EphA2 contributes to vasculogenic mimicry formation of head and neck squamous cell carcinoma," *Biomed Res Int*, vol. 2014, p. 803914, 2014, doi: 10.1155/2014/803914.
- [130] H. S. Kim *et al.*, "Morphological characteristics of vasculogenic mimicry and its correlation with EphA2 expression in gastric adenocarcinoma," *Sci Rep*, vol. 9, no. 1, p. 3414, Mar. 2019, doi: 10.1038/s41598-019-40265-7.
- [131] J.-Y. Wang *et al.*, "Functional significance of VEGF-a in human ovarian carcinoma: role in vasculogenic mimicry," *Cancer Biol Ther*, vol. 7, no. 5, pp. 758–766, May 2008, doi: 10.4161/cbt.7.5.5765.
- [132] K. Harada, M. Negishi, and H. Katoh, "HGF-induced serine 897 phosphorylation of EphA2 regulates epithelial morphogenesis of MDCK cells in 3D culture," *Journal of Cell Science*, vol. 128, no. 10, pp. 1912–1921, May 2015, doi: 10.1242/jcs.163790.
- [133] D. Delgado-Bellido, S. Serrano-Saenz, M. Fernández-Cortés, and F. J. Oliver, "Vasculogenic mimicry signaling revisited: focus on non-vascular VE-cadherin," *Mol Cancer*, vol. 16, no. 1, p. 65, Mar. 2017, doi: 10.1186/s12943-017-0631-x.
- [134] F. Bladt, D. Riethmacher, S. Isenmann, A. Aguzzi, and C. Birchmeier, "Essential role for the c-met receptor in the migration of myogenic precursor cells into the limb bud," *Nature*, vol. 376, no. 6543, pp. 768–771, Aug. 1995, doi: 10.1038/376768a0.
- [135] H.-N. Mo and P. Liu, "Targeting MET in cancer therapy," *Chronic Dis Transl Med*, vol. 3, no. 3, pp. 148–153, Jul. 2017, doi: 10.1016/j.cdtm.2017.06.002.
- [136] P. C. Ma, G. Maulik, J. Christensen, and R. Salgia, "c-Met: structure, functions and potential for therapeutic inhibition," *Cancer Metastasis Rev*, vol. 22, no. 4, pp. 309–325, Dec. 2003, doi: 10.1023/a:1023768811842.
- [137] Y. Uehara *et al.*, "Placental defect and embryonic lethality in mice lacking hepatocyte growth factor/scatter factor," *Nature*, vol. 373, no. 6516, pp. 702–705, Feb. 1995, doi: 10.1038/373702a0.
- [138] J. T. Buijs, A.-M. Cleton, V. T. H. B. M. Smit, C. W. G. M. Löwik, S. E. Papapoulos, and G. van der Pluijm, "Prognostic significance of periodic acid-Schiff-positive patterns in primary breast cancer and its lymph node metastases," *Breast Cancer Res Treat*, vol. 84, no. 2, pp. 117–130, Mar. 2004, doi: 10.1023/B:BREA.0000018408.77854.d1.
- [139] B. Sun *et al.*, "Identification of metastasis-related proteins and their clinical relevance to triple-negative human breast cancer," *Clin Cancer Res*, vol. 14, no. 21, pp. 7050–7059, Nov. 2008, doi: 10.1158/1078-0432.CCR-08-0520.
- [140] H. Sun *et al.*, "Anti-angiogenic treatment promotes triple-negative breast cancer invasion via vasculogenic mimicry," *Cancer Biol Ther*, vol. 18, no. 4, pp. 205–213, Apr. 2017, doi: 10.1080/15384047.2017.1294288.

- [141] J. Kollias, C. A. Murphy, C. W. Elston, I. O. Ellis, J. F. Robertson, and R. W. Blamey, "The prognosis of small primary breast cancers," *Eur J Cancer*, vol. 35, no. 6, pp. 908–912, Jun. 1999, doi: 10.1016/s0959-8049(99)00056-8.
- [142] L. Qiao *et al.*, "Advanced research on vasculogenic mimicry in cancer," *J Cell Mol Med*, vol. 19, no. 2, pp. 315–326, Feb. 2015, doi: 10.1111/jcmm.12496.
- [143] R. E. B. Seftor *et al.*, "Tumor cell vasculogenic mimicry: from controversy to therapeutic promise," *Am J Pathol*, vol. 181, no. 4, pp. 1115–1125, Oct. 2012, doi: 10.1016/j.ajpath.2012.07.013.
- [144] P. Xing *et al.*, "ALDH1 Expression and Vasculogenic Mimicry Are Positively Associated with Poor Prognosis in Patients with Breast Cancer," *Cell Physiol Biochem*, vol. 49, no. 3, pp. 961–970, 2018, doi: 10.1159/000493227.
- [145] D. P. Zelinski, N. D. Zantek, J. C. Stewart, A. R. Irizarry, and M. S. Kinch, "EphA2 overexpression causes tumorigenesis of mammary epithelial cells," *Cancer Res*, vol. 61, no. 5, pp. 2301–2306, Mar. 2001.
- [146] D. M. Brantley-Sieders *et al.*, "The receptor tyrosine kinase EphA2 promotes mammary adenocarcinoma tumorigenesis and metastatic progression in mice by amplifying ErbB2 signaling," *J Clin Invest*, vol. 118, no. 1, pp. 64–78, Jan. 2008, doi: 10.1172/JCI33154.
- [147] A. B. Larsen, M. W. Pedersen, M.-T. Stockhausen, M. V. Grandal, B. van Deurs, and H. S. Poulsen, "Activation of the EGFR gene target EphA2 inhibits epidermal growth factor-induced cancer cell motility," *Mol Cancer Res*, vol. 5, no. 3, pp. 283–293, Mar. 2007, doi: 10.1158/1541-7786.MCR-06-0321.
- [148] D. Vaught, D. M. Brantley-Sieders, and J. Chen, "Eph receptors in breast cancer: roles in tumor promotion and tumor suppression," *Breast Cancer Res*, vol. 10, no. 6, p. 217, 2008, doi: 10.1186/bcr2207.
- [149] H. Miao *et al.*, "EphA2 promotes infiltrative invasion of glioma stem cells in vivo through cross-talk with Akt and regulates stem cell properties," *Oncogene*, vol. 34, no. 5, pp. 558–567, Jan. 2015, doi: 10.1038/onc.2013.590.
- [150] J. Huang *et al.*, "EphA2 promotes epithelial-mesenchymal transition through the Wnt/ β -catenin pathway in gastric cancer cells," *Oncogene*, vol. 33, no. 21, pp. 2737–2747, May 2014, doi: 10.1038/onc.2013.238.
- [151] E. Binda *et al.*, "The EphA2 receptor drives self-renewal and tumorigenicity in stem-like tumor-propagating cells from human glioblastomas," *Cancer Cell*, vol. 22, no. 6, pp. 765–780, Dec. 2012, doi: 10.1016/j.ccr.2012.11.005.
- [152] T. Tawadros, M. D. Brown, C. A. Hart, and N. W. Clarke, "Ligand-independent activation of EphA2 by arachidonic acid induces metastasis-like behaviour in prostate cancer cells," *Br J Cancer*, vol. 107, no. 10, pp. 1737–1744, Nov. 2012, doi: 10.1038/bjc.2012.457.
- [153] C. Schmidt *et al.*, "Scatter factor/hepatocyte growth factor is essential for liver development," *Nature*, vol. 373, no. 6516, pp. 699–702, Feb. 1995, doi: 10.1038/373699a0.
- [154] J. M. Siegfried, L. A. Weissfeld, J. D. Luketich, R. J. Weyant, C. T. Gubish, and R. J. Landreneau, "The clinical significance of hepatocyte growth factor for non-small cell lung cancer," *Ann Thorac Surg*, vol. 66, no. 6, pp. 1915–1918, Dec. 1998, doi: 10.1016/s0003-4975(98)01165-5.
- [155] L. Goyal, M. D. Muzumdar, and A. X. Zhu, "Targeting the HGF/c-MET Pathway in Hepatocellular Carcinoma," *Clin Cancer Res*, vol. 19, no. 9, pp. 2310–2318, May 2013, doi: 10.1158/1078-0432.CCR-12-2791.
- [156] S. P. Hack, J.-M. Bruey, and H. Koeppen, "HGF/MET-directed therapeutics in gastroesophageal cancer: a review of clinical and biomarker development," *Oncotarget*, vol. 5, no. 10, pp. 2866–2880, May 2014.
- [157] T. A. Yap and J. S. de Bono, "Targeting the HGF/c-Met axis: state of play," *Mol Cancer Ther*, vol. 9, no. 5, pp. 1077–1079, May 2010, doi: 10.1158/1535-7163.MCT-10-0122.

- [158] P. Carmeliet and R. K. Jain, "Molecular mechanisms and clinical applications of angiogenesis," *Nature*, vol. 473, no. 7347, pp. 298–307, May 2011, doi: 10.1038/nature10144.
- [159] M. Potente, H. Gerhardt, and P. Carmeliet, "Basic and therapeutic aspects of angiogenesis," *Cell*, vol. 146, no. 6, pp. 873–887, Sep. 2011, doi: 10.1016/j.cell.2011.08.039.
- [160] Cancer Genome Atlas Network, "Comprehensive molecular portraits of human breast tumours," *Nature*, vol. 490, no. 7418, pp. 61–70, Oct. 2012, doi: 10.1038/nature11412.
- [161] P. Lal, L. K. Tan, and B. Chen, "Correlation of HER-2 status with estrogen and progesterone receptors and histologic features in 3,655 invasive breast carcinomas," *Am J Clin Pathol*, vol. 123, no. 4, pp. 541–546, Apr. 2005, doi: 10.1309/YMJ3-A83T-B39M-RUT9.
- [162] H. Sung *et al.*, "Global Cancer Statistics 2020: GLOBOCAN Estimates of Incidence and Mortality Worldwide for 36 Cancers in 185 Countries," *CA: A Cancer Journal for Clinicians*, vol. 71, no. 3, pp. 209–249, 2021, doi: 10.3322/caac.21660.
- [163] M. G. Cerrito *et al.*, "Metronomic combination of Vinorelbine and 5Fluorouracil is able to inhibit triple-negative breast cancer cells. Results from the proof-of-concept VICTOR-0 study," *Oncotarget*, vol. 9, no. 44, pp. 27448–27459, Jun. 2018, doi: 10.18632/oncotarget.25422.
- [164] C. L. Shapiro and A. Recht, "Side Effects of Adjuvant Treatment of Breast Cancer," *N Engl J Med*, vol. 344, no. 26, pp. 1997–2008, Jun. 2001, doi: 10.1056/NEJM200106283442607.
- [165] "Rationalizing combination therapies," *Nat Med*, vol. 23, no. 10, Art. no. 10, Oct. 2017, doi: 10.1038/nm.4426.
- [166] M. A. Wilson *et al.*, "Copy Number Changes Are Associated with Response to Treatment with Carboplatin, Paclitaxel, and Sorafenib in Melanoma," *Clin Cancer Res*, vol. 22, no. 2, pp. 374–382, Jan. 2016, doi: 10.1158/1078-0432.CCR-15-1162.
- [167] P. B. Gaule, J. Crown, N. O'Donovan, and M. J. Duffy, "c-MET in triple-negative breast cancer: is it a therapeutic target for this subset of breast cancer patients?," *Expert Opin Ther Targets*, vol. 18, no. 9, pp. 999–1009, Sep. 2014, doi: 10.1517/14728222.2014.938050.
- [168] T. Okuyama *et al.*, "EPHA2 antisense RNA modulates EPHA2 mRNA levels in basal-like/triple-negative breast cancer cells," *Biochimie*, vol. 179, pp. 169–180, Dec. 2020, doi: 10.1016/j.biochi.2020.10.002.
- [169] I. Nikas *et al.*, "EPHA2, EPHA4, and EPHA7 Expression in Triple-Negative Breast Cancer," *Diagnostics (Basel)*, vol. 12, no. 2, p. 366, Feb. 2022, doi: 10.3390/diagnostics12020366.
- [170] X. Zhao *et al.*, "Clinicopathological and prognostic significance of c-Met overexpression in breast cancer," *Oncotarget*, vol. 8, no. 34, pp. 56758–56767, May 2017, doi: 10.18632/oncotarget.18142.
- [171] "c-Met as a potential therapeutic target in triple negative breast cancer," *Cancer-Leading Proteases*, pp. 295–326, Jan. 2020, doi: 10.1016/B978-0-12-818168-3.00011-5.
- [172] "Impact of MET status on treatment outcomes in papillary renal cell carcinoma: A pooled analysis of historical data - ClinicalKey." <https://www.clinicalkey.com/#!/content/playContent/1-s2.0-S0959804922002313?returnurl=https%2F%2Flinkinghub.elsevier.com%2Fretrieve%2Fpii%2FS0959804922002313%3Fshowall%3Dtrue&referrer=https%2F%2Fpubmed.ncbi.nlm.nih.gov%2F> (accessed Mar. 23, 2023).
- [173] S. L. Organ and M.-S. Tsao, "An overview of the c-MET signaling pathway," *Ther Adv Med Oncol*, vol. 3, no. 1 Suppl, pp. S7–S19, Nov. 2011, doi: 10.1177/1758834011422556.
- [174] R. Straussman *et al.*, "Tumour micro-environment elicits innate resistance to RAF inhibitors through HGF secretion," *Nature*, vol. 487, no. 7408, pp. 500–504, Jul. 2012, doi: 10.1038/nature11183.
- [175] M. Wang *et al.*, "Role of tumor microenvironment in tumorigenesis," *J Cancer*, vol. 8, no. 5, pp. 761–773, Feb. 2017, doi: 10.7150/jca.17648.

- [176] C. Liebmam, "Regulation of MAP kinase activity by peptide receptor signalling pathway: paradigms of multiplicity," *Cell Signal*, vol. 13, no. 11, pp. 777–785, Nov. 2001, doi: 10.1016/s0898-6568(01)00192-9.
- [177] J. Zhang *et al.*, "Recent advances in the development of dual VEGFR and c-Met small molecule inhibitors as anticancer drugs," *Eur J Med Chem*, vol. 108, pp. 495–504, Jan. 2016, doi: 10.1016/j.ejmech.2015.12.016.
- [178] P. Zhao, D. Jiang, Y. Huang, and C. Chen, "EphA2: A promising therapeutic target in breast cancer," *Journal of Genetics and Genomics*, vol. 48, no. 4, pp. 261–267, Apr. 2021, doi: 10.1016/j.jgg.2021.02.011.
- [179] D. Mitra *et al.*, "Phosphorylation of EphA2 receptor and vasculogenic mimicry is an indicator of poor prognosis in invasive carcinoma of the breast," *Breast Cancer Res Treat*, vol. 179, no. 2, pp. 359–370, Jan. 2020, doi: 10.1007/s10549-019-05482-8.
- [180] C. Lefebvre and A. L. Allan, "Anti-proliferative and anti-migratory effects of EGFR and c-Met tyrosine kinase inhibitors in triple negative breast cancer cells," *Precision Cancer Medicine*, vol. 4, no. 0, Art. no. 0, Mar. 2021, doi: 10.21037/pcm-20-62.
- [181] V. Eterno *et al.*, "Adipose-derived mesenchymal stem cells (ASCs) may favour breast cancer recurrence via HGF/c-Met signaling," *Oncotarget*, vol. 5, no. 3, pp. 613–633, Oct. 2013.
- [182] V. S. Hughes and D. W. Siemann, "Failures in preclinical and clinical trials of c-Met inhibitors: evaluation of pathway activity as a promising selection criterion," *Oncotarget*, vol. 10, no. 2, pp. 184–197, Jan. 2019, doi: 10.18632/oncotarget.26546.
- [183] D. M. Brantley-Sieders, W. B. Fang, D. J. Hicks, G. Zhuang, Y. Shyr, and J. Chen, "Impaired tumor microenvironment in EphA2-deficient mice inhibits tumor angiogenesis and metastatic progression," *The FASEB Journal*, vol. 19, no. 13, pp. 1884–1886, 2005, doi: 10.1096/fj.05-4038fje.
- [184] M. Tandon, S. V. Vemula, and S. K. Mittal, "Emerging strategies for EphA2 receptor targeting for cancer therapeutics," *Expert Opin Ther Targets*, vol. 15, no. 1, pp. 31–51, Jan. 2011, doi: 10.1517/14728222.2011.538682.
- [185] A. Coxon *et al.*, "Soluble c-Met receptors inhibit phosphorylation of c-Met and growth of hepatocyte growth factor: c-Met-dependent tumors in animal models," *Mol Cancer Ther*, vol. 8, no. 5, pp. 1119–1125, May 2009, doi: 10.1158/1535-7163.MCT-08-1032.
- [186] R. Cashman, H. Cohen, R. Ben-Hamo, A. Zilberberg, and S. Efroni, "SENP5 mediates breast cancer invasion via a TGF β RI SUMOylation cascade," *Oncotarget*, vol. 5, no. 4, pp. 1071–1082, Feb. 2014.
- [187] S. Dasgupta *et al.*, "RGS5-TGF β -Smad2/3 axis switches pro- to anti-apoptotic signaling in tumor-residing pericytes, assisting tumor growth," *Cell Death Differ*, vol. 28, no. 11, pp. 3052–3076, Nov. 2021, doi: 10.1038/s41418-021-00801-3.
- [188] K. R. Amato *et al.*, "EPHA2 blockade overcomes acquired resistance to EGFR kinase inhibitors in lung cancer," *Cancer Res*, vol. 76, no. 2, pp. 305–318, Jan. 2016, doi: 10.1158/0008-5472.CAN-15-0717.
- [189] M. Sameni *et al.*, "Cabozantinib (XL184) Inhibits Growth and Invasion of Preclinical TNBC Models," *Clin Cancer Res*, vol. 22, no. 4, pp. 923–934, Feb. 2016, doi: 10.1158/1078-0432.CCR-15-0187.
- [190] N. Kawase *et al.*, "SRC kinase activator CDCP1 promotes hepatocyte growth factor-induced cell migration/invasion of a subset of breast cancer cells," *Journal of Biological Chemistry*, vol. 298, no. 3, Mar. 2022, doi: 10.1016/j.jbc.2022.101630.
- [191] D. Saha *et al.*, "Lupeol and Paclitaxel cooperate in hindering hypoxia induced vasculogenic mimicry via suppression of HIF-1 α -EphA2-Laminin-5 γ 2 network in human oral cancer," *J Cell Commun Signal*, Sep. 2022, doi: 10.1007/s12079-022-00693-z.
- [192] K. Tao, M. Fang, J. Alroy, and G. G. Sahagian, "Imagable 4T1 model for the study of late stage breast cancer," *BMC Cancer*, vol. 8, p. 228, Aug. 2008, doi: 10.1186/1471-2407-8-228.

- [193] O. Bello-Monroy *et al.*, "Hepatocyte growth factor enhances the clearance of a multidrug-resistant Mycobacterium tuberculosis strain by high doses of conventional chemotherapy, preserving liver function," *Journal of Cellular Physiology*, vol. 235, no. 2, pp. 1637–1648, 2020, doi: 10.1002/jcp.29082.
- [194] X. Zhang *et al.*, "Lupeol inhibits the proliferation and migration of MDA-MB-231 breast cancer cells via a novel crosstalk mechanism between autophagy and the EMT," *Food & Function*, vol. 13, no. 9, pp. 4967–4976, 2022, doi: 10.1039/D2FO00483F.
- [195] S. Ghosh, A. Pal, and M. Ray, "Methylglyoxal in combination with 5-Fluorouracil elicits improved chemosensitivity in breast cancer through apoptosis and cell cycle inhibition," *Biomed Pharmacother*, vol. 114, p. 108855, Jun. 2019, doi: 10.1016/j.biopha.2019.108855.
- [196] K. Wilson, E. Shiuan, and D. M. Brantley-Sieders, "Oncogenic functions and therapeutic targeting of EphA2 in cancer," *Oncogene*, vol. 40, no. 14, pp. 2483–2495, Apr. 2021, doi: 10.1038/s41388-021-01714-8.
- [197] B. Wang *et al.*, "Cancer-Associated Fibroblasts Promote Radioresistance of Breast Cancer Cells via the HGF/c-Met Signaling Pathway," *Int J Radiat Oncol Biol Phys*, pp. S0360-3016(22)03679–3, Dec. 2022, doi: 10.1016/j.ijrobp.2022.12.029.
- [198] S. Yan, X. Jiao, H. Zou, and K. Li, "Prognostic significance of c-Met in breast cancer: a meta-analysis of 6010 cases," *Diagn Pathol*, vol. 10, p. 62, Jun. 2015, doi: 10.1186/s13000-015-0296-y.
- [199] K. Miura *et al.*, "Involvement of EphA2-mediated tyrosine phosphorylation of Shp2 in Shp2-regulated activation of extracellular signal-regulated kinase," *Oncogene*, vol. 32, no. 45, Art. no. 45, Nov. 2013, doi: 10.1038/onc.2012.571.
- [200] B. P. Schneider *et al.*, "Triple-negative breast cancer: risk factors to potential targets," *Clin Cancer Res*, vol. 14, no. 24, pp. 8010–8018, Dec. 2008, doi: 10.1158/1078-0432.CCR-08-1208.
- [201] M. Yousefi, R. Nosrati, A. Salmaninejad, S. Dehghani, A. Shahryari, and A. Saberi, "Organ-specific metastasis of breast cancer: molecular and cellular mechanisms underlying lung metastasis," *Cell Oncol.*, vol. 41, no. 2, pp. 123–140, Apr. 2018, doi: 10.1007/s13402-018-0376-6.
- [202] C. Neophytou, P. Boutsikos, and P. Papageorgis, "Molecular Mechanisms and Emerging Therapeutic Targets of Triple-Negative Breast Cancer Metastasis," *Frontiers in Oncology*, vol. 8, 2018, Accessed: Apr. 08, 2022. [Online]. Available: <https://www.frontiersin.org/article/10.3389/fonc.2018.00031>
- [203] C. M. Ho-Yen, J. L. Jones, and S. Kermorgant, "The clinical and functional significance of c-Met in breast cancer: a review," *Breast Cancer Res*, vol. 17, no. 1, p. 52, 2015, doi: 10.1186/s13058-015-0547-6.
- [204] K. P. Raghav *et al.*, "c-MET and Phospho-c-MET Protein Levels in Breast Cancers and Survival Outcomes," *Clinical Cancer Research*, vol. 18, no. 8, pp. 2269–2277, Apr. 2012, doi: 10.1158/1078-0432.CCR-11-2830.
- [205] N. Sharma, P. Palia, A. Chaudhary, Shalini, K. Verma, and I. Kumar, "A Review on Pharmacological Activities of Lupeol and its Triterpene Derivatives," *Journal of Drug Delivery and Therapeutics*, vol. 10, no. 5, Art. no. 5, Sep. 2020, doi: 10.22270/jddt.v10i5.4280.
- [206] S. Bhattacharyya *et al.*, "CDKN2A-p53 mediated antitumor effect of Lupeol in head and neck cancer," *Cell Oncol.*, vol. 40, no. 2, pp. 145–155, Apr. 2017, doi: 10.1007/s13402-016-0311-7.
- [207] S. Rauth *et al.*, "Lupeol evokes anticancer effects in oral squamous cell carcinoma by inhibiting oncogenic EGFR pathway," *Mol Cell Biochem*, vol. 417, no. 1–2, pp. 97–110, Jun. 2016, doi: 10.1007/s11010-016-2717-y.
- [208] L. K *et al.*, "Lupeol and its derivatives as anticancer and anti-inflammatory agents: Molecular mechanisms and therapeutic efficacy," *Pharmacological research*, vol. 164, Feb. 2021, doi: 10.1016/j.phrs.2020.105373.

- [209] S. Che, S. Wu, and P. Yu, "Lupeol induces autophagy and apoptosis with reduced cancer stem-like properties in retinoblastoma via phosphoinositide 3-kinase/protein kinase B/mammalian target of rapamycin inhibition," *J Pharm Pharmacol*, vol. 74, no. 2, pp. 208–215, Feb. 2022, doi: 10.1093/jpp/rgab060.
- [210] K. Hata, K. Hori, and S. Takahashi, "Differentiation- and apoptosis-inducing activities by pentacyclic triterpenes on a mouse melanoma cell line," *J Nat Prod*, vol. 65, no. 5, pp. 645–648, May 2002, doi: 10.1021/np0104673.
- [211] M. Saleem, S. Kaur, M.-H. Kweon, V. M. Adhami, F. Afaq, and H. Mukhtar, "Lupeol, a fruit and vegetable based triterpene, induces apoptotic death of human pancreatic adenocarcinoma cells via inhibition of Ras signaling pathway," *Carcinogenesis*, vol. 26, no. 11, pp. 1956–1964, Nov. 2005, doi: 10.1093/carcin/bgi157.
- [212] T. K. W. Lee, A. Castilho, V. C. H. Cheung, K. H. Tang, S. Ma, and I. O. L. Ng, "Lupeol targets liver tumor-initiating cells through phosphatase and tensin homolog modulation," *Hepatology*, vol. 53, no. 1, pp. 160–170, Jan. 2011, doi: 10.1002/hep.24000.
- [213] S. C. Thomasset, D. P. Berry, G. Garcea, T. Marczylo, W. P. Steward, and A. J. Gescher, "Dietary polyphenolic phytochemicals--promising cancer chemopreventive agents in humans? A review of their clinical properties," *Int J Cancer*, vol. 120, no. 3, pp. 451–458, Feb. 2007, doi: 10.1002/ijc.22419.
- [214] E. L. Nguemfo *et al.*, "Anti-oxidative and anti-inflammatory activities of some isolated constituents from the stem bark of *Allanblackia monticola* Staner L.C (Guttiferae)," *Inflammopharmacology*, vol. 17, no. 1, pp. 37–41, Feb. 2009, doi: 10.1007/s10787-008-8039-2.
- [215] L. Farrand, S.-W. Oh, Y. S. Song, and B. K. Tsang, "Phytochemicals: A Multitargeted Approach to Gynecologic Cancer Therapy," *Biomed Res Int*, vol. 2014, p. 890141, 2014, doi: 10.1155/2014/890141.
- [216] J. a. O. Ojewole, "Antiinflammatory, analgesic and hypoglycemic effects of *Mangifera indica* Linn. (Anacardiaceae) stem-bark aqueous extract," *Methods Find Exp Clin Pharmacol*, vol. 27, no. 8, pp. 547–554, Oct. 2005, doi: 10.1358/mf.2005.27.8.928308.
- [217] Y. Aratanechemuge, H. Hibasami, K. Sanpin, H. Katsuzaki, K. Imai, and T. Komiya, "Induction of apoptosis by lupeol isolated from mokumen (*Gossampinus malabarica* L. Merr) in human promyelotic leukemia HL-60 cells," *Oncol Rep*, vol. 11, no. 2, pp. 289–292, Feb. 2004.
- [218] J. Nautiyal *et al.*, "Curcumin Enhances Dasatinib Induced Inhibition of Growth and Transformation of Colon Cancer Cells," *Int J Cancer*, vol. 128, no. 4, pp. 951–961, Feb. 2011, doi: 10.1002/ijc.25410.
- [219] P. Dandawate, S. Padhye, A. Ahmad, and F. H. Sarkar, "Novel strategies targeting cancer stem cells through phytochemicals and their analogs," *Drug Deliv Transl Res*, vol. 3, no. 2, pp. 165–182, Apr. 2013, doi: 10.1007/s13346-012-0079-x.
- [220] S. Shankar *et al.*, "Resveratrol Inhibits Pancreatic Cancer Stem Cell Characteristics in Human and KrasG12D Transgenic Mice by Inhibiting Pluripotency Maintaining Factors and Epithelial-Mesenchymal Transition," *PLoS One*, vol. 6, no. 1, p. e16530, Jan. 2011, doi: 10.1371/journal.pone.0016530.
- [221] M. Gallo and M. Sarachine, "Biological Activities of Lupeol," 2009. Accessed: Jun. 14, 2023. [Online]. Available: <https://www.semanticscholar.org/paper/Biological-Activities-of-Lupeol-Gallo-Sarachine/a64119fb1a24650b56bebfff5d7c5e1373f9050>
- [222] Y.-J. You, N.-H. Nam, Y. Kim, K.-H. Bae, and B.-Z. Ahn, "Antiangiogenic activity of lupeol from *Bombax ceiba*," *Phytother Res*, vol. 17, no. 4, pp. 341–344, Apr. 2003, doi: 10.1002/ptr.1140.
- [223] T. C. Chou and P. Talalay, "Quantitative analysis of dose-effect relationships: the combined effects of multiple drugs or enzyme inhibitors," *Adv Enzyme Regul*, vol. 22, pp. 27–55, 1984, doi: 10.1016/0065-2571(84)90007-4.

- [224] T.-C. Chou and P. Talalay, "Analysis of combined drug effects: a new look at a very old problem," *Trends in Pharmacological Sciences*, vol. 4, pp. 450–454, Jan. 1983, doi: 10.1016/0165-6147(83)90490-X.
- [225] G. Silva-Santana *et al.*, "Clinical hematological and biochemical parameters in Swiss, BALB/c, C57BL/6 and B6D2F1 *Mus musculus*," *Animal Model Exp Med*, vol. 3, no. 4, pp. 304–315, Dec. 2020, doi: 10.1002/ame2.12139.
- [226] Meta-analysis Group In Cancer *et al.*, "Efficacy of intravenous continuous infusion of fluorouracil compared with bolus administration in advanced colorectal cancer," *J Clin Oncol*, vol. 16, no. 1, pp. 301–308, Jan. 1998, doi: 10.1200/JCO.1998.16.1.301.
- [227] D. B. Longley, D. P. Harkin, and P. G. Johnston, "5-fluorouracil: mechanisms of action and clinical strategies," *Nat Rev Cancer*, vol. 3, no. 5, pp. 330–338, May 2003, doi: 10.1038/nrc1074.
- [228] J. E. Ferguson and R. A. Orlando, "Curcumin reduces cytotoxicity of 5-Fluorouracil treatment in human breast cancer cells," *J Med Food*, vol. 18, no. 4, pp. 497–502, Apr. 2015, doi: 10.1089/jmf.2013.0086.
- [229] C. Gjerdrum *et al.*, "Axl is an essential epithelial-to-mesenchymal transition-induced regulator of breast cancer metastasis and patient survival," *Proc Natl Acad Sci U S A*, vol. 107, no. 3, pp. 1124–1129, Jan. 2010, doi: 10.1073/pnas.0909333107.
- [230] J. Chen *et al.*, "PKD2 mediates multi-drug resistance in breast cancer cells through modulation of P-glycoprotein expression," *Cancer Lett*, vol. 300, no. 1, pp. 48–56, Jan. 2011, doi: 10.1016/j.canlet.2010.09.005.
- [231] "A tissue-engineered 3D microvessel model reveals the dynamics of mosaic vessel formation in breast cancer - PMC." <https://www.ncbi.nlm.nih.gov/pmc/articles/PMC7541732/> (accessed Apr. 09, 2022).



CHAPTER 5
PUBLICATIONS

REVIEW ARTICLE

Madhuca indica Inhibits Breast Cancer Cell Proliferation by Modulating COX-2 Expression

Paramita Ghosh, Debarpan Mitra, Sreyashi Mitra, Sudipta Ray, Samir Banerjee and Nabendu Murmu*

Department of Signal Transduction and Biogenic Amines, Chittaranjan National Cancer Institute, 37, S.P. Mukherjee Road, Kolkata-700026, India

Abstract: Background: *Madhuca indica* belongs to the family sapotaceae, commonly known as Mahua. It is primarily known for alcoholic beverage production and is reported to have anti-inflammatory, analgesic and antipyretic properties. *Madhuca indica* has also been reported to be effective in several diseases.

Objective: This study was undertaken to check the anticancer efficacy and chemopreventive effect of methanolic extract of Mahua flower (ME) on human breast cancer cell lines MCF-7 and MDA-MB-468.

Method: The cytotoxic and anti-proliferative effects on MCF-7 and MDA-MB-468 cells were studied by MTT, hexosaminidase and colony formation assay. Expression of caspase 3/7 was assessed by flow cytometry and western blot analysis. Expression of COX-2 was evaluated by western blot analysis, luciferase assay and mRNA analysis.

Results: ME inhibited the proliferation of breast cancer cells by inducing apoptosis through up-regulating the expression of Caspase 3/7 ($P < 0.0001$). Our results showed a decrease in the expression of COX-2 mRNA and COX-2 protein in both MCF-7 and MDA-MB-468 cells with an increase in ME concentration. Furthermore synergistic effect of ME and chemotherapeutic drug paclitaxel was also studied in MCF-7 and MDA-MB-468 cells which were found to be more effective ($P < 0.0001$) than treatment of either ME or paclitaxel alone. Results were analyzed by ANOVA and Pearson correlation analysis.

Conclusion: All these experiments suggest that ME inhibits breast cancer cell proliferation and apoptosis by inhibiting the expression of COX-2 in MCF-7 and MDA-MB-468 cells. This work further highlighted that ME may enhance the potentiality of paclitaxel in breast cancer treatment.

ARTICLE HISTORY

Received: March 15, 2018
Revised: June 21, 2018
Accepted: November 29, 2018

DOI:
10.2174/1566524019666181212100808

Keywords MCF-7, MDA-MB-468, ME, COX-2, paclitaxel, AKT, NF- κ B.

1. INTRODUCTION

Breast cancer is the most common form of cancer among women worldwide. Its incidence in developed countries is higher, while relative mortality is highest in comparatively less developed countries [1, 2]. It is estimated that around 1.4 million women are diagnosed with breast cancer every year worldwide, while approximately 458,000 die of this disease [3, 4]. Based on molecular profiling, breast cancer subtypes are defined as luminal A, luminal B, luminal/human epidermal growth factor receptor 2 (HER2), HER2 enriched, basal-like, and triple negative (TN) non basal. Among all these types, basal subtype accounts for

approximately fifteen percent of one million global cases diagnosed each year [5, 6]. Triple-negative, lacks the estrogen, progesterone, and Her2/neu receptors which fuel most breast cancer growth and development [7, 8] Lack of these receptors in the tumor cells make it ineffective to most targeted and hormonal therapies [9]. The effective treatment of breast cancer includes chemotherapy, radiotherapy and surgery but the patients often suffer from various side effects, poor survival and recurrence. These ordeals have led to the use of the alternative form of treatment such as the use of natural products [10]. Phytochemicals are essential bioactive, non-nutritive molecules found abundantly in fruits, vegetables, grains, and other plant-based foods. In recent years, the use of chemoprevention by edible phytochemicals has attracted the attention of scientists because of their diverse roles, multiple targets, inexpensiveness and accessible approach for the cancer control and management [11].

*Address correspondence to this author at the Department of Signal Transduction and Biogenic Amines, Chittaranjan National Cancer Institute, 37, S. P. Mukherjee Road, Kolkata-700026, India; Tel: 9133-2476-5101; Ext: 322; Fax: 9133-2475-7606; E-mail: nabendu.murmu@cnci.org.in



ELSEVIER

Contents lists available at ScienceDirect

Microvascular Research

journal homepage: www.elsevier.com/locate/yvmre

Reversing effect of Lupeol on vasculogenic mimicry in murine melanoma progression



Sayantana Bhattacharyya^a, Debarpan Mitra^a, Sudipta Ray^a, Nirjhar Biswas^a, Samir Banerjee^a, Biswanath Majumder^b, Saunak Mitra Mustafi^c, Nabendu Murmu^{a,*}

^a Department of Signal Transduction and Biogenic Amines, Chittaranjan National Cancer Institute, 37, S. P. Mukherjee Road, Kolkata 700026, India

^b Department of Molecular Pathology and Cancer Biology, Mitra Biotech, 202, Narayana Nethralaya, Hosur Main Road, Bangalore 560099, India

^c Department of Pathology, Chittaranjan National Cancer Institute, 37, S. P. Mukherjee Road, Kolkata 700026, India

ARTICLE INFO

Keywords:

Melanoma
Vasculogenic mimicry
Dacarbazine
Lupeol
Cancer stem cells
Endothelial progenitor cells

ABSTRACT

Vasculogenic mimicry, an endothelia-independent tumor microcirculation has been found in various cancers and is thought to be achieved by cancer stem like cells. Dacarbazine resistance is one of the most common features of melanoma and recent studies suggest that the mode of resistance is closely related to the formation of vasculogenic mimicry. In our work, we examined the anticancer effect of Lupeol, a novel phytochemical with Dacarbazine *in vivo* and *in vitro*. Results demonstrated adequate cytotoxicity followed by down regulation of CD 133 expression in Lupeol treated B16-F10 cell line. In solid tumor model the drug also inhibited vasculogenic mimicry along with angiogenesis by altering both the cancer stem cell as well as the endothelial progenitor cell population. Lupeol hindered the maturation of bone marrow derived endothelial progenitors and thus, retarded the formation of rudimentary tumor microvessels. Notably, Dacarbazine treatment demonstrated unresponsiveness to B16-F10 cells in both *in vivo* and *in vitro* model via upregulation of CD 133 expression and increased formation of vasculogenic mimicry tubes. Together, these data indicate that Lupeol alone can become a proficient agent in treating melanoma, inhibiting vasculogenic mimicry and might play a significant role in subduing Dacarbazine induced drug resistance.

1. Introduction

Angiogenesis and Vasculogenic Mimicry (VM) are the two major routes of communication in a tumor and both processes require extreme remodelling of the extracellular matrix (ECM) and highly plastic cells to achieve proper architecture. Although there is plenty of report available on the mode of action and molecular signalling driving angiogenesis, a little is known about the other, relatively new machinery. When Maniotis et al. first described the formation of endothelial cell independent vessel-like structures in Uveal melanoma model (Maniotis et al., 1999), an entirely new field of cancer research emanated. Until 1999, it had been taken for granted that all intra-tumoral vascular channels were formed and lined by endothelial cells. This new discovery described the functional plasticity of aggressive cancer cells in expressing a multipotent, stem cell-like phenotype and forming ECM-rich and patterned vessel-like networks in three-dimensional matrix. Initially the hypothesis ignited a spirited debate for several years and earned distinction as a citation classic (Qiao et al., 2014). Today, however it is a well-established mechanism carried out by highly plastic

cancer cells present in the tumor microenvironment and it has been recorded in multiple cancer models including glioma, triple negative breast cancer (TNBC), hepatocellular carcinoma and head and neck squamous cell carcinoma (HNSCC) (Francescone et al., 2012; Liu et al., 2013; Guzman et al., 2007; Wang et al., 2010).

When a tumor tends to grow beyond a certain size (1–2 mm³), pre-existing blood vessels commence to form nascent endothelia and the mode of action is thought to be driven by endothelial progenitor cells (EPC) - a group of hemangioblast derived cells that play major roles in the regeneration of the endothelial lining of blood vessels (Basak et al., 2009). Studies have shown that ischemic stimuli lures EPCs from bone marrow and their incorporation into the target site, promote tumor vascularisation (Asahara et al., 1997; Sepúlveda et al., 2007; Nolan et al., 2007) and the maturation is signified by marked upregulation of Vascular Endothelial Cadherin (VE-cadherin), a cell adhesion glycoprotein present in matured endothelial cells (Medina et al., 2010; Lee et al., 2012). Before Asahara et al. first described the presence of EPCs (Asahara et al., 1997), it was thought that angiogenesis is only achieved by matured endothelial cells. The discovery of EPC mediated



Phosphorylation of EphA2 receptor and vasculogenic mimicry is an indicator of poor prognosis in invasive carcinoma of the breast

Debarpan Mitra¹ · Sayantan Bhattacharyya¹ · Neyaz Alam² · Sagar Sen² · Saunak Mitra³ · Syamsundar Mandal⁴ · Shivani Vignesh⁶ · Biswanath Majumder^{5,6} · Nabendu Murmu¹

Received: 12 July 2019 / Accepted: 23 October 2019
© Springer Science+Business Media, LLC, part of Springer Nature 2019

Abstract

Purpose The occurrence of vasculogenic mimicry (VM) and EphA2-mediated tumour progression are associated with poor prognosis in various solid tumours. Here, we aimed to investigate the prognostic implications of VM and its association with phosphorylated EphA2 receptor in invasive carcinoma of the breast.

Methods The patients were stratified based on CD-31/PAS dual staining and subsequently the expression status of phospho-EphA2 (S897), FAK, phospho-ERK1/2 and Laminin 5Y2 was analysed by immunohistochemistry. Survival of patients was correlated within the stratified cohort.

Results The pathologically defined VM phenotype and phospho-EphA2 (S897) expression status were significantly associated with lower disease-free survival (DFS) and overall survival (OS). Both the features were also found to be significantly associated with higher nodal status, poor Nottingham Prognostic Index (NPI) and were more prevalent in the triple-negative breast cancer (TNBC) group. Incidentally, there were no significant association between age of the patient, grade and size of the tumour with VM and phospho-EphA2 (S897). The effector molecules of phospho-EphA2 (S897) viz., Focal Adhesion Kinase (FAK), phospho-ERK1/2 and Laminin 5Y2 were significantly upregulated in the VM-positive cohort. Survival analysis revealed that the VM and phospho-EphA2 (S897) dual-positive cohort had poorest DFS [mean time = 48.313 (39.992–56.633) months] and OS [mean time = 56.692 (49.055–64.328) months]. Individually, VM-positive [Hazard Ratio (HR) 6.005; 95% confidence interval (CI) 2.002–18.018; $P=0.001$ for DFS and HR 11.654; 95% CI 3.195–42.508; $P<0.0001$ for OS] and phospho-EphA2 (S897)-positive (HR 4.342; 95% CI 1.717–10.983; $P=0.002$ for DFS and HR 5.853; 95% CI 1.663–20.602; $P=0.006$ for OS) expression proved to be independent indicators of prognosis.

Conclusion This study evaluated tumour dependency on oncogenic EphA2 receptor regulation and VM in invasive carcinoma of the breast and their prognostic significance. Significant correlations between VM, phospho-EphA2 and several clinicopathologic parameters of breast cancer were found. Subsequently, the occurrence of VM or phospho-EphA2 expression proved to be major contributors for poor prognosis in patients with breast cancer but their simultaneous expression failed to be an independent risk factor.

Keywords Breast cancer · Vasculogenic mimicry · EphA2 · Prognosis · Overall survival

Introduction

Breast cancer is the most commonly diagnosed malignancy accounting for 1 in 4 cases among women [1]. Although a widespread understanding of the molecular subtypes of breast cancer has led to the evolution of molecularly guided personalised therapies and improved response rate, a large number of patients do not get any durable benefit [2]. The better understanding of the molecular and phenotypic basis of disease progression, recurrence and metastasis is an unmet need for effective management of the diseases. One of

Electronic supplementary material The online version of this article (<https://doi.org/10.1007/s10549-019-05482-8>) contains supplementary material, which is available to authorized users.

✉ Nabendu Murmu
nabendu.murmu@cnci.org.in

Extended author information available on the last page of the article

Research Article

Botanical from *Piper capense* Fruit Can Help to Combat the Melanoma as Demonstrated by *In Vitro* and *In Vivo* Studies

Brice E. N. Wamba,^{1,2} Paramita Ghosh,¹ Armelle T. Mbaveng,² Sayantan Bhattacharya,¹ Mitra Debarpan,¹ Saha Depanwita,¹ Mustafi Mitra Saunak,³ Victor Kuete,² and Nabendu Murmu¹

¹Department of Signal Transduction and Biogenic Amines, Chittaranjan National Cancer Institute, 37, S.P. Mukherjee Road, Kolkata 700026, India

²Department of Biochemistry, Faculty of Science, University of Dschang, Dschang, Cameroon

³Department of Pathology, Chittaranjan National Cancer Institute, 37, S. P. Mukherjee Road, Kolkata 700026, India

Correspondence should be addressed to Victor Kuete; kuetevictor@yahoo.fr and Nabendu Murmu; nabendu.murmu@cnci.org.in

Received 25 September 2020; Revised 16 November 2020; Accepted 16 December 2020; Published 18 January 2021

Academic Editor: Saheed Sabiu

Copyright © 2021 Brice E. N. Wamba et al. This is an open access article distributed under the Creative Commons Attribution License, which permits unrestricted use, distribution, and reproduction in any medium, provided the original work is properly cited.

Piper capense belongs to Piperaceae family and has long been used as a traditional medicine to treat various diseases in several parts of Africa. The present study aims to investigate the effect of *Piper capense* fruit extract (PCFE) alone and in combination with dacarbazine on metastatic melanoma cell line B16-F10 and *in vivo* in C57BL/6J mice. Cytotoxic effects of PCFE alone and in association with dacarbazine on B16-F10 cells were studied by 3-(4, 5-dimethylthiazol-2-yl)-2, 5-diphenyl tetrazolium bromide (MTT) assay and colony formation assay. Wound healing assay, immunofluorescence staining, and western blot analysis were performed to evaluate the individual and combined effect of PCFE and dacarbazine on epithelial-mesenchymal transition (EMT). For *in vivo* studies, C57BL/6J mice were subcutaneously injected with B16-F10 cells (5×10^5 cells/mL), and the effect of PCFE and dacarbazine was studied on tumor development. The alteration of EMT was evaluated by targeting E-cadherin, vimentin, and CD133 in PCFE alone and in combination with dacarbazine-treated tumor tissues by western blot analysis. Phytochemical screening of PCFE reveals the presence of certain secondary metabolites. Our results showed that PCFE alone and in association with dacarbazine has a good activity in preventing B16-F10 melanoma cell progression and clonogenicity. This extract also regulated EMT. *In vivo* results showed that PCFE (100 mg/kg body weight) reduced tumor size in C57BL/6J mice along with the decrease in the expression of vasculogenic mimicry (VM) tubes as well as an improvement in the qualitative and quantitative expression of markers involved in EMT. Our study suggests that PCFE may be useful for managing the growth and metastasis of melanoma.

1. Introduction

Cancer is increasingly recognized as a critical public health problem worldwide, specifically in some parts of Africa where people are poor and do not have the financial means to obtain adequate treatment even though the survival rates are lower compared to other countries [1].

The latest World Health Organization (WHO) global data show 18.1 million new cases and 9.6 million cancer deaths in 2018 [2]. It is recognized as the leading and the second leading cause of death, respectively, in economically

developed and developing countries [3]. WHO Bulletin in 2018 reports 15769 cases of cancer detected against 10533 cases of deaths or more than half of the incidence in Cameroon [2]. There are more than a hundred different cancers depending on the organ affected. Malignant melanoma is the most aggressive form of skin cancer. About 96480 new cases of melanoma have been diagnosed (57220 in men and 39260 in women) and 7230 cases of death (4740 in men and 2490 in women) from this disease in the United States in 2019 according to the work of Siegel et al. [4]. Melanomas which are not of epithelial origin develop from

Orchestrated expression of vasculogenic mimicry and laminin-5 γ 2 is an independent prognostic marker in oral squamous cell carcinoma

Depanwita Saha¹ | Debarpan Mitra¹ | Neyaz Alam² | Sagar Sen² |
 Saunak Mitra Mustafi³ | Syamsundar Mandal⁴ | Biswanath Majumder⁵ |
 Nabendu Murmu¹

¹Department of Signal Transduction and Biogenic Amines, Chittaranjan National Cancer Institute, Kolkata, India

²Department of Surgical Oncology, Chittaranjan National Cancer Institute, Kolkata, India

³Department of Pathology, Chittaranjan National Cancer Institute, Kolkata, India

⁴Department of Epidemiology and Biostatistics, Chittaranjan National Cancer Institute, Kolkata, India

⁵Departments of Molecular Profiling, Cancer Biology and Molecular Pathology, Mitra Biotech, Bangalore, India

Correspondence

Nabendu Murmu, Department of Signal Transduction and Biogenic Amines, Chittaranjan National Cancer Institute, 37, S. P. Mukherjee Road, Kolkata 700026, India.
 Email: nabendu.murmu@cnici.ac.in

Present address

Biswanath Majumder, Oncology Division, Bugworks Research, C-CAMP, Bangalore, India

Funding information

This work was financially supported by the Science and Engineering Research Board (SERB), Government of India, under Grant Project No: EEQ/2016/000345.

Abstract

Vasculogenic mimicry (VM), an endothelial cell-independent alternative mechanism of blood supply to the malignant tumour, has long been considered as an adverse prognostic factor in many cancers. The correlation of VM with laminin-5 γ 2 and the assessment of their harmonized expression as an independent risk factor have not been elucidated yet in oral squamous cell carcinoma (OSCC). CD31/PAS staining stratified 116 clinically diagnosed OSCC specimens into VM+ and VM- cohorts. The expression pattern of laminin-5 γ 2 and its upstream modulator MMP2 was evaluated by immunohistochemistry and Western blot. The Kaplan-Meier and Cox regression analyses were performed to assess the survival and prognostic implications. The presence of VM demonstrated a significant correlation with the expression of laminin-5 γ 2 ($p < .001$) and MMP2 ($p < .001$). This pattern was mirrored by the significant upregulation of laminin-5 γ 2 and MMP2 in VM+ cohorts compared with the VM- ones. Furthermore, co-expression of VM and laminin-5 γ 2 was significantly associated with tumour grade ($p = .010$), primary tumour size ($p < .001$), lymph node metastasis ($p = .001$) and TNM stages ($p < .001$) but not with patients' age, gender, tobacco and alcohol consumption habit. Vasculogenic mimicry and laminin-5 γ 2 double-positive cohort displayed a significantly poorer disease-free survival (DFS) and overall survival (OS). Vasculogenic mimicry, laminin-5 γ 2 and their subsequent dual expression underlie a significant prognostic value for DFS [hazard ratio (HR) = 9.896, $p = .028$] and OS [HR = 21.401, $p = .033$] in OSCC patients. Together, our findings imply that VM along with laminin-5 γ 2 is strongly linked to the malignant progression in OSCC and VM and laminin-5 γ 2 coordination emerges as a critical prognostic biomarker for OSCC.

KEYWORDS

co-expression, laminin-5 γ 2, OSCC, prognosis, survival, vasculogenic mimicry

Increasing incidence of colorectal cancer among Indians: Concerns and the way forward

We read the article by Tahiliani *et al.* titled, "Retrospective analysis of histopathological spectrum of premalignant and malignant colorectal lesions," with great interest.^[1] The article highlights the increasing incidence of colorectal cancers (CRCs) in developing countries such as India and Africa, which could be attributed to lifestyle changes.^[2] The study conducted in patients ($N = 150$) from the Gujarat Cancer Society Medical College reported ulcerative colitis to be the most common premalignant lesion and adenocarcinoma to be the most common malignant colorectal lesion. They also reported that these lesions advance with age and have a higher incidence among male patients. The rectum was reportedly the most common site of the lesions. Most of the findings of this study corroborated the findings of previous studies with some variations; for instance, the most common premalignant lesion was reported to be tubular adenoma in CRCs by two previous independent studies.^[3,4]

While Tahiliani *et al.*'s study showed that most patients affected with CRC are in the sixth decade of life, akin to the findings of previous studies, an interesting observation in this study was that around 22.8% of the patients were aged less than 40 years.^[1] First, CRC is not as frequent in developing countries such as ours, and second, the increasing incidence of CRC among the youth is a definite cause for alarm. A number of factors could be responsible for this drastic rise of CRC among Indian youth, ranging from lifestyle changes to dietary habits.^[5] Recently, over-usage of antibiotics has been linked to a higher incidence of colon cancer, and India, as we know, is one of the largest consumers of antibiotics.^[6] This higher risk may be due to the disruption of the gut microbiota in the colorectal region.^[7] Post coronavirus disease-2019 (COVID-19), with the indiscriminate and unwarranted usage of antibiotics among patients,^[8,9] this concern is even larger and needs to be addressed and understood only through future studies keeping the negative impact of the pandemic in mind. To truly understand the effect of lifestyle changes and dietary habits on the increasing incidence of CRC among Indian youth, we must stratify the youth with CRC from rural and urban areas. This stratification will help in the delineation of how the sedentary lifestyle and fast-food consumption by the urban youth put them at a relatively higher risk of developing CRC compared to their rural counterparts, leading a more active life and consuming traditional Indian diet.

Although this study sheds some light on the prevalence of CRC in the Indian population, it suffers from several drawbacks, some of which have been mentioned by the authors themselves. First, a cohort comprising only 150 patients is too small to draw any significant conclusion.^[1] A more extensive statistical analysis is required with higher number of patients. Second, the study was conducted among majorly tertiary patients with stage IIIB cancer,^[1] and hence, more patients with less advanced disease such as stage IIA, I, and IIC need to be included to expand the evidence. Third, along with age, the anatomical site, and sex of the patients, more patient information should have been recorded such as antibiotic usage, whether the patient lived in an urban or rural area, the level of daily physical activity (active versus sedentary), and dietary habits. All these parameters along with the parameters already mentioned in this study would lead to a more comprehensive study on CRC in Indian patients, which will pose a plethora of important questions and hopefully lead to greater awareness among people.

Financial support and sponsorship

Nil.

Conflicts of interest

There are no conflicts of interest.

NABENDU MURMU, DEBARPAN MITRA, GAURAV DAS


Department of Signal Transduction and Biogenic Amines,
Chittaranjan National Cancer Institute, Kolkata, West Bengal,
India

Address for correspondence: Dr. Nabendu Murmu,
Department of Signal Transduction and Biogenic Amines,
Chittaranjan National Cancer Institute, 37, Shyama Prasad
Mukherjee Road, Bakul Bagan, Bhowanipore, Kolkata - 700 026,
West Bengal, India.
E-mail: nabendu.murmu@cnci.ac.in

REFERENCES

1. Tahiliani HT, Purohit AP, Desai SC, Jarwani PB. Retrospective analysis of histopathological spectrum of premalignant and malignant colorectal lesions. *Cancer Res Stat Treat* 2021;4:472-8.
2. Aster JC. The gastrointestinal tract. In: Vinay K, Abdul KA, Jon CA, editors. *Robbins and Cotran Pathologic Basis of Disease*. 10th ed. Philadelphia: Elsevier; 2021. p. 814.
3. Umana IO, Obasek DE, Ekanem VJ. The clinicopathological features of lower gastrointestinal tract endoscopic biopsies in Benin City, Nigeria. *Saudi Surg J* 2017;5:9-20.
4. Sheikh B, Ambreen B, Summaiya F, Ruby R, Farzaana M, Sheikh J. Spectrum of colorectal lesions on colonoscopic biopsies; a

Lupeol and Paclitaxel cooperate in hindering hypoxia induced vasculogenic mimicry via suppression of HIF-1 α -EphA2-Laminin-5 γ 2 network in human oral cancer

[Depanwita Saha](#), [Debarpan Mitra](#), [Neyaz Alam](#), [Sagar Sen](#), [Saunak Mitra Mustafi](#), [Pradip K. Majumder](#), [Biswanath Majumder](#) & [Nabendu Murmu](#) 

Journal of Cell Communication and Signaling (2022) | [Cite this article](#)

Abstract

Vasculogenic mimicry (VM), defined as an endothelial cell independent alternative mechanism of blood and nutrient supply by dysregulated tumor cells, is associated with poor prognosis in oral squamous cell carcinoma (OSCC). Here we aim to investigate the underlying molecular mechanism of the synergistic effect of phytochemical Lupeol and standard microtubule inhibitor Paclitaxel in reversing the hypoxia induced VM formation in OSCC. The results demonstrated that the hypoxia induced upregulation of HIF-1 α led to augmentation of signaling cascade associated with extracellular matrix remodeling and EMT phenotypes that are mechanistically linked to VM. Induction of HIF-1 α altered the expression of EMT/CSC markers (E-Cadherin, Vimentin, Snail, Twist and CD133) and enhanced the ability of cell migration/invasion and spheroid formation. Subsequently, the targeted knockdown of HIF-1 α by siRNA led to the perturbation of matrigel mediated tube formation as well as of Laminin-5 γ 2 expression with the down-regulation of VE-Cadherin, total and phosphorylated (S-897) EphA2, pERK1/2 and MMP2. We also observed that Lupeol in association with Paclitaxel resulted to apoptosis and the disruption of VM associated phenotypes in vitro. We further validated the impact of this novel interventional approach in a patient derived tumor explant culture model of oral malignancy. The ex vivo tumor model mimicked the in vitro anti-VM potential of Lupeol-Paclitaxel combination through down-regulating HIF-1 α /EphA2/Laminin-5 γ 2 cascade. Together, our findings elucidated mechanistic underpinning of hypoxia induced Laminin-5 γ 2 driven VM formation highlighting that Lupeol-Paclitaxel combination may serve as novel therapeutic intervention in perturbation of VM in human OSCC.



Cite this: DOI: 10.1039/d2nj03481f

A new “turn-on” molecular switch for idiosyncratic detection of Al³⁺ ion along with its application in live cell imaging†

 Amitav Biswas,^a Rahul Naskar,^a Debarpan Mitra,^b Akash Das,^a Saswati Gharami,^a Nabendu Murmu^b and Tapan Kumar Mondal^{b,*}

A highly sensitive, reversible, reusable and fluorogenic “turn-on” probe (HBTC) is fabricated for the sole detection of Al³⁺. On incremental addition of Al³⁺ in a solution of HBTC in ACN:H₂O (4:1), a sharp “turn-on” emission enhancement is observed at 480 nm. The reversibility of the probe (HBTC) was displayed on the addition of F⁻ solution. The detection limit is found to be of the order of 10⁻⁹ M which suggests that HBTC can detect Al³⁺ at a very minute level. The mechanism for Al³⁺ detection in ACN:H₂O (4:1) is attributed to forbidding C=N isomerization and ESIPT process simultaneously turning on the chelation-enhanced fluorescence process. The reusability and real-time application of the probe are also studied. Bioimaging study reveals that HBTC can detect Al³⁺ in human breast cancer cells (MDA-MB-231). Electronic structure of the probe is explained by density functional theory.

Received 14th July 2022,
Accepted 21st October 2022

DOI: 10.1039/d2nj03481f

rsc.li/njc

Introduction

Nowadays undue use of ionic pollutants in industry and the farming sector has become a menace to the environment.^{1,2} Hence rapid and accurate detection of those ions has become a promising part in the research field in modern times. It is well known that aluminium is the most abundant metallic element in earth's crust. And it has become an integrated part of daily lifestyle such as in drinking water supplies, utensils, packaging of foods, powder, cosmetic products, processed dairy products, cookware, bleached flour, component of medicine, medicine storage containers and manufacturing of cars.^{3–7} The WHO (World Health Organization) stated that the average consumption of Al³⁺ in the human body through several ways is about 3–10 mg per kg per day and the maximum recommended limit Al-contaminated water is 7.42 μM.^{8–10} Although it has negative effects on both biological and environment systems, it is extensively used on a daily basis. The central nervous system is deeply affected by overexposure of Al.¹¹ Abnormal concentration of Al in the human body is related to many neurological disorders including Alzheimer's disease, Parkinson's disease and dementia.^{12–14} On the other hand, regular intake of Al

beyond permissible limits causes bone disease, damage in the gastrointestinal tract, encephalopathy, microcytic hypochromic anaemia, myopathy, bone softening, impaired lung function, fibrosis and chronic renal failure.^{15–18} Therefore, it is imperative to develop probes that can detect and track aluminium ions with high sensitivity using minimal resources and under biological conditions. Among different sensing tools for detection of such kinds of environmental hazardous metal, fluorescence-based chemosensors are considered to be efficient for specifically detecting target analytes.¹⁹ Different mechanisms like excited-state intra-/intermolecular proton transfer (ESIPT), chelation-enhanced fluorescence (CHEF), metal–ligand charge transfer, photoinduced electron/energy transfer, fluorescence resonance energy transfer, intramolecular charge transfer, and –C=N– isomerisation are considered to be the reason for chemosensing processes.^{20,21} A strong oxidising site is preferred for the CHEF process, through which a radiative process gets turn on.²² Comparing with different transition metal ions, chemosensors detecting solely Al³⁺ are limited, due to poor coordination power, strong hydration enthalpy and lack of spectroscopic characteristics.^{23,24} Being a hard acid, Al³⁺ always prefers to bind hard centres like N and O donor sites. Schiff bases possess excellent coordinating capabilities, showing different biological activities and have potential analytical application.^{25,26} Hence, development of probes with such binding sites causing metal–ligand CHEF is an interesting approach due to a fluorescence “turn-on” mechanism on interaction with a guest.

Recently in 2021, Singh *et al.* reported a silatrane-based Schiff base-functionalized probe which can detect Al³⁺ ions

^a Department of Chemistry, Jadavpur University, Kolkata, 700032, India.

E-mail: tapank.mondal@jadavpuruniversity.in

^b Department of Signal Transduction and Biogenic Amines (STBA),

Chittaranjan National Cancer Institute, Kolkata, 700026, India

† Electronic supplementary information (ESI) available. See DOI: <https://doi.org/10.1039/d2nj03481f>

RESEARCH ARTICLE

Azophenyl appended Schiff base probe for colorimetric detection of Cu²⁺ in semi-aqueous medium and live cell imaging

Samrat Dev¹ | Souvik Pandey² | Suwendu Maity¹ | Debarpan Mitra³ | Gaurav Das³ | Nabendu Murmu³ | Chittaranjan Sinha¹

¹Department of Chemistry, Jadavpur University, Kolkata, India

²Department of Chemistry, Sister Nivedita University, Kolkata, India

³Department of Signal Transduction and Biogenic Amines, Chittaranjan National Cancer Institute (CNCI), Kolkata, India

Correspondence

Chittaranjan Sinha, Department of Chemistry, Jadavpur University, Kolkata-700032, West Bengal, India.
Email: chittaranjan.sinha@jadavpuruniversity.in

Funding information

University Grant Commission (UGC); National Cancer Institute; Jadavpur University, Grant/Award Number: Nil

Abstract

A phenylazo appended *ortho*-vanillin Schiff base scaffold (HAZ) has been used for selective colorimetric sensing of Cu²⁺ in semi-aqueous medium (methanol–water, 1:1, v/v) in the presence of 16 cations and 20 anions, and the limit of detection is 1.8×10^{-7} M. The structures of HAZ and Cu (II) complex, [Cu (AZ)₂], have been characterised by spectroscopic data (UV–Vis, Fourier transform infrared and electron paramagnetic resonance) and established by the single crystal X-ray diffraction measurement. The Job's plot from the absorption studies has also confirmed the 1:2 stoichiometry of Cu²⁺:HAZ. The absorption spectrum of [Cu (AZ)₂] has returned to the spectrum of HAZ on the addition of Na₂EDTA solution which is again recovered upon the addition of Cu²⁺ solution. Discrete Fourier transform computations were carried out using the coordinates of the X-ray structures of the compounds, and the molecular functions were used to correlate the solution spectroscopic properties. In addition to this, the probe is treated on MDA-MB 231 breast cancer cells to check the cytotoxicity. The probe is used for the detection of trace quantity of Cu²⁺ in the cancer cell.

KEYWORDS

cell imaging assay, cytotoxicity study, colorimetric sensor of Cu²⁺ ions, phenylazo appended *ortho*-vanillin Schiff base, X-ray structures

1. INTRODUCTION

Metal ions are very crucial in biology and chemical sciences; they act as important cofactors in enzymes and vitamins; they regulate cell metabolism; and some of them transport oxygen such as iron in haemoglobin or myoglobin.^[1,2] However, their de-regulation in cells can lead to a wide variety of disorders, like their elevation or sudden depression can cause havoc damage to a human body and often be fatal.^[1,3] Their easy, reliable, sensitive, and selective detection at trace level using reliable chemosensors is

essential^[4–6] and much needed. Numerous measurement methods for metal ions have been formulated, but it has been found that detection using colour-changing techniques is most effective.^[7] Many reports already exist whereby metal ion, like Cu²⁺, has been successfully detected using spectrophotometric techniques.^[8–12] The importance of Cu²⁺ is numerous in the development of civilisation (The Copper Age!) and the sustenance of living bodies. Cu is the third most abundant trace metal in a healthy adult human being (behind iron and zinc) with a total amount of 75–100 mg per human body (70 kg).^[13,14]

Fabrication of a New Coumarin Based Fluorescent “turn-on” Probe for Distinct and Sequential Recognition of Al^{3+} and F^- Along With Its Application in Live Cell Imaging

Atanu Maji, Rahul Naskar, Debarpan Mitra, Saswati Gharami, Nabendu Murmu & Tapan Kumar Mondal 

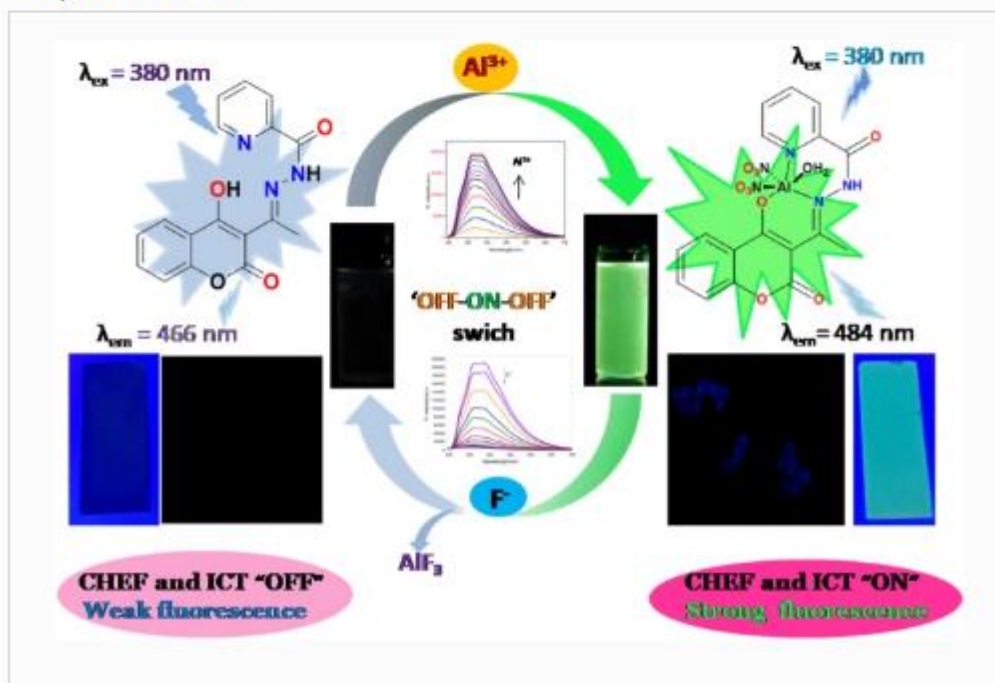
Journal of Fluorescence (2023) | [Cite this article](#)

127 Accesses | [Metrics](#)

Abstract

A new coumarin based fluorescent switch PCEH is fabricated which displays high selective sensing towards Al^{3+} among other metal cations at physiological pH. On gradual addition of Al^{3+} , PCEH shows a brilliant “turn-on” emission enhancement in MeOH/ H_2O (4/1, v/v) solution. This new fluorescent switch is proven to be a reversible probe by gradual addition of F^- into the PCEH- Al^{3+} solution. Detection limit as well as binding constant values are calculated to be in the order of 10^{-9} M and 10^4 M^{-1} respectively. We have also explored its potential as a biomarker in the application of live cell imaging using breast cancer cells (MDA-MB-231 cell).

Graphical Abstract



A biphenyl thiosemicarbazide based fluorogenic chemosensor for selective recognition of Cd²⁺: application in cell bioimaging †



Amitav Biswas,^a Debarpan Mitra,^b Rahul Naskar,^a Atanu Maji,^a Akash Das,^a Nabendu Murmu^b and Tapan Kumar Mondal

*a

Author affiliations

Abstract

A diversified biphenyl thiosemicarbazide based chemosensor (HBMC) has been fabricated and reported for the specific detection of Cd²⁺ in a MeOH : H₂O (4 : 1) solution. We observed a chromogenic change from colorless to light yellow colour, and it showed a “turn-on” fluorogenic change from non fluorescent to blooming cyan colour. In fluorometric titration a sharp “turn-on” emission for Cd²⁺ was observed with a ~16 fold increase in fluorescence intensity value at 496 nm by incremental addition of Cd²⁺ ions in the MeOH : H₂O (4 : 1) solution. The reversibility of the chemosensor (HBMC) was confirmed by a sequential addition of the EDTA solution. Again the binding stoichiometry of HBMC with Cd²⁺ was found to be 2 : 1, as confirmed by Job's plot analysis and HRMS spectra of the HBMC–Cd²⁺ complex. The mechanism for Cd²⁺ sensing in MeOH : H₂O (4 : 1) is based upon the inhibition of C=N isomerization and ESIPT process and simultaneously turning on the CHEF (chelation enhanced fluorescence) process. The limit of detection for Cd²⁺ was found to be in the order of 10⁻⁸ (M), which implies that HBMC is an efficient probe to detect Cd²⁺ at the microscopic level. A reusability study was performed and on-sight detection of cadmium ions by the chemosensor (HBMC) was established by dip-stick experiment. *In vitro* detection of Cd²⁺ in human breast cancer cells (MDA-MB-231) by HBMC discloses its cell permeability and biocompatible nature. Computational studies (DFT and TDDFT) with the probe HBMC and HBMC–Cd²⁺ complex were also performed.

